Binding of vanadium ions and complexes to proteins and enzymes in aqueous solution

João Costa Pessoa[a,*], Marino F. A. Santos[a,b], Isabel Correia[a], Daniele Sanna[c], Giuseppe Sciortino[d,e], Eugenio Garribba[d,*]

[a] *Centro de Química Estrutural and Departamento de Engenharia Química, Instituto Superior Técnico, Universidade de Lisboa, Av. Rovisco Pais, 1049-001 Lisboa, Portugal*

[b] *UCIBIO, Applied Molecular Biosciences Unit, Departamento de Química, Faculdade de Ciências e Tecnologia, Universidade Nova de Lisboa, 2829-516 Caparica, Portugal*

[c] *Istituto CNR di Chimica Biomolecolare, Trav. La Crucca 3, I-07100 Sassari, Italy*

[d] *Dipartimento di Chimica e Farmacia, Università di Sassari, Via Vienna 2, I-07100 Sassari, Italy*

[e] *Institute of Chemical Research of Catalonia (ICIQ), The Barcelona Institute of Science and Technology (BIST), 43007 Tarragona, Spain*

* Corresponding authors.
E-mail addresses: joao.pessoa@ist.utl.pt (J. Costa Pessoa); garribba@uniss.it (E. Garribba).

Abstract

The understanding of the role of vanadium enzymes and of vanadium compounds (VCs) in biology, as well as the design of new vanadium-based species for catalysis, materials science and medicinal chemistry has exponentially increased during the last decades. In biological systems, VCs may rapidly interconvert under physiological conditions and several V-containing moieties may be formed and bind to proteins. These interactions play key roles in the form transported in blood, in their uptake by cells, in inhibition properties and mechanism of action of essential and pharmacologically active V species. In this review, we focus on the recent advances made, namely in the application of the theoretical methodologies that allowed the description of the *coordinative* and *non-covalent* VC–protein interactions. The text is organized in six main topics: a general overview of the most important experimental and computational techniques useful to study these systems, a discussion on the nature of binding process, the recent advances on the comprehension of the V-containing natural and artificial enzymes, the interaction of mononuclear VCs with blood and

other physiologically relevant proteins, the binding of polyoxidovanadates(V) to proteins and, finally, the biological and therapeutic implications of the interaction of pharmacologically relevant VCs with proteins and enzymes. Recent developments on vanadium-containing nitrogenases, haloperoxidases, nitrate reductases, transferrin, albumins, immunoglobulins, hemoglobin, lysozyme, myoglobin, ubiquitin and cytochrome *c* are discussed. Challenges and ideas about desirable features and potential drawbacks of VCs in biology and medicine and future directions to explore this chemistry area are also presented. The deeper understanding of the interactions of V-species with proteins, and the discussed data may provide the basis to undertake the investigation, design and development of new potentially active VCs with a more solid knowledge to predict their binding to biological receptors at a molecular point of view.

Keywords: Vanadium-protein binding; Vanadium enzymes; Biophysical characterization; Computational Methods; Polyoxidovanadates; Vanadium drugs

Contents

1. Introduction

Advances in the development of vanadium compounds (VCs) in areas of catalysis, materials science, and medicinal chemistry has been exponential since the 2000s. In addition, the environmental impact of VCs resulting from exploration of natural resources and industrial activities, and the corresponding risk for human health, also continue being active topics of intense research.

Being widely distributed in water, soil and crude oil, and – depending on the place and conditions – also in air, vanadium is an element easily available for living beings. With a concentration of ca. 35

nM in sea water, it is the 2nd most abundant transition metal, exceeded only by molybdenum. Consequently, biological systems made use of it and there are several organisms, namely macroalgae, bacteria and fungi that contain V-dependent enzymes such as haloperoxidases or nitrogenases [1-5]. Haloperoxidases catalyze the two electron oxidation of halides by H_2O_2, while nitrogenases have a remarkable reducing power, being capable of catalyzing the conversion of atmospheric N_2 to ammonia, as well as CO and CO_2 to hydrocarbons [6-11].

Some organisms such as ascidians [12, 13], *Polychaetes* [14] and mushrooms [1, 15] developed remarkably selective and efficient systems for uptake, transport and storage of V. Ascidians are able to extract vanadium from seawater and reduce it to V^{III}, several proteins, namely vanabins, participating in the processes of storage and reduction of vanadium [12, 13]. Other marine organisms such as *Polychaetes* and the tube-dwelling fan worms of the family of *Sabellidae* also accumulate high amounts of vanadium in vacuoles of the epithelial cells, using several low molecular mass proteins to bind vanadium [14]. In *Amanita muscaria* vanadium forms amavadin, a non-oxido V^{IV}-complex with the bioligand *N*-hydroxyimino-2,2'-diisopropionic acid (H_3hidpa). In this way V is accumulated ca. 400 times the amounts found in other mushrooms of the same type [15-17]. Besides these examples, essentiality to mammals has been proposed, but not yet firmly established [18]. It is also highly probable, but not proven, that vanadium is also an essential element for humans [4].

During the last years, many studies addressed the effects of VCs on living beings, mainly associated to their environmental impact and possible applications in medicine [19]. This latter prospective necessarily gave rise to many studies addressing the interactions of VCs with proteins [1, 19-25]. Studies on protein binding have developed in parallel with those on the biological and pharmacological effects of vanadium-based compounds as potential therapeutics, in particular to treat diabetes and cancers [19, 26-29]. In fact, the interaction of VCs with blood proteins, namely human serum transferrin (HTF), human serum albumin (HSA), and hemoglobin (Hb), the modification of the conformation of proteins upon binding and the inhibition of phosphatases and ATP-dependent enzymes, are all factors that have relevance in the transport, cellular uptake and biological action of VCs [22]. In this context, important issues are how vanadium is transported in blood, how it is taken up by cells and which are the chemical form(s) present under physiological conditions. The type and strength of the interactions established by vanadium species with proteins are particularly important in this respect, but – despite the fact that they have deserved a throughout discussion – several aspects are still not well understood [5, 27, 30-33].

One of the most important characteristics of vanadate(V) is its chemical similarity with phosphate [22, 27, 34]. This and the versatility of vanadium ions in changing their coordination geometry, and

the ability to form phosphate-transition state analogues with low energy, allows vanadium to interfere and possibly modulate the function of many phosphate-related enzymes, participating in biologically critical processes such as the transport of cations in mammalians [35, 36]. However, there are differences, namely the fact that in contrast to phosphate, vanadate forms stable 5-coordinate compounds and is accessible to one-electron reduction. A comprehensive overview emphasizing why vanadate(V) is able to effectively interfere with a wide diversity of enzymes, enabling its broad scope of bioactivity, was previously made [22].

In aqueous solution or in biological media, VCs can easily undergo hydrolysis, ligand exchange and redox reactions, as well as changes in geometry, coordination number and nuclearity (Scheme 1). In particular, at low concentrations, the main species that form may totally differ from the compound initially introduced in the media; thus the identification of the active species and proposals of mechanism of action are not easily made. Only rather recently researchers started taking this into consideration and tried to understand the complex speciation that takes place in biological media [37-41].

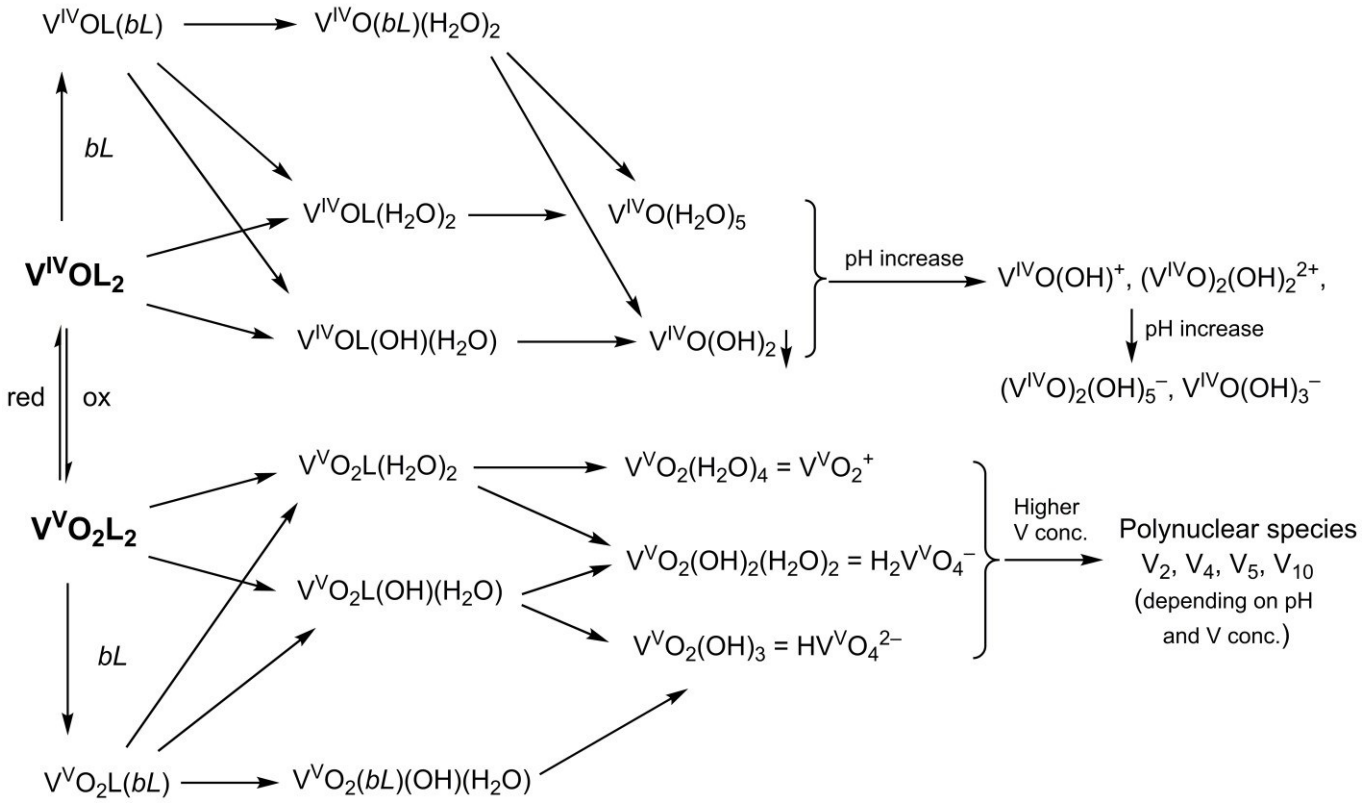

Scheme 1. Outline of possible hydrolysis, ligand exchange and redox reactions for V^{IV} and V^{V} complexes.

Because of the rapid interconversion of VCs in biological media, a variety of distinct V-containing species may form and their interactions with proteins and enzymes may spread out to several distinct metabolic processes and cell cycles. It is not trivial to identify the species formed and to distinguish their actions. Therefore, establishing the effects of VCs may be an extremely complex task and it is difficult to predict or adequately explain their *in vivo* roles [21, 42]. To comprehend the consequences of therapies involving long-term administration of VCs and to evaluate risks connected to their potential deleterious effect, as well as of possible disorders associated with reactive oxygen species (ROS) unbalances, requires a much deeper knowledge and careful accession of beneficial and toxic effects resulting from their use [21]. Notwithstanding, there are several prospective clinical applications of VCs which continue to drive the interest of many researchers [19, 26, 28].

Based on these assumptions, understanding the several types of binding that may be established between VCs and proteins/enzymes is very important because their action may be modified and/or inhibited, and the structure and properties of the original complex be changed. Several reviews were published addressing the vanadium bioinorganic chemistry and/or the role of VCs in biology [4, 5, 27, 34], however since 2015 none addressed their binding to proteins [22]. Thus, one of the objectives of the present review is to make an account of the new findings during the past 7 years, particularly due to the improvements achieved in theoretical techniques and their applications [23, 32, 43-45]. We made a systematic account of the possible interactions of VCs with proteins addressing the most important recent works, and mainly focusing on their behavior in aqueous media rather than on X-ray diffraction studies. Challenges and ideas about desirable features and potential drawbacks and toxicity of vanadium compounds, future directions to explore and adequately use the available methodologies are also presented.

The text is organized in nine sections: a general overview of the experimental and computational techniques useful in this field (sections 2-3), a discussion on the nature of binding processes of VCs to proteins (section 4), the recent advances on V-containing natural and artificial enzymes (section 5), the interaction of mononuclear VCs with blood, physiological and model proteins (sections 6 and 7), the binding of promising antitumor, antibacterial and antiviral polyoxidovanadates(V) agents (section 8), the biological and therapeutic implications due to the interaction of pharmacologically relevant VCs with proteins and enzymes (section 9) and, finally, the challenges and future directions (section 10). The presented data on the type of possible interactions of VCs in the biological systems may provide the basis to undertake the investigation, design and development of new potentially active VCs with a more solid knowledge to predict their critical binding to biological receptors.

2. Instrumental techniques

Several techniques have been applied to characterize vanadium–protein adducts, namely X-ray diffraction, EXAFS, UV-Vis, EPR, ESEEM, ENDOR, NMR and CD spectroscopy. Techniques such as polarography and voltammetry, ICP-MS, size exclusion chromatography, gel-electrophoresis, cryo-EM and others have also been employed. Each has advantages and limitations and, typically, should be used in combination with other techniques. NMR and EPR measurements (and others) require relatively high V concentrations (ca. 0.1-1.0 mM) to ensure adequate signal-to-noise ratios, largely exceeding those determined in healthy persons (0.2-15 nM) [19, 46, 47], or in humans treated with vanadium inorganic salts (1-10 μM) [47, 48] or with complexes such as BMOV or BEOV (BMOV is $[V^{IV}O(ma)_2]$ with ma = maltolato, while BEOV is $[V^{IV}O(ema)_2]$ with ema = ethylmaltolato) [47-49]. Mass spectrometric (MS) techniques, particularly ElectroSpray Ionization (ESI) and Matrix-Assisted Laser Desorption/Ionization (MALDI), are more adequate for physiological concentrations and may be applied to understand the role of metal-based drugs in samples of biological relevance, and to access the interactions established with proteins [50, 51].

2.1. UV-Vis

UV-Vis or electronic absorption spectroscopy involves the study of electronic transitions. The electronic absorption of a molecule depends on the chemical nature and molecular environment of its chromophores. Consequently, UV-Vis is a suitable technique to follow ligand binding and conformational transitions in proteins. For metal complexes, the energy of the transitions is dependent on the oxidation state, geometry, electronic structure as well as on the type of transition, i.e. *d-d* absorptions, metal-to-ligand charge transfers (MLCT), ligand-to-metal charge transfers (LMCT) and ligand-to-ligand charge transfers (LLCT).

V^{III} has a $[Ar]3d^2$ electronic configuration. For a regular octahedron with O_h symmetry (e.g. $[V^{III}(H_2O)_6]^{3+}$ and other hexa-coordinated species with monodentate or bidentate ligands), the ground state is $^3T_{1g}$, derived from t_{2g}^2 configuration; three transitions to the excited states $^3T_{2g}$ and $^3T_{1g}(P)$ from $t_{2g}^1\ e_g^1$ configuration and $^3A_{2g}$ (e_g^2) are expected, and observed at 580, 390 and 265 nm for the aqua ion. UV difference spectra in the system with human lactoferrin allowed to assign to V^{III} the same coordination environment as Fe^{III} [52].

Considering crystal field theory, in axially distorted octahedral or square pyramidal $V^{IV}O^{2+}$ complexes, like $[V^{IV}O(H_2O)_5]^{2+}$, the $3d^1$ electron occupies the d_{xy} orbital. The compression along the z axis causes a separation of the degenerated orbitals d_{xz}, d_{yz} from d_{xy} and of d_{z^2} from $d_{x^2-y^2}$. The

three electronic transitions $^2B_2 \rightarrow {}^2E$, $^2B_2 \rightarrow {}^2A_1$ and $^2B_2 \rightarrow {}^2B_1$ are expected in the range 900-620 nm, 690-530 nm, and 480-330 nm. These are observed at 760, 625 and ~400 nm for $[V^{IV}O(H_2O)_5]^{2+}$ [53]. The degeneracy of the d_{xz}/d_{yz} orbitals can be removed when the square pyramidal geometry of a $[V^{IV}OL_2]$ complex is distorted towards the trigonal bipyramid. This happens, for example, in complexes with α-hydroxycarboxylates such as citrate, lactate and tartrate. In these systems, four transitions may be detected in the range 400-420 nm, 530-550 nm, 580-610 nm and 800-860 nm, and the distortion degree can be related to the steric hindrance of the R group on the C–OH group [54-57].

Vanadium(V), with $[Ar]3d^0$ configuration, has no d electrons, and the electronic absorptions are associated with LMCT and LLCT transitions.

Proteins typically show maxima between 275 and 280 nm, mostly due to the absorbance of the amino acid residues containing aromatic side groups. Several authors used titrations followed by UV spectra measurements of proteins such as bovine serum albumin (BSA) or human serum albumin to determine binding constants. Albumins show bands at *ca.* 220 and 280 nm; the former band is associated with the n-π* transitions of C=O in peptide bonds, and the lower energy band stems from the aromatic rings of Trp, Tyr and Phe residues, whereas conformational changes affect both bands. Examples abound in the literature, but most of the times the stability of the complexes in buffered solutions is not evaluated prior to the binding studies, oxygen is not always excluded from the experimental setup, and linearization of the spectral data at selected wavelengths is used, instead of non-linear fitting, all factors that may introduce errors. As an example [58], the binding of vanadium(IV)–salen complexes to BSA and ovalbumin (OVA) were evaluated using absorption titration, and binding constants of *ca.* 10^4 were determined using the Scatchard equation [59]. For V(V) complexes formed by Schiff bases derived from 2-hydroxy-5-(phenyldiazenyl)benzaldehyde and *S*-benzyldithiocarbazate binding constants in the range $0.8\text{-}3\times10^4$ were found, as well as the values for the thermodynamic parameters ΔH, ΔS and ΔG, which suggest hydrogen bond (H-bond) or van der Waals (vdW) interactions between the compounds and BSA [60]. Typically, absorption titrations are only used qualitatively to evaluate conformational transitions, focusing on the absorption changes of the band at 280 nm and its spectral shifts [61-64].

2.2. Circular Dichroism

Circular dichroism (CD) is a spectrophotometric technique that may be applied to study biological and non-biological samples and to access structural characteristics of the interaction of metal ions with small or large biomolecules such as proteins.

In a CD spectropolarimeter, beams of left and right circular polarized light alternately pass through the quartz cell containing the sample. The extinction coefficients for the right (ε_D) and left (ε_L) circular polarized light are measured and the values of $\Delta\varepsilon = (\varepsilon_L - \varepsilon_D)$ are obtained. If the solution contains an optically active solute, non-zero values of $\Delta\varepsilon$ may be measured. The $\Delta\varepsilon$ values as a function of λ give the CD spectrum of the sample. At a particular wavelength, $\Delta\varepsilon \neq 0$ if the solution contains a chiral substance that absorbs light of that wavelength. CD spectra are normally measured in the visible or UV range (but may be recorded in other wavelength regions), the CD bands being obtained at the same λ values as those of the electronic absorption bands of the solution under examination [65].

For a coordination compound, a CD spectrum can only be measured if there is some chirality source and CD spectroscopy may be used to prove the interaction of metal centers with chiral molecules, these being either small ones such as amino acids or large complex molecules like proteins. The essential feature is that the chromophore, the metal complex, must be situated in a chiral environment, this implying that the V-species and the protein must be somehow closely connected. This is relevant for d-d electronic transitions in coordination compounds, as CD bands may be recorded in ranges of λ values where the protein does not absorb, which highly simplifies the interpretation of the measured data [65].

Circular dichroism measured in the 190-250 nm range, where proteins absorb radiation, may be used to provide information on the secondary structure of a protein, namely its content in β-strands, α-helix and random coils. If, by adding a compound, the CD spectrum in such a λ range is modified, this means that the interaction of the protein and metal complex is taking place. When metal ions or complexes are involved, CD may be measured at wavelengths corresponding to charge-transfer or d-d bands; if $\Delta\varepsilon \neq 0$ are measured, this provides confirmation of binding of a metal species to chiral donor groups of the protein.

CD spectroscopy has been used to study interactions of several proteins with vanadium compounds [66-68]. For example, relatively strong CD bands were observed in solutions containing $V^{IV}O^{2+}$ ions and apo-human serum transferrin (apo-HTF) [66, 67]. These correspond to induced chirality in the d-d or charge transfer electronic transitions resulting from the binding of V^{IV} to chiral residues of the protein. Besides confirming the coordination of the $V^{IV}O^{2+}$ ions to donor atoms of the protein, CD data allowed the identification and calculation of conditional formation constants for the $(V^{IV}O)_2$(apo-HTF) and $(V^{IV}O)$(apo-HTF) adducts [66, 67]. In systems involving covalent binding of a single amino acid donor of a protein to V^{IV}, such as in the $[V^{IV}O(pic)_2]$–Lyz adduct, where Hpic is picolinic acid and Lyz is lysozyme, the measured CD spectrum is very weak [69].

Addition of a non-chiral ligand to a solution containing a $V^{IV}O^{2+}$ salt and a protein may lead to changes in the CD spectrum. If a pattern distinct from the CD spectrum of the $V^{IV}O^{2+}$- protein is recorded, this means that the ligand is also participating in the binding of the metal to the protein, possibly forming mixed-ligand complexes. For example, CD spectroscopy was applied to confirm binding of $V^{IV}O^{2+}$ ions to serum proteins, and the distinct CD spectra measured when either $[V^{IV}O(acac)_2]$ or $[V^{IV}O(phen)_2]^{2+}$ were added (Hacac = acetylacetone, phen = 1,10-phenanthroline), allowed to distinguish situations where binding of $V^{IV}O(acac)^{+}$ to apo-HTF [68], or of $V^{IV}O(phen)^{2+}$ to albumin [39] takes place. This type of measurements was also carried out to probe the formation of mixed-ligand complexes of $V^{IV}O^{2+}$ with HSA and apo-HTF [66, 67] with several ligands (examples are acac, dhp, maltol, Hdhp being 1,2-dimethyl-3-hydroxy-4(1*H*)-pyridinone).

2.3. Fluorescence

Fluorescence corresponds to the light emitted spontaneously during irradiation with electromagnetic radiation of a substance, due to transitions from excited singlet states to vibrational levels of the electronic ground state. Fluorescence depends on several parameters that can be monitored in steady-state or time-resolved mode, which give information about the physico-chemical nature of the fluorophore. Fluorescence emission properties of proteins are provided by tyrosine (Tyr), tryptophan (Trp) and phenylalanine (Phe), but Trp is the most relevant [70]. Since these residues may be located on different protein domains, they might display different fluorescence decay profiles and different accessibility, factors that may lead to useful information in protein binding studies.

When compared to absorption, the higher sensitivity of spectrofluorimetry allows the use of lower concentrations (10^{-6}-10^{-7} M), an advantage regarding aggregation and precipitation phenomena. However, this may have implications when dealing with labile metal ions such as vanadium, since at low concentrations complexes may hydrolyze, and the quenching may be due to several species and not to a single one, with the consequence that the binding constants determined may be meaningless. To properly address vanadium-protein systems, their speciation should be evaluated; this has been recently addressed [31], as well as other tricky aspects that most researchers typically do not take into account [70, 71].

Fluorescence quenching titrations have been extensively used to investigate ligand-protein binding. Albumins are among the most studied proteins, particularly BSA and HSA. The fluorescence quenching can be modelled using the Stern-Volmer equation (eq. 1):

$$\frac{I_0}{I} = 1 + k_q \tau_0 [Q] = 1 + K_{SV}[Q] \quad \text{(eq. 1)}$$

In eq. 1, I and I_0 represent, respectively, the fluorescence intensities in the presence and absence of the quencher, $[Q]$ is the molar concentration of the free quencher, K_{SV} is the Stern-Volmer quenching constant, τ_0 is the lifetime of the fluorophore in the absence of the quencher and k_q is the bimolecular quenching constant. To obtain the conditional binding constant, K, and number of binding sites, n, usually eq. 2 is used:

$$\log\left[\frac{I_0 - I}{I}\right] = \log K + n \log[Q] \quad \text{(eq. 2)}$$

This equation is valid only when a non-fluorescent complex forms; it has several limitations, but this discussion is outside the scope of this review [70, 71]. Weak binding results in higher concentrations of the complex in the plasma, and short lifetime or poor distribution, while strong binding yields lower concentrations in plasma, possibly improving distribution and pharmacological effects of the compounds.

Several studies on the binding of potentially therapeutic VCs to BSA have been published in the last 10 years using these approaches. Both V(IV) and V(V) complexes were examined. Here we are providing only a part of the references [39, 58, 60-64, 68, 72-88]. 3D fluorescence, which is the collection of emission spectra at different excitation wavelengths, has also been used to gain further insight into these systems [60, 64]. Human serum transferrin has several Trp residues, thus interpretation of quenching measurements is not straightforward. Binding of $[V^{IV}O(acac)_2]$ to apo-HTF led to concentration dependent fluorescence quenching, which was quantified with $K = 1.0\times10^4$ M^{-1}, and its doubtful meaning was discussed considering the complex solution speciation of the $[V^{IV}O(acac)_2]$–HTF system [68].

2.4. EPR

Electron Paramagnetic Resonance (EPR) spectroscopy can be useful in the characterization of any species having one or more unpaired electrons and, among them, of transition metal complexes. The theory is described in some excellent books or reviews [90-94]. For a paramagnetic mononuclear species with a single unpaired electron, the spin Hamiltonian parameters to be considered are the g factor, which defines the position of the resonances, and A, the hyperfine coupling (HFC) constant between the metal nucleus and the unpaired electron. For an *isotropic* spectrum these are indicated

by g_{iso} and A_{iso}, while for a *rigid limit* or *anisotropic* spectrum these are g_x, g_y, g_z and A_x, A_y, A_z [92]. The $\boldsymbol{g}$ and $\boldsymbol{A}$ tensors depend on the chemical environment around the metal, and the observed changes can provide important information on the structure of the complex being characterized.

For V^{IV}, [Ar]$3d^1$ configuration, the values of the HFC constants arise from the interaction between the spin-angular momentum of the ^{51}V nucleus (I = 7/2) with the spin-angular momentum of the electron (S = 1/2). For $V^{IV}O$ complexes with symmetry approaching C_{4v} and ground state based mostly on the d_{xy} orbital, for example the aqua ion, a 'tetragonal' spectrum with two g and A values is observed [95]. The order $g_z < g_x \sim g_y < g_e$ and $A_z > A_x \sim A_y > 0$ is expected. In these cases, the values of A_z and g_z are more sensitive to the changes in the coordination sphere than A_x and A_z; if the electron donor capability of the ligand is increased, a decrease of the experimental A_z and an increase of g_z is observed. Typically, the A_z values span from 182×10^{-4} cm^{-1} of $[V^{IV}O(H_2O)_5]^{2+}$ [95] to 134×10^{-4} cm^{-1} of $[V^{IV}O(ethane\text{-}1,2\text{-}dithiolato)_2]^{2-}$ [96]. The values of $|A_x–A_y|$ are related to the trigonal bipyramidal distortion of an ideal square-pyramidal geometry [54, 56]. The empirical rule, known as the “additivity relationship”, assigns a contribution to each donor in the equatorial plane and allows to estimate A_{iso} or A_z within approximately $\pm3\times10^{-4}$ cm^{-1} from those experimentally measured [95, 97]. EPR spectra of hexa-coordinated non-oxido V^{IV} species show A values in the range $(90\text{-}155)\times10^{-4}$ cm^{-1}, depending on the metal geometry and composition of the singly occupied molecular orbital (SOMO) [98].

In frozen solutions, e.g. at 77 K, for small complexes a *rigid limit* spectrum is expected, because the molecules are blocked in their positions, while at room temperature, when the rotational motion proceeds faster than the EPR timescale, an *isotropic* spectrum is obtained [99]. In contrast, for large $[V^{IV}OL_x]$–protein adducts, the spectra approach the *rigid limit* or *slow tumbling* type as the rotational motion is slowed down [100, 101].

The spin Hamiltonian parameters, namely the ^{51}V HFC $\boldsymbol{A}$ tensor, can be successfully estimated using Density Functional Theory (DFT) methods [98, 102-105]. This approach allowed to assign the coordination modes to unknown complexes or, also, to V–protein adducts [100, 106, 107], and EPR spectroscopy has been often used to determine the binding sites of $V^{IV}O^{2+}$ when bound to proteins and enzymes (see sections 6 and 7).

For systems with more than one unpaired electron and $S > ½$, for example V^{III} (S = 1), the zero-field splitting (ZFS), expressed by the term $\hat{\mathbf{S}}\cdot\mathbf{D}\cdot\hat{\mathbf{S}}$ in the Hamiltonian, must be considered. Very few examples of EPR spectra were reported because in normal conditions they give “EPR-silent” systems; this results from their large ZFS in the $^3T_{1g}$ ground state combined with integer spin number (non-Kramers ions) [108, 109]. For these systems, high-frequency and high-field EPR

(HFEPR) allows a qualitative and quantitative analysis of the formed species and to relate the values of ZFS to their electronic structure [110].

2.5. ENDOR and ESEEM

In most cases, the broad spectral lines observed in an EPR spectrum (usually larger than 10 Gauss) preclude to resolve the coupling between the unpaired electron(s) and the nuclei directly bound to the metal or close to it. This coupling is named superhyperfine coupling (SHFC) and is indicated with A^{L}, where L specifies the coupled nucleus (for example ^{1}H, ^{14}N or ^{31}P). The nature, position and orientation of the bound ligand determine the SHFC constant measured for ^{14}N [111, 112]; for proteins, the coupling with imidazole-N has been examined to assess the binding of His residues to V. Information on the SHFC constant can be obtained by Electron-Nuclear Double Resonance (ENDOR) [97, 113] and Electron Spin Echo Envelope Modulation (ESEEM) [114, 115] techniques. ENDOR spectroscopy allows to resolve SHFC normally lost in EPR experiments, fixing the magnetic field to study a specific EPR signal and irradiating with a microwave radiation of sufficient power to saturate the transition. Subsequently, a radiofrequency scan is carried out over the range of the probable resonances. Depending on the spatial arrangement of the donors around the metal ion valuable information can be obtained about the structure of the metal complex in solution. For $V^{IV}O^{2+}$-substituted proteins and enzymes, ENDOR was used to explore the metal environment, for example for $V^{IV}O^{2+}$–D-xylose isomerase and imidazoleglycerol-phosphatase dehydratase, the isotropic SHFC of *ca*. 7 MHz is consistent with a coordination of histidine imidazole nitrogen(s) [116, 117].

ESEEM is a pulsed technique, in which the irradiation by a continuous microwave is replaced by a series of microwave pulses that are followed by a waiting period. If the magnetic field is set to a particular resonance and two microwave pulses are applied, the emission of a microwave signal is revealed. ESEEM methods, similarly to ENDOR, were used to measure the SHFC with ^{14}N nucleus in $V^{IV}O$ systems, especially vanadium–enzymes [118]. The ^{14}N SHFC constant corresponding to the coordination of an equatorial His-N is in the range 6.5-7.0 MHz; significantly lower values are expected for a N donor bound in *trans* position to V^{IV}=O [119]. For HTF, values of 6.6 MHz measured in the ESEEM spectra suggested the equatorial coordination of a His-N, and this obviously may be His249 or His585 of the Fe binding sites [120]. Similar values were detected for the reduced form of vanadium bromoperoxidase [121], and these were assigned to His486 and His418 – the residues bound to V^{V} in the native protein in a trigonal bipyramidal geometry. The SHFC constant of 7.2 MHz allowed proving the coordination of Lys-NH_2 to V^{IV} in vanabin2, one of the five proteins that bind V in the cytoplasm of vanadocytes of ascidians [122]. In contrast,

experimental modulation frequency below 2.5 MHz suggested the axial binding of His14 residue in $V^{IV}O^{2+}$–substituted IGPD [23] and of Lys175 in $V^{IV}O^{2+}$–CF_1-ATPase [123].

2.6. ^{51}V NMR

The information that is usually extracted from a Nuclear Magnetic Resonance (NMR) spectrum is the chemical shift (δ) and the coupling constant (*J*) and – less commonly – the relaxation rate [124, 125]. Comparing with EPR, the chemical shift δ corresponds to the *g* factor and the coupling constant *J* to the HFC constant *A* [126]. NMR can be applied to diamagnetic and paramagnetic systems, while EPR only to paramagnetic molecules with one or more unpaired electrons.

Due to its small quadrupole moment (≈ -0.05×10^{-28} m^2), large gyromagnetic ratio, nuclear spin of 7/2 and natural abundance (99.76%) [127], the ^{51}V nucleus is a good NMR probe; in addition, ^{51}V chemical shift values may significantly change with modifications in the coordination environment of V^V. Therefore, ^{51}V NMR is an excellent tool for detailed studies of V^V, and is easily accessible in conventional NMR spectrometers, as well as more sophisticated studies, including 2D and solid-state NMR. In systems involving V^V bound to proteins the resonance lines are normally extremely broad, and thus often not observed. In some cases, as with apo-HTF, the ^{51}V NMR resonances are sharp and even allow distinction of the two metal binding sites [128]. This rather unusual situation results from the motional properties of the protein-bound vanadate(V), which fall outside the extreme narrowing limit [129, 130]. Among the first examples exploring the favourable NMR properties of the ^{51}V nucleus, were the studies of the interaction between V^V and proteins such as ribonuclease [131] and peroxidase from *Ascophyllum nodosum* [132]. Both unspecific vanadate(V) protein binding as well as coordination to the metal binding sites were observed [133].

A few studies have been reported in the last years, particularly regarding binding of oligovanadates(V) to proteins and mycobacteria. ^{51}V NMR spectroscopy was applied to study the interactions of two decavanadates (V_{10}), one of them functioning as ligand of two Co(II) ($V_{10}Co$) and two Cu(II) centers ($V_{10}Cu$), with model and serum proteins, under conditions mimicking protein crystallization [134]. Line broadening was used to evaluate binding affinity of VCs to the proteins and different affinities were found for the two species.

Crans *et al.* reported a very elegant study that compared the effect of V_{10} and monovanadate(V) (V_1) on two mycobacterial strains using ^{51}V NMR and speciation. The spectra of the growth media at several V concentrations and time points during the growth experiment showed that redox processes occur and that the mycobacteria probably excrete a compound that is able to interact with V_{10}, causing the redox reactions and the hydrolysis of V_{10} [135]. Žižić *et al.* used ^{51}V NMR

spectroscopy for the detection and identification of cell-associated vanadate(V) species after exposure to *Phycomyces blakesleeanus* mycelium [136, 137].

Computational docking studies and the NMR technique designated by ^{1}H saturation transfer difference (STD) were used to study the interactions of $[V^{V}O_2(ma)_2]^-$ and $[V^{V}O_2(dhp)_2]^-$ with HSA, the data indicating a preference of the species $[V^{V}O_2(ma)_2]^-$ and $[V^{V}O_2(dhp)(H_2O)(OH)]^-$ for HSA binding [138].

Regarding solid state ^{51}V NMR, its measurement relies greatly on magical angle spinning (MAS), since it allows the narrowing of the resonance lines by averaging dipolar, anisotropic chemical shielding and first order quadrupolar effects [133]. ^{51}V MAS NMR can yield relevant information on chemical characteristics of the V center and ligand environments. This approach is particularly powerful when coupled with DFT and quantum mechanical/molecular mechanical (QM/MM) models, and was used for e.g. the study of the active site geometry and protonation equilibria of the vanadium chloroperoxidase from *Curvularia inaequalis* (see section 5) [139, 140].

A study was recently reported on helicase DnaB and on ATP-binding cassette (ABC) transporter, BmrA [141], in which the authors investigated the binding of ATP using several magnetic resonance approaches that included solid state ^{51}V NMR. It was concluded that vanadate(V) is a reasonable ATP-transition state mimic for BmrA, while ADP–vanadate(V) is not a suitable ATP-transition state mimic in helicase DnaB, most likely binding to it in an unspecific manner [141].

2.7. Electrophoresis and Chromatography

The production of recombinant proteins requires electrophoretic (namely Na^+ dodecylsulfate-polyacrylamide gel electrophoresis, SDS-PAGE, and native-PAGE) and chromatographic (namely size-exclusion chromatography, SEC, as well as immobilized metal-affinity chromatography, IMAC) procedures to guarantee an isolated and purified sample to be used in the subsequent biochemical, biophysical or structural characterization steps [142-145]. Vanadium-related proteins are not an exception and throughout the present and past reviews, several examples can be found regarding different protein classes, including nitrogenases and haloperoxidases, that were isolated and purified using these procedures.

Notwithstanding, both electrophoresis and chromatography have also been often used to obtain other relevant insights such as the oligomerization state of the protein, and some examples may be mentioned. For example, Sippel *et al*. by molybdenum depletion produced a vanadium nitrogenase from *A. vinelandii*, which was purified by a two-step anion exchange chromatography followed by running a SEC [10]. The last step allowed to determine the protein molecular mass (235.3 kDa), suggesting a heterohexamer ($VnfD_2K_2G_2$) as further confirmed by SDS-PAGE. In a later study,

SEC and SDS-PAGE data disclosed a V-nitrogenase variant with a citrate-substituted cofactor with a different internal organization and a molecular mass of *ca*. 180 kDa [146]. By a combined use of ion exchange chromatography, SEC, SDS-PAGE and native-PAGE, Gunasinghe *et al* characterized V-binding proteins from the blood plasma and intestine of the sea squirt *Halocynthia roretzi*, showing the presence as a dimer and a monomer, respectively, [147]. IMAC and SDS-PAGE were also used to assess the metal selectivity of the V-binding protein VBP-129 from *Ascidia sydneiensis samea* [148].

Some other electrophoresis-based techniques have also been important in the characterization of V-proteins including Western blot analysis [147, 149, 150]. Denaturing urea polyacrylamide gel electrophoresis (urea-PAGE), often used to evaluate changes in conformation of proteins and respective variants upon ligand binding, should be also mentioned [151, 152]. In the context of vanadium-related proteins, urea-PAGE has been applied to detect human serum transferrin interactions with V-based complexes [153, 154]. In recent years, two studies by Costa Pessoa *et al.* used urea-PAGE to characterize the binding of V^{V}, V^{IV} and V^{III} as well as four $[V^{IV}OL_n]$ complexes (L = ma, dhp, pic, and dipic, where H_2dipic is 2,6-dipicolinic acid) to apo-HTF revealing that: i) V^{III} binds very strongly forming $(V^{III})_2$–HTF which corresponds to a closed conformation, similar to $(Fe^{III})_2$–HTF, ii) for all ligands, $(V^{IV}O)_2$–HTF species do not involve the protein closing, and iii) $(V^{V})_2$–HTF remains in an open conformation. Interestingly, both studies were carried out with a desalting procedure with size exclusion columns to remove the ligand and free V excess and determine the number of V centers bound, highlighting the importance of chromatographic methods in these topics [155, 156].

Levina and Lay investigated the effect of V^{IV} and V^{V} binding to transferrin in cellular V uptake, and *in vitro* antiproliferative activity [30]. Urea-PAGE was used to mimic the endosomal Fe release analyzing samples of cell culture medium with partially or fully Fe^{III} saturated transferrin and V^{IV}/V^{V} species, suggesting that the presence of vanadium influences the metal release and the protein conformational changes.

2.8. X-ray absorption spectroscopy, EXAFS and XANES

X-ray absorption spectroscopy (XAS) is a remarkable tool to determine the structural features of crystalline or amorphous samples and is complementary to single-crystal X-ray diffraction (XRD). In XAS, an element is excited selectively through a synchrotron radiation, providing the electronic structure characterization and information on the chemical environment of a specific compound [157, 158]. In V-proteins or V-enzymes, the target element may be vanadium or, alternatively, a donor in the binding site. Unlike XRD and NMR, XAS methods provide information on the region

of the biomolecule around ~5 Å from the absorbing atom and, in this range, is as precise and accurate as a crystallographic determination or magnetic resonance. A XAS spectrum is normally divided in three regions: the first is named 'pre-edge', the second region around the edge is X-ray Absorption Near Edge Structure (XANES), and the higher energy region is abbreviated as EXAFS (Extended X-ray Absorption Fine Structure Spectroscopy) [159].

XANES signal is due to the excitation of a core electron that is promoted to a partially filled or empty orbital of the absorbing atom and are sensitive to the metal oxidation state and coordination geometry, making this tool adequate for V, which in the biological systems shows three oxidation states and a large variety of coordination environments [160]. EXAFS signal results from the interference of the wave emitted by the absorbing atom after the ejection of the core electrons with the wave scattered by the electron shells of surrounding atoms. From the analysis, the coordination number and distances, e.g. bond lengths between V and surrounding atoms, can be accurately determined. For vanadium, the K-edge is usually examined, which is associated to the 1s $\rightarrow$ 4p transition with the eventual detection of 1s $\rightarrow$ 3d promotion in the 'pre-edge' region [161].

EXAFS and XANES have been employed mainly to determine the structure of vanadium haloperoxidases [2]. The weak 'pre-edge' absorption 1s $\rightarrow$ 3d of *Ascophyllum nodosum* bromoperoxidase [162] is consistent with the trigonal bipyramidal structure with His-N coordination as determined by XRD [163]; in contrast, for tetrahedral vanadate(V) species such an absorption would be very strong. The XAS spectrum of the reduced form shows that the coordination environment of the metal drastically changes, accounting for the inactivity after the reduction [164]. K-edge XAS spectrum of the vanadium chloroperoxidase (VClPO) (native and peroxido forms) from *C. inaequalis* indicates that V is bound in the native enzyme to three equatorial O-donors at 1.54, 1.69, 1.69 Å, another O-donor at 1.93 Å, and to His496 at 2.02 Å; the study allowed to also confirm the interactions with positively charged residues, namely from Arg360, Arg489 and Lys353 [165]. Lay and co-workers published a library of XANES data for $V^{III/IV/V}$ complexes with biologically relevant ligands that allowed to confirm the structure of vanadium bromoperoxidase (VBrPO) from *A. nodosum* [166].

Recently, measurements by XANES and EXAFS allowed to establish that the binding of decavanadate(V) to G-actin causes a conformational reorientation of the protein, which favors the oxidation of Cys residues (with the formation of $V^{IV}O^{2+}$), with subsequent protein aggregation to F-actin [167].

The non-oxido nature of V-nitrogenase and amavadine and oxidation state of vanadium has been clearly demonstrated by XANES and EXAFS [164, 168], in the latter case before the XRD determination.

2.9. SAXS

SAXS, Small-angle X-ray scattering, may be used in the characterization of both inorganic and biological molecules (namely proteins) in solution, is widely used as a complement to other high-resolution structural methodologies, providing relevant insights on the characterization of native protein, protein-protein and protein-ligand systems [169-171]. Traditionally, SAXS data are useful to detect protein shape, conformational changes and oligomerization states, but a recent investigation also proposes its use as a screening method to determine binding affinities [172].

Despite its constant development and increasing popularity in the last years, there are only a few examples of studies using SAXS to characterize V-protein interactions. Complemented by other experimental methods, the interactions established between $[V^{IV}O(acac)_2]$ and apo-HTF were evaluated by SAXS, and the data support that, despite the globular structure being conserved, the protein conformation is clearly changed upon ligand binding, suggesting the presence of VCs–apo-HTF interactions [68]. A combined voltammetric, spectrometric and SAXS study, focusing on the interactions of inorganic $V^{IV}SO_4$ and $NaV^{V}O_3$ salts with apo- and holo-HTF was also reported. Upon addition of the vanadium salts, a partial closing of apo-transferrin was demonstrated. In parallel, noticeable differences in the SAXS profile and parameters were found between the native apo- and holo-HTF samples. However, due to the potential aggregation, the influence of either $V^{IV}OSO_4$ or $NaV^{V}O_3$ in the conformation of holo-HTF was not conclusive, but the maintenance of the conformation was suggested [173].

2.10. Mass spectrometry

Mass spectrometric techniques are well-established with a mass range spanning from single atoms to complex molecules of megadaltons. Ionization techniques established in the early 90's used protein and peptide fragmentation, while the discovery of milder techniques for the ionization, like ESI and MALDI allowed extending studies to large proteins without derivatization, leading to the development of proteomics and the elucidation of protein-ligand binding [50, 174].

These techniques enable the study of intact (metal complex)–protein adducts in the gas phase. In an ESI experiment, singly to multiply charged ions are generated upon deprotonation or formation of adducts with either protons or alkali metals, while MALDI yields mostly singly charged ions of metallodrug–protein adducts. Experimentally, in ESI a mixture of sample and liquid carrier is sprayed by raising the potential on the spray capillary and applying back pressure, generating charged droplets. In MALDI an inert molecule of low volatility and viscosity is mixed with the

sample; the matrix/analyte mixture is then irradiated by a laser, that produces desorption and ionization of the sample.

Despite its relevance, not many MALDI-MS studies were done addressing the binding of VCs to proteins. Costa Pessoa *et al*. reported the interaction of vanadium salts, $V^{IV}OSO_4$ and $NH_4V^{V}O_3$ to holo-HTF and apo-HTF [173] and also of $[V^{IV}O(acac)_2]$ to apo-HTF and HSA by MALDI-TOF-MS (TOF, time of flight), corroborating the binding of vanadium to HTF. No binding of $[V^{IV}O(acac)_2]$ to HSA was observed [68], while the interaction of $V^{IV}O$–phen complexes with BSA was also established using this technique [39].

Being a soft technique, ESI-MS may be used to study both *non-covalent* interactions and *covalent* bond formation of labile metal complexes, for example of vanadium and copper with biomolecules [24, 51, 175]. In systems containing vanadium, ESI-MS allows: i) to examine low concentrations such as 1-100 μM, i.e. not much higher than those found for vanadium under *in vivo* conditions [176]; ii) to demonstrate if a VC complex is bound to a protein or in some other form [24]; iii) to identify *covalent* and *non-covalent* binding [25]; iv) to access the type and number of metal–L moieties ($n[V^{III,IV,V}L]$, $m[V^{III,IV,V}L_2]$, etc.) involved in the interaction with proteins [176]; v) to reveal the simultaneous existence in aqueous solution of adducts involving different oxidation states (V^{III}, $V^{IV}O/V^{IV}$ and $V^{V}O/V^{V}O_2$) [177]. On the other hand, the major limitations are: i) ESI-MS does not give any information on the 3D structure of the adducts detected; ii) in most cases, the amino acid donors involved cannot be identified; iii) the concentration of the species in solution cannot be related to the intensity of the peaks observed in the ESI spectra.

Garribba *et al*. applied ESI-MS to study the speciation of different $V^{III/IV/V}$–based drugs in biological samples and characterized the adducts formed with model proteins, namely with ubiquitin (Ub), myoglobin (Mb) and lysozyme at the molecular level [24, 25, 177-180]. The interaction of vanadium containing molecule amavadin ($[V^{IV}(hidpa)_2]^{2-}$) with Lyz was also reported by the authors [24].

2.11. Electrochemistry

Electron transfer is ubiquitous in chemical and biological systems and electrochemistry studies the interconversion of electrical and chemical energy in molecular systems. Most of the redox reactions involve metals ions, and in the human body metals participate in most of the redox chemistry. Electrochemistry is suitable for investigating the interactions between proteins and metal ions because of its high sensitivity, selectivity, rapid analysis, ease of operations, and possibility of studying simultaneously several distinct solutes and determining kinetic and thermodynamic parameters. Two of the most commonly used electrochemical techniques are differential pulse

voltammetry (DPV) and cyclic voltammetry (CV). Both involve applying a potential (E) to an electrode and record the resulting current (i) passing through the electrochemical cell. In cyclic voltammetry, the current at each potential step is measured and a plot of current *vs.* potential is recorded. The potential applied at the working electrode is varied in both forward and reverse directions at selected scan rates. The relevant parameters in CV are the currents (i_{pa}, i_{pc}) and potentials (E_{pa}, E_{pc}) of the anodic and cathodic peaks, respectively. If electron transfer proceeds fast compared with processes such as diffusion, the electrochemical process is considered as reversible.

DPV is a controlled-potential method that uses pulse modulation programming to extract the faradaic current response from an electrochemical system. The current is measured just before applying the pulse and also at the end of the pulse. The difference between the current recorded for each pulse at these stages is plotted against the potential.

Vanadium has four easily interconverted oxidation states +V, +IV, +III, and +II, resulting in a rich redox chemistry. A review by Floris *et al.* was published a few years ago on the electrochemistry of vanadium and its complexes [181]. Research on vanadium electrochemistry has been focusing on vanadium redox flow batteries, but a few studies can be found addressing the electrochemistry of adducts formed between vanadium and proteins.

A study by Costa Pessoa *et al.* reported the electrochemical behavior of vanadate(V) and its interaction with holo-HTF and apo-HTF, as analysed by DPP and CV at a mercury electrode [173]. In the presence of holo-HTF or of apo-HTF, the voltammetric behaviour of V remained the same, revealing the sequential reductions $V^{V} \rightarrow V^{IV}$ and $V^{IV} \rightarrow V^{II}$, as well as the same peak potentials, but the peak currents decreased with increasing protein concentration; therefore, proof of the existence of electrochemically inert vanadium–protein adducts was provided. Altogether, the data supported the formation of $(V^{V})_2$–apo-HTF complexes and, in the V^{V}-holo-HTF system, a mixture of 1:1 and 2:1 adducts; the formation constants were determined and are in agreement with those obtained with other techniques for the V^{V}–apo-HTF system [128, 182].

Recently Yang *et al.* reported voltammetric studies of nitrogenase cofactors from *Azotobacter vinelandii* [183]. Cyclic voltammetry revealed that the isolated V-cluster yielded a quasi-reversible redox process, with an $E_{1/2}$ of -0.414 V versus standard hydrogen electrode (SHE) that increased with higher scan rates, and an irreversible reduction at E_{pc} = -1.06 V versus SHE. When compared to the M-cluster, the V-cluster undergoes a shift of both peak potentials to more negative values of *ca.* 100 mV.

2.12. Biochemical Methods

Biochemical methods, namely enzymatic and inhibition assays, can be used to both confirm vanadium binding to proteins and give further insights on available structural data. The inhibition of phosphatases by vanadate due to its well-established phosphate analogy is one of the classical examples and several references are available on this topic [3, 22, 34, 149, 150, 184]. Nevertheless, other vanadium-related protein classes have been characterized with a biochemical perspective. As an example, the recent report on a V-nitrogenase variant from *Azotobacter vinelandii* with a citrate-substituted cofactor includes a section dedicated to the characterization of its substrate-reducing activity (H^+, N_2, C_2H_2, CO and CN^-), revealing a significant increase of the N_2-reducing-activity if compared with the wild-type [146].

On the other hand, the description of biochemical experiments to determine the activity of different haloperoxidases – namely for the halogenation of monochlorodimedone – was recently reviewed [185, 186]. An alternative fluorescence-based assay (halogenation of 4-methyl-7-diethylamino-coumarin) has been also suggested [187]. Biochemical assays also play an important role to characterize the production of ROS resulting from the haloperoxidase activity as described by Punitha and coworkers [188].

The bromoperoxidase and iodoperoxidase activities of two recombinant vanadium-dependent iodoperoxidases, Zg-VIPO1 and Zg-VIPO2 from *Zobellia galactanivorans*, were assessed by the thymol blue colorimetric assay, suggesting iodide specificity. Subsequently, the thymol blue colorimetric assay was also used with twelve Zg-VIPO1 variants, revealing loss of haloperoxidase activity, gain of bromoperoxidase activity and different kinetic parameters depending on the mutation [189]. The thymol blue colorimetric assay allowed to determine the haloperoxidase activity during the early embryogenesis of the seaweed *Fucus vesiculosus*, showing that, following fertilization, both iodoperoxidase and bromoperoxidase activities gradually increase till the third day when they appear to be stabilized [190].

We highlight that whenever using a biochemical method to quantify interactions of vanadium complexes with a biological target, namely a protein, particularly when using low concentrations of the metal species, care should be taken to sort out if the output of the property measured results from the VC added and/or from species derived from its hydrolysis [39].

2.13. Calorimetry methods

Calorimetric methods – namely Differential Scanning Calorimetry (DSC) and Isothermal Titration Calorimetry (ITC) – have been often applied to describe interactions in protein-protein and protein-ligand systems, determining different thermodynamic parameters, as well as measuring the

respective binding affinities through equilibrium association (K_{ass}) and dissociation constants (K_{dis}) [191-193].

In the last decades ITC and DSC have been used to characterize metal–protein binding events [194]. Vanadium is not an exception and different examples are available in the literature. ITC results were important to demonstrate the potential use of decavanadate as inhibitor (K_{dis}: 1.4 μM) of bovine pancreatic ribonuclease A [195], and both techniques were employed to study the interactions between $V^{IV}OSO_4$, $NaV^{V}O_3$ and BMOV with HTF [196]. ITC was also applied to compare the binding of $NH_4V^{V}O_3$ to apo-HTF and to nicatransferrin (transferrin with a single lobe) from the ascidian *Ciona intestinalis*. The binding affinity of vanadate to both proteins was similar but, unlike apo-HTF, nicatransferrin requires the presence of HCO_3^- as synergistic anion [197].

ITC was applied to determine the dissociation constant for the binding of a small-molecule inhibitor of the human low-molecular-mass protein tyrosine phosphatase (LMPTP) as 8.0 μM, thus disclosing a weak interaction. Interestingly, upon addition of vanadate(V) to the protein, the ligand affinity significantly increased to 1.4 μM, which was interpreted as compatible with an uncompetitive inhibition: a *covalent* adduct is formed between vanadate(V) and the cysteine in the LMPTP active site, allowing the binding of the inhibitor and, ultimately, to prevent the phosphate release [198].

In the recent years, other calorimetric techniques have progressively gained popularity namely MicroScale Thermophoresis (MST) [199], but – to our knowledge – no studies of MST applied to vanadium-related proteins have been reported.

2.14. Cryo-EM

From a historical point of view, X-ray crystallography has been the undisputable method for protein structure determination. In the last decades, cryogenic electron microscopy (cryo-EM) techniques are becoming more and more important despite offering low-resolution structures. Among the advantages, cryo-EM can be applied to samples in solution, eliminating the need of well-ordered crystals [200-202]. Several cryo-EM techniques – namely single particle analysis and cryo-electron tomography – are increasingly being used to characterize different systems including ribosomes, membrane proteins and transcription complexes [203-205], with significant improvement in resolution.

A few examples of structures of vanadium-related proteins were determined applying cryo-EM and were deposited in the PDB (Protein Data Bank) and are mainly related with use of ADP–vanadate complexes to obtain the intermediate state formed during the ATP hydrolysis of several ATP-binding cassette (ABC) transporters reconstituted into nanodiscs. A 6.0 Å rabbit sarcoplasmic

reticulum Ca^{2+}-ATPase (Ca^{2+}-free), using decavanadate and thapsigargin as inhibitors, was deposited (PDB: 1KJU); combined with a Ca^{2+}-bound crystal structure, conformational rearrangements of the protein caused by the calcium binding were analyzed, allowing the proposal of a structural mechanism for the catalytic cycle [206].

Recently, a 4.8 Å resolution structure of ABC transporter MsbA, responsible for flipping the glycolipid lipopolysaccharide from *Escherichia coli* became available (PDB: 5TTP) [207]. Single particle cryo-EM was employed to compare the nucleotide-free MsbA (PDB: 5TV4) with the transition state obtained by the use of vanadate(V) which presents a closed conformation, interpreted as the one adopted by MsbA after the glycolipid dissociation [207]. Similarly, in 2019, single particle cryo-EM was used to describe both LptB2FG and the complex LptB2FG-LptC in their nucleotide-free and ADP-vanadate intermediate conformation forms (PDB: 6MHZ and 6MI8), at 4.1 Å and 4.3 Å resolution, respectively [208].

The bacterial ABC transporter TmrAB from *Thermus thermophilus*, a model for the human transporter associated with antigen processing, involved in the immune system, was also characterized by cryo-EM (2.8-4.2 Å resolution) covering different stages of the transport cycle. Two vanadate-trapped hydrolysis transition states (PDB: 6RAK and 6RAJ, with 3.3 Å and 3.5 Å resolution) were modeled [209].

TRPM4 is a Ca^{2+}-activated, non-selective cation channel, and the structure of a human TRPM4 channel bound to Ca^{2+} and V_{10} was reported using cryo-EM. A unique architecture was disclosed among the TRPM family, providing a basis for modulation and selectivity of decavanadate over TRPM4 [210].

In 2020, two new single particle cryo-EM vanadate-induced intermediate state ABC transporters became available: NaAtm1 from *Novosphingobium aromaticivorans* and MlaFEDB from *Acinetobacter baumannii* [211, 212]. NaAtm1 (ABC transporter of mitochondria), was stabilized by disulfide crosslinks revealing different conformations related with the position of the transmembrane helix 6. The 3.0 Å resolution structure with $MgADPVO_4$ (PDB: 6VQT), mimicking the post-ATP hydrolysis state, shows a closed state in which the substrate-binding space is eliminated by a rearrangement of the referred helix [211]. The complex MlaFEDB, implied in the maintenance of the lipid membrane by transporting in glycerophospholipids, was solved in a nucleotide-free state, providing insights on its assembly and glycerophospholipid binding. Vanadate originated a closed conformation of a 4.0 Å resolution structure (PDB: 7D0A), showing the absence of the substrate-binding cavity due to the movement of both MlaD and MlaE [212].

3. Computational techniques

Dealing with (metal species)–protein interactions is a not trivial task from a computational perspective. The simulations should account with several aspects related to the metal binding: i) the characterization of the biologically active species, which lead to the formation of metal–protein adducts; ii) the exploration of the protein space to detect potential metal binding site(s); iii) the electronic properties of the metal and its environment, oxidation state, geometry distortions or ligand exchange during binding; iv) the wide conformational space of the protein receptor prior and upon metal interactions; and v) the formation of secondary interactions such as vdW or H-bonds, etc.) between the organic ligand(s) bound to the VC and protein scaffold.

Density functional theory, dealing with a chemical system at electronic level with reasonable computational cost, has been increasingly applied to complex systems like metalloenzymes or metallodrugs. In the context of VCs, DFT approaches are routinely used for structural, energetic and fine molecular properties prediction such as spin Hamiltonian parameters [98, 213-215] or UV-Vis electronic transitions [216]. When no clear biospeciation profiles can be drawn by instrumental techniques, DFT methods, comparing the experimental with the computed parameters, can fill the gap discriminating between different putative coordination modes and becoming a fundamental tool in bioinorganic chemistry [23, 107, 215, 217]. The most popular functionals used in vanadium chemistry are B3P86 and B3LYP for geometry optimization and prediction of thermodynamic properties [218, 219], BHandHLYP and B2PLYP for EPR parameter simulation of $V^{IV}O$ and 'bare' V^{IV} species [98, 213], and BHandHLYP or CAM-B3LYP for predicting electronic transitions and UV-Vis spectra [216, 220]. Generally, the selected basis set affects the quality of the calculations only slightly. Considering a dataset of 32 $V^{IV}O$ complexes, the mean absolute deviation (MAD) in the prediction of V–L distance with B3P86 functional and 6-311g basis set is 0.034 Å, which decreases to 0.019 Å if the optimization is carried out accounting for the solvent effects with polarizable continuum model (PCM). The MAD for $O{=}V{-}L_{eq}$ and $L_{eq}{-}V{-}L'_{eq}$ angles is 2.5° and 0.9° in the gas phase and 2.1° and 0.9° in solution [218]. Concerning the prediction of the hyperfine $\boldsymbol{A}$ tensor of the EPR spectrum of a $V^{IV}O$ complex, BHandHLYP functional allows to predict A_z with a mean absolute percent deviation (MAPD) below 4% without the inclusion of the second-order spin-orbit term (SO), while PBE0 gives a MAPD ~6% considering the SO interaction; for non-oxido V^{IV} species MAPD is ~3% with B2PLYP. By comparing the experimental and simulated A_z values, the methods were used to characterize the binding sites of a VC in a protein [215]. For amavadin the percent deviation (PD) is -2.0% at the level of theory B2PLYP/VTZ [98]. Up to now, it has not been possible to obtain a quantitative prediction of the UV-Vis spectra and to find – within the framework of time-dependent density functional theory (TD-DFT) – a general protocol.

In the case of VCs the order of performance of the tested functionals is long-range corrected > half-and-half hybrid > hybrid > standalone [216]. However, data indicate that a qualitative agreement can be reached, as well as the character of the transitions (d-d, MLCT, LMCT and LLCT). The ^{14}N SHFC constants of the ESEEM spectra can be predicted with BHandH functional followed by B3PW91 and B3P86. The value of PD is rather high when the N coordination is in the axial position, while when N donors are equatorially bound the prediction is quite satisfactory [215, 221]. Pure quantum mechanical (QM) approaches are viable for a limited number of atoms (about 300), reflecting the possibility to treat only a reduced fraction of the system, typically the metal ion, its ligands and a few amino acids [222, 223]. When examining (metal species)–protein systems, a conventional approach proposed by Himo *et al*. [224, 225] consists in cutting out the metal containing region generating cluster models without considering the entire size of the system. Valuable alternatives are represented by the multilevel QM/MM methods that split the system in two or more layers treating the metal-containing region under QM formalism and the rest of the protein at the less expensive MM level. MM approaches, neglecting electrons and computing the potential energy on the base of the nuclei position, are fast techniques commonly applied for structural analysis of proteins and metalloproteins.

When dealing with biological systems, bulk water effects become particularly relevant and thus should be modelled during the simulations. Including explicit solvation shells is entitlement of QM/MM or MM-based methods, where the bulk is described under MM formalism. However, within the pure QM framework, only a limited number of water molecules can be included, and continuum models result in a good balance between accuracy and computational time. One of the wide popular implicit schemes is the Self-Consistent Reaction Field (SCRF) that treats the solute-solvent interaction as a classical electrostatic problem [226, 227]. Among the most popular SCRF-based methods, the above mentioned PCM [228], SMD (Solvation Model Based on Density) [229], and COSMO (COnductor-like Screening MOdel) [230] should be mentioned.

In the MM framework, protein-ligand dockings, built on top of efficient Genetic or Monte Carlo search algorithms and simplified intermolecular force-fields (Scoring Functions, SF), are able to fast evaluate host-guest complementarity and binding affinity. When combined with pattern recognition algorithms [231] and adequate SF accounting for metal *covalent* or *coordinative* [43, 44] and *non-covalent* [99] interactions, they can offer a fast and accurate identification of the binding sites and binding modes of metallospecies in proteins. The background of docking is discussed in refs. [223, 232-240]. Among pattern recognition algorithms available in the literature [241], BioMetAll – based on the backbone preorganization hypothesis [231] – has been successfully applied for fast screening of proteins searching regions with two or more specific amino acid side-

chains prone to coordinate vanadium moieties. This information allows to reduce subsequent docking explorations to those regions identified in this preliminary step, avoiding time-consuming explorations [23, 25, 80, 107, 177, 178].

Concerning docking for metal-containing species, some of us recently improved the docking technique to describe a *coordinative* metal–donor bond using the Gold software [43-45]. The method takes advantage of the description of H-bonds, the spearhead of docking SF treating with high accuracy both bond lengths and directionality to virtually describe the coordination bond. From a force-field point of view, the metal is described as a new *atom type* and its coordination vacancies filled by fictitious hydrogens making the metal able to interact as an H-bond donor toward the Lewis bases of the protein. The *GoldScore* SF is represented in eq. 3 [242]:

$$Fitness\ (F) = \alpha \cdot S_{\text{H-bond}}^{ext} + \beta \cdot S_{\text{vdW}}^{ext} + \gamma \cdot S_{\text{H-bond}}^{int} + \delta \cdot \left(S_{\text{vdW}}^{int} - S_{\text{tors}} \right) \qquad \text{(eq. 3)}$$

with $S_{\text{H-bond}}^{ext}$, S^{ext} and $S_{\text{H-bond}}^{int}$, S^{int}_{vdW} describing the inter- and intramolecular H-bond and vdW interactions, and S_{tors} the energetic change related to the molecular torsions. Each term is weighed by a series of specific empirical parameters, namely α, β, γ, and δ.

The force constants of metals with each Lewis base of the biological receptor and equilibrium distances have been optimized for 15 main group and transition metals and validated towards a dataset of 64 X-ray structures covering metal compounds with different coordination numbers (4-6), vacancies in the sites (1-4) and geometries (square planar, tetrahedral, square pyramidal, trigonal bipyramidal, and octahedral) [43-45, 99]. For V, the force constants are reported in ref [45]. For VCs, the new methodology has been further validated through specific benchmarks containing all the available X-ray structures in the PDB: $V^{V}O_3$(benzohydroxamato) coordinated by Ser-O^{-} chymotrypsin A (PDB: 2P8O [243]); $V^{V}O_4$ bound to Cys-S^{-}, Ser-O^{-} and His-N, donors of tyrosine, alkaline and acid phosphatase, respectively (PDB: 3I80 [244], 1B8J [245] and 1RPT [246]); *cis*-$V^{IV}O(pic)_2$ moiety coordinated to Asp-COO^{-} of lysozyme (PDB: 4C3W [69]); and His-N bound to $V^{IV}O^{2+}$ in α-ketoglutarate-dependent taurine dioxygenase and *cyt* cb_{562} (PDB: 6EDH [247] and (PDB: 6DYL [248]). The ability of the dockings to reproduce subtle thermodynamic effects such as chiral discrimination of the binding region has been also evaluated with Lyz which, among the eight isomers of *cis*-[$V^{IV}O(pic)_2(H_2O)$], selectively binds *OC*-6-23-Δ upon displacement of the labile equatorial water by Asp52 [69]. After DFT optimization of the most stable isomers (*OC*-6-23-Λ/Δ and *OC*-6-24-Λ/Δ), the activated moieties were blindly docked on the Lyz scaffold obtaining *OC*-6-23-Δ as the highest affinity adduct, thus reproducing the experimental behaviour. The relative affinity predicted by docking also matched that computed at QM/MM theory level, projecting the

methodology as a new fast and accurate tool to identify (metal species)–protein interactions (Fig. 1) [45].

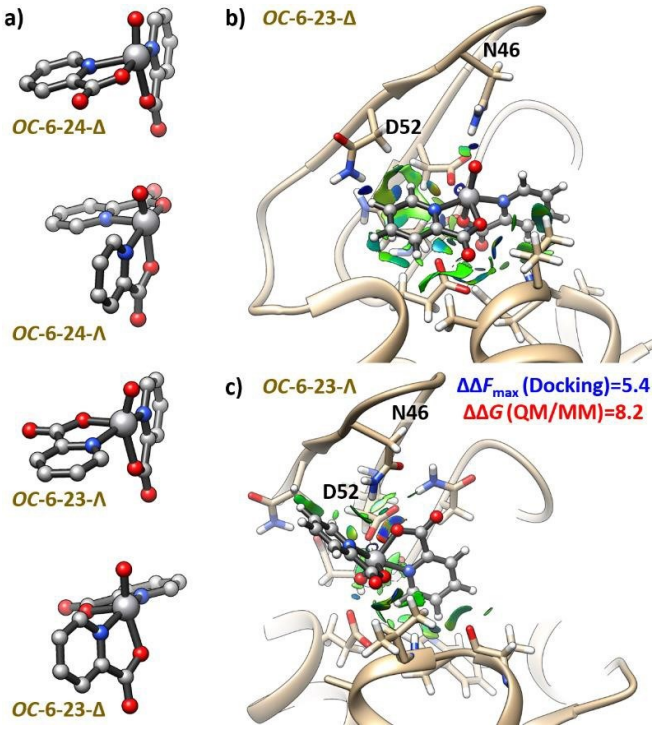

Fig. 1. a) Representation of *OC*-6-23/24 series of the most stable isomers of the $V^{IV}O(pic)_2$ moiety. The predicted adducts at the active site of Lyz with highest *Fitness F* of the series are shown in b) for *OC*-6-23-Δ isomer and in c) for *OC*-6-23-Λ isomer. The NCIplot map showing the intermolecular secondary interactions behind the chiral selectivity of the binding region is shown. Blue, red and green regions indicate strong attractive (dipole-dipole or H-bond), repulsive and vdW interactions, respectively.

Finally, a further updated version of *GoldScore* SF was proposed in the context of *non-covalent* dockings of VCs. The intermolecular H-bond contribution to the scoring is generally underestimated for metal compounds. Thus, the hard work consisted in fine tuning the coefficients of intermolecular H-bond and vdW interactions in eq. 3, assigning 1.0 and 0.3 to α and β, respectively. With this approach, the experimental relative affinity of a series of $[V^{IV}OL_2]$ compounds formed by flavonoid ligands for Lyz, ascertained by EPR spectroscopy, was reproduced [99], distinguishing the VCs that strongly bind to the protein (at least in the EPR timescale) and defining the value of maximum and average *Fitness* (F_{max} and F_{mean}) – which depends on the ligand and metal complex features – that marks the transition from a strong (detection of a *rigid limit* or anisotropic EPR spectrum) to a weak interaction (*slow tumbling* or isotropic spectrum) [99].

Despite their high performance, general docking methods are often limited by the local treatment of the motion of both metal compound (bond rotation) and protein (side-chain rotamers). In the case of highly flexible systems, this limitation can be overcome integrating Molecular Dynamics (MD) at different stages of the simulation to account for wide conformational changes of the receptors, eventually induced upon binding, and to describe the metal moiety accommodation into the protein scaffold. For metalloproteins, the MM force-fields on which MDs are based, must be implemented by custom-generated metal parameters [249-251]. The readers interested in dealing with metals in MM or MD based techniques can refer to the papers cited in ref. [252].

Among other post-treatment tools, the popular DFT based NCIPlot (Non Covalent Interaction Plot) [253] must be mentioned for its capability to characterize intra- and intermolecular host-guest interactions (see Fig. 1).

To summarize, the metal compound binding process should be treated by an integrated combination of different techniques and level of theory adequate to the specific phenomenon under analysis: i) DFT methods can be used to define the species responsible for the interaction; ii) MDs to evaluate the natural conformational changes of the protein in solution; iii) pattern recognition algorithms to identify the potential binding region of the target; iv) protein-ligand dockings to ascertain the possibility of metal binding on those identified regions; v) if necessary, further MD calculations to evaluate the binding induced fit and adaptation of the metal moiety to the protein scaffold; vi) DFT refinement and prediction of the spectroscopic properties, focusing on the metal containing region(s) through the methods of Himo and co-workers [224, 225], and comparison with the experimental data to discriminate between possible binding sites and modes; and finally vii) post-treatment methods such as NCIPlots to identify factors behind the recognition selectivity and preferential binding modes.

Moreover, considering the complex and multivariable nature of these systems a wise analysis of the experimental data is essential to guide the simulations. In the case of VCs, ^{51}V NMR and EPR can be used to define the metal oxidation state, its equilibria in biological media, as well as eventual changes on its first coordination sphere upon protein interaction. These data could be integrated with other structural and speciation data, provided by UV-Vis, CD, ESI-MS, MALDI and other techniques presented in section 2, that can contribute to identify the number and type of the metal–protein adducts.

Several examples of the application of computational methods to the characterization of VC–protein adducts will be presented in sections 4-8.

4. Binding modes of vanadium compounds to proteins

4.1. Specific and non-specific binding

The interaction between VCs and proteins can be described in two different ways: depending on the type of site, *specific* and *non-specific*, and on the type of binding, *covalent* or *coordinative* and *non-covalent*. A specific site is a region of a protein which is complementary to the metal moiety for size, charge and hydro/lipophilic character, and is able to selectively coordinate a specific metal species. Such sites ensure high stability of the formed adducts through the simultaneous interaction of several residues with the metal ion. In most cases, the stabilization is increased by secondary interactions, like H-bonds or vdW contacts. An example of specific binding is found in human serum albumin which transports several metal ions in the blood serum. HSA possesses two *specific* sites: one for Ni^{2+} and Cu^{2+} in the *N*-terminal site (NTS) with (NH_2, N^-, N^-, His3-N) donor set, where N^- is the deprotonated nitrogen of the backbone amide [254], and the multi-metal binding site (MBS) with (His67, His247, Asp-249, Asn99-CO) where Zn^{2+} specifically interacts [254, 255]. In contrast, $V^{III,IV,V}$ (and other metal ions) can bind to *non-specific* sites, generally accessible on the protein surface, formed in particular by His and Asp/Glu residues. In these cases, the strength of the interaction depends on the number of residues – which can be calculated through pattern recognition algorithms such as BioMetAll [231], see section 3 – and on the stabilization through secondary interactions. The vanadium binding to HTF in $(V^{III})_2$(HTF), very similar to Fe^{III}, is another example of *specific* binding [156].

4.2. Covalent and non-covalent binding

Covalent or *coordinative* binding occurs when one or more amino acid donors (stemming from the side-chains or backbone) replace the solvent molecules and/or the ligand L, while *non-covalent* binding takes place when the first coordination sphere of the VCs remains unaltered, without ligand exhange, and the interaction is based only on secondary interactions, namely vdW contacts and H-bonds, with accessible groups of the protein [42, 99, 179]. Depending on the type of interaction, the stereochemistry of the metal moiety could change (Fig. 2).

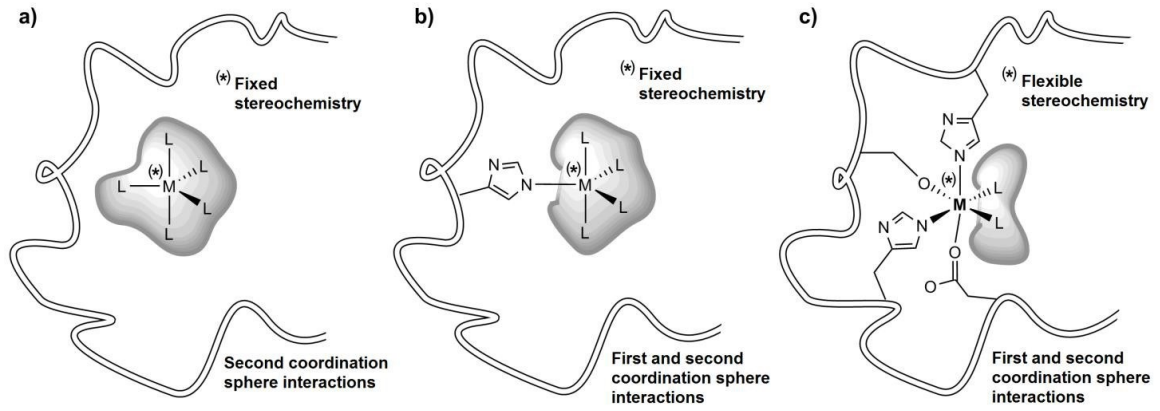

Fig. 2. Binding of a metal complex to a protein: a) *non-covalent* binding with second sphere interaction and fixed stereochemistry and chirality; b) *covalent* binding with only one M–donor bond and fixed stereochemistry and chirality; c) *covalent* binding with several M–donor bonds and stereochemistry and chirality defined by the interactions. Reprinted with permission from ref. [44]. Copyright (2019) American Chemical Society.

The *coordinative* binding can be exemplified by the case of $V^{3+}/V^{IV}O^{2+}/V^{V}O_2^{+}$ ions to apo-transferrin, which transports iron in the blood, in the Fe binding sites [22, 52]. These two sites, in the *N*-terminal and *C*-terminal region, bind $V^{III,IV,V}$ (for V^{III} see comment above) with high values of log*K* (Fig. 3). Another example is the adduct formed by *cis*-$V^{IV}O(pic)_2$ moiety to lysozyme through Asp52, demonstrated by XRD, spectroscopic and computational methods [45, 69].

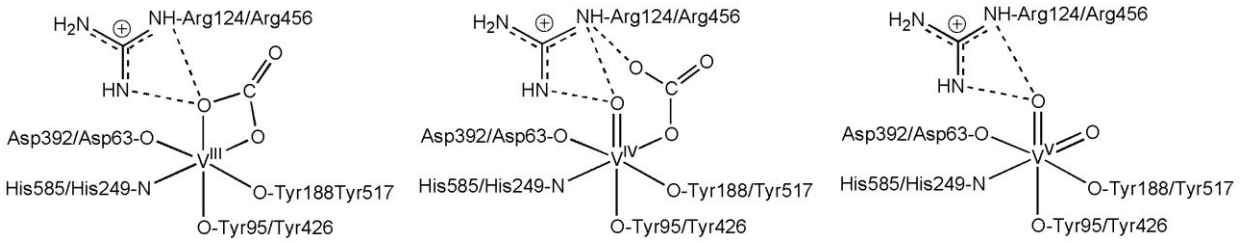

Fig. 3. Vanadium *coordinative* binding to HTF specific sites: a) V^{III}; b) $V^{IV}O^{2+}$; c) $V^{V}O_2^{+}$. The residues in the *N*- and *C*-terminal region are indicated. Adapted from ref. [22].

Usually, in a *covalent* bond, the V-donor distances fall in the range 1.8-1.9 up to 2.2-2.3 Å. Direct coordination is often overlooked in the literature, but should be considered when the V concentration approaches to the physiological values (1-50 μM) at which, due to the hydrolysis, the formation of $V^{III,IV,V}$–L species with available coordination sites – as proved by MS [173, 177, 180] – is expected. Several factors influence the *coordinative* binding: i) the availability of coordinating residues, mainly His-N and Asp/Glu-COO for V; ii) the presence of weak ligands in the metal

species that may be replaced by amino acid side-chains (for example, water molecules); iii) the strength of H-bonds and vdW contacts that can stabilize the adducts; iv) the steric hindrance of VCs and v) their electric charge [179]. While the first point is associated with the protein structure, the last ones mainly depend on the chemical and steric features of the ligands. For example, the comparison of *cis*-$[V^{IV}O(hqs)_2(H_2O)]^{2-}$ and *cis*-$[V^{IV}O(Hpip)_2(H_2O)]^{2+}$, where H_2hqs is 8-hydroxyquinoline-5-sulfononic acid and Hpip is pipemidato ligand with piperazine-NH^+ protonated, revealed that the formation of the adduct with Asp52 and Glu51 of ubiquitin (Ub) is favoured for $[hqs]^{2-}$ when compared to [Hpip], due to the strong H-bond established with Arg74 (Fig. 4, a-b) and the lower steric hindrance (Fig. 4, c-d) [179]. C*ovalent* docking studies, performed with Gold software and the updated version of *GoldScore* (see section 3) [43-45], also suggested that the deprotonation of piperazine-N to give the fragment *cis*-$V^{IV}O(pip)_2$ has a marked effect on the complexation process to Ub. This changes the order in the interaction strength for the sites between isomers Λ (favored for the neutral moiety $V^{IV}O(pip)_2$) and Δ (favored for $V^{IV}O(Hpip)_2^{2+}$). Moreover, the affinity for some potential sites is reversed: for example, His68 prefers the charged fragment $V^{IV}O(Hpip)_2^{2+}$, while Glu24 the neutral one $V^{IV}O(pip)_2$ (not shown in Fig. 4).

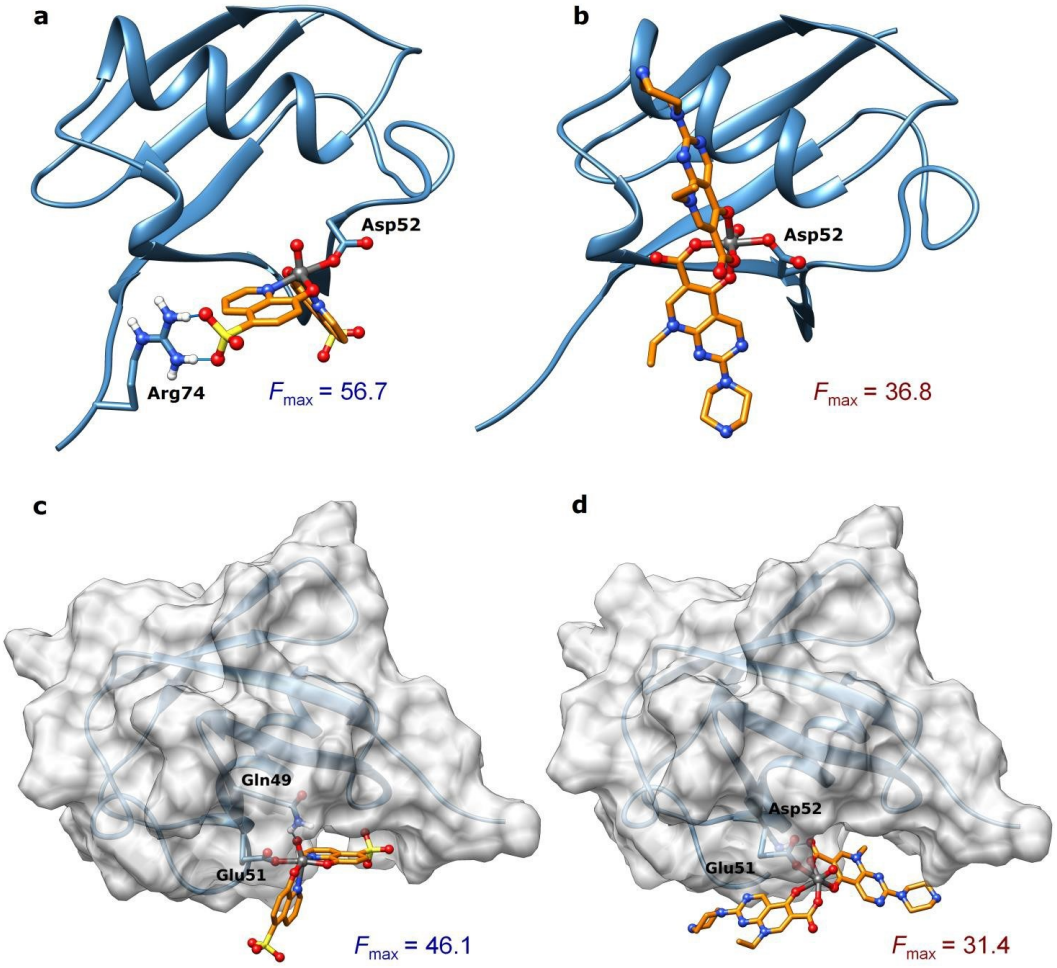

Fig. 4. Docking solution for the binding of *cis*-$V^{IV}O(hqs)_2^{2-}$ and *cis*-$V^{IV}O(Hpip)_2^{2+}$ moieties with ubiquitin: a) Asp52 with *OC*-6-42-Λ-$V^{IV}O(hqs)_2^{2-}$; b) *OC*-6-32-Δ-$V^{IV}O(Hpip)_2$; c) Glu51 with *OC*-6-44-Λ-$V^{IV}O(hqs)_2^{2-}$; d) Glu51 with *OC*-6-24-Λ-$V^{IV}O(Hpip)_2$. H-bonds are depicted in solid blue lines. Adapted from ref. [179].

Non-covalent bonding, stabilized by second coordination sphere interactions such as vdW, electrostatic or H-bonds, occurs for thermodynamically stable VCs which cannot increase the coordination number, or when *coordinative* binding sites of proteins are unavailable. Similarly to what was discussed above for *covalent* binding, this interaction is driven by some of the factors mentioned above, in particular in points iii-v. With aroylhydrazone ligands incorporating naphthalene moieties, the *non-covalent* binding of non-oxido $[V^{IV}L_2]$ species on the surface of Lyz depends on the substitution in position 2 of the phenolic ring, –OH or $–NH_2$. With the hydroxyl derivative, strong H-bonds are expected between the ligand phenolic –OH and the COO^- group of Asp52, NH of Trp62 and Trp63, CO of Asn109 and NH_2 of Arg112, while with the amino derivative these contacts are not possible and the interaction is significantly weaker [42].
Distinguishing a *non-covalent* from a *coordinative* bond is not a trivial task because in solution both interactions may occur and, often, the spectroscopic techniques do not provide enough information. In addition, the determination of the strength of *non-covalent* binding is often problematic and computational methods may be critical and should be integrated with the conventional instrumental techniques (section 3). An interesting example is represented by the *non-covalent* surface interaction of $[V^{IV}O(flavonoidato)_2]$ with Lyz; such a binding is quite strong and blocks the rotational motion of the complex in the EPR timescale, giving a rigid limit signal at room temperature [99]. Docking results using the *non-covalent* approach (section 3) indicated that polar residues, such as Arg, Trp, Ser, Asn, Gln, Asp and Glu, are involved in the interaction with OH and CO functionalities of the flavonoids [99]. Through an integrated EPR, ESI-MS and computational strategy, it was possible to distinguish two types of binding at pH 7.4 between Lyz and $[V^{IV}O(nal)_2]$ and *cis*-$[V^{IV}O(nal)_2(H_2O)]$ (where nal is nalidixato ligand). ESI-MS spectra established the formation of adducts $[V^{IV}O(nal)_2]_n$–Lyz, (n = 1-4) without distinguishing unambiguously between *coordinative* from *non-covalent* binding. EPR analysis as a function of $[V^{IV}O(nal)_2(H_2O)]$/Lyz molar ratio demonstrated that 1-2 equivalents of $V^{IV}O(nal)_2$ bind to Lyz in a *coordinative* way interacting through Asp/Glu-COO^- donors, while the excess interacts in a *non-covalent* fashion with the protein surface. The best docking solutions suggested a *covalent* binding of *OC*-6-32-Λ and *OC*-6-34-Λ isomers to Asp52 and Asp87, and *non-covalent* surface interaction of *SPY*-5-13 with Tyr20,

Arg21, Lys96 and Ser100 and of *SPY*-5-12 with Lys13 and Arg14 (Fig. 5), to form the final adduct with formula $[V^{IV}O(nal)_2]_4$–Lyz [25].

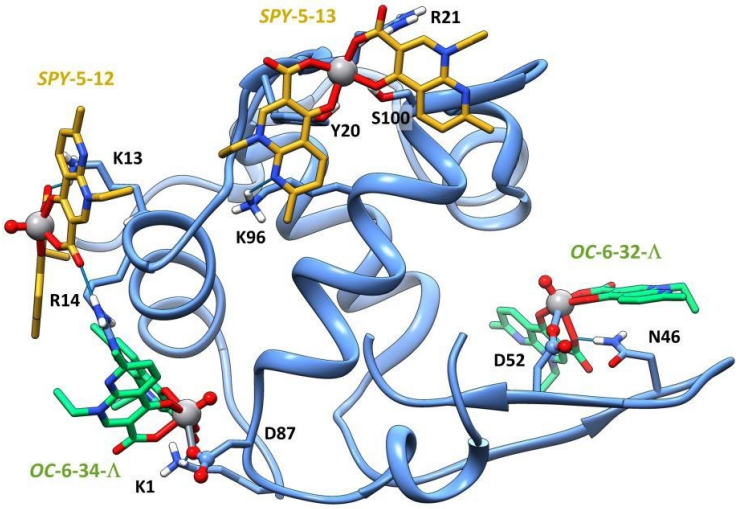

Fig. 5. Best docking solutions for the binding of $V^{IV}O(nal)_2$ moiety with Lyz. In green the *coordinative* adduct $[V^{IV}O(nal)_2]_2$-Lyz and in yellow the two *non-covalent* adducts to form the final $[V^{IV}O(nal)_2]_4$–Lyz species. Reproduced from ref. [25] by permission of The Royal Society of Chemistry.

4.3. V^{IV} and V^{V} binding

To summarize, the binding of $V^{IV}O^{2+}/V^{V}O_2^{+}$ ions and V^{IV} and V^{V} compounds depends on the protein and type of ligands bound to V. When the protein possesses specific binding sites, 'bare' $V^{IV}O^{2+}$ and $V^{V}O_2^{+}$ interact with the residues of these sites, as occurs for two 'iron sites' of HTF or NTS and MBS of HSA. In the literature there has been much debate in recent years whether also the moieties $V^{IV}OL/V^{IV}OL_2$ and $V^{V}O_2L_2/V^{V}O_2L$ could bind to the specific sites [22], this being a relevant issue to sort out as the binding strength of V to the protein could be significantly different.

For proteins without specific sites, 'bare' $V^{IV}O^{2+}$ and $V^{V}O_2^{+}$ ions may form stable adducts on the surface as well as buried into the protein if at least two amino acid donors, particularly His-N or Asp/Glu-COO, are available for the metal coordination. Carbonyl-O from backbone could also bind the metal [44], while the deprotonation and coordination of peptide NH is not favored for V at physiological pH [256]. When not saturated by side-chain groups, the first metal coordination sphere could be completed by H_2O or OH^- ligands, depending on the pH and residues that may favor the water dissociation (Fig. 6, a-b). Moreover, metal coordination may be stabilized by H-bonds between the oxido ligand and amino acids as Thr, Lys, Tyr, Cys, Arg, Trp, etc. Usually, H-bond formation may be the driving force stabilizing these adducts.

When $V^{IV}OL_2$ species are considered, the binding takes place in three different modes. When the geometry is *cis*-octahedral, *cis*-$[V^{IV}OL_2(H_2O)]$, adducts with composition $[V^{IV}OL_2]_n$–Protein can be

formed, where an amino acid donor replaces the equatorial H_2O and *n* is the number of available residues (Fig. 6, c). In general, metal coordination through carboxylate groups of Asp or Glu takes place when accessible His are lacking, or when they are not exposed enough (this is the case of lysozyme, that has a unique His residue, His15 [45]), or if H-bonds are so strongly formed that revert the order of stability His-N > Asp/Glu-COO^-, based on basicity. For square pyramidal complexes $[V^{IV}OL_2]$, the axial site is not prone toward coordination and only very weak *coordinative* binding or *non-covalent* interaction is expected (Fig. 6, d) [257]. When the hydrolysis favors the formation of $[V^{IV}OL(H_2O)_2]^+$, after the loss of one ligand L^- from neutral $[V^{IV}OL_2]$, and when suitable or adequately positioned donor atoms of the protein are present, the formation of $[VOL]_n$–Protein is expected through a couple of amino acid donors (usually His-N and/or Asp/Glu-COO^-) (Fig. 6, e) [178, 180]. The axial interaction with a third side-chain donor (Z in Fig. 6, e) is possible, but unlikely and depends on the type of protein. The formation of $[V^{IV}OL]_n$–Protein and $[V^{IV}OL_2]_n$–Protein is related to the intrinsic thermodynamic stability of the bis-chelated $[V^{IV}OL_2]$ species. For strong ligands L, $[V^{IV}OL_2]$ partly survives in solution and interacts in an unaltered form; if L has an intermediate strength, the dissociation of one ligand is favored, particularly at low concentrations, leading to the $V^{IV}OL^+$ fragment that may form ternary species with the protein [24]. A final situation is expected when L is a tridentate ligand and one equatorial and one axial positions are available in the V^{IV} coordination sphere (Fig. 6, f).

When considering V^V and L is a bidentate ligand, with $[V^VO_2L_2]$ *non-covalent* interactions are predicted when the complex maintains its identity in solution, while equatorial (and eventually axial) binding is possible for the hydrolyzed moiety $V^VO_2L^+$ (Fig. 6, g). When L is tridentate, only a weak apical coordination or a *non-covalent* interaction is predicted (Fig. 6, h).

Finally, for non-oxido $V^{IV,V}$ species the binding can be exclusively *non-covalent* since an increase of the coordination number is not possible. For these species, *covalent* binding in solution occurs or could occur when the transformation to $V^{IV}O/V^VO_2$ takes place [42].

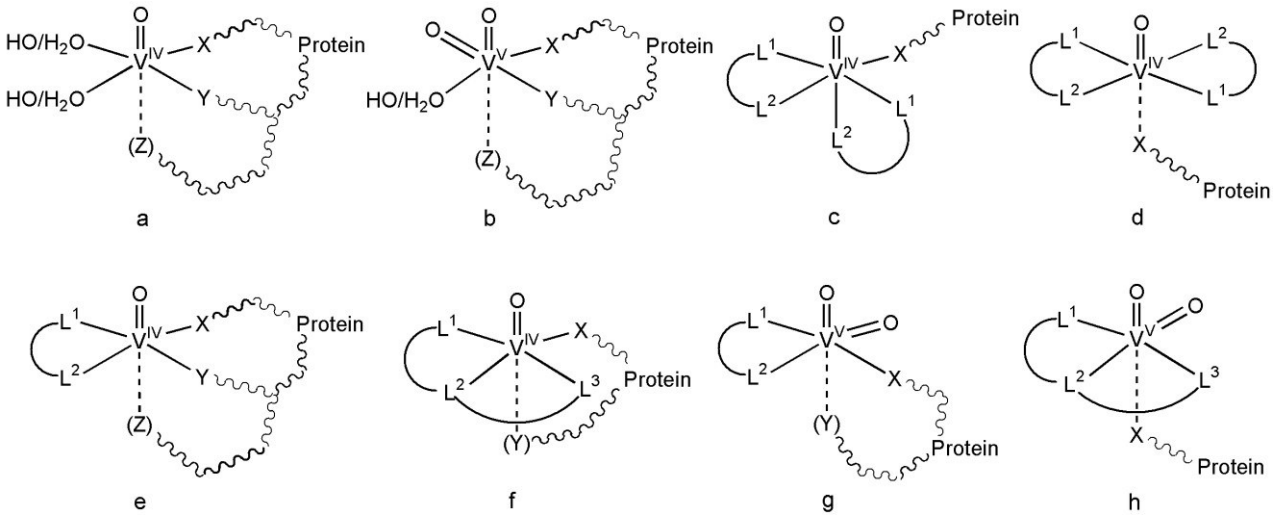

Fig. 6. General binding modes of $V^{IV}O^{2+}$ (a), $V^{V}O_2^{+}$ (b), $V^{IV}OL_2/V^{IV}OL^{+}$ (c-f), and $V^{V}O_2L$ (g-h). X, Y and Z are the amino acid donors of the protein. The potential weak axial donor is represented between round parentheses.

5. Vanadium enzymes

Vanadium enzymes play a quite remarkable role in nature. Vanadium nitrogenases from cyanobacteria or *Azotobacter* contribute to fixation of nitrogen, supplying ammonium for plant growth, and vanadium haloperoxidases from macroalgae are relevant in regulation of ozone levels, as they are responsible for a significant part of the supply of methylhalides to the atmosphere.

Other tasks of vanadium associated to function, metabolism and growth of bacteria have been reported in the last two decades. This may become of great interest for detoxification of e.g., ground water in areas impacted by mining activities or in other environmental remediation related to vanadium overload. Vanadium-dependent nitrate reductases may become relevant in this context, and research has become significant in the field.

Considering its role in homogeneous catalysis and in biocatalysis, vanadium attracted growing attention in the field of artificial metalloenzymes (ArMs) for industrial processes in mild conditions using green solvents (water) and oxidants (for example, H_2O_2 and O_2).

5.1. Nitrogenases

Nitrogenases are enzymes produced by bacteria, such as *Azotobacter vinelandii* and *Azotobacter chroococcum*, which effectively catalyze the reduction of N_2 to NH_4^{+}. This topic has been discussed in several reviews [1, 22, 258, 259] as well as book chapters [127, 260, 261], which should be consulted if detailed information is required on these systems.

Nitrogenases encompass three known isozymes: V-nitrogenase (V-Nase), Mo-nitrogenase (Mo-Nase), and Fe-nitrogenase (Fe-Nase), each encoded by unique gene clusters: Mo-Nase by *nif*, V-Nase by *vnf*, and Fe-Nase by *anf* [262]. The expression of each nitrogenase by *Azotobacter* is regulated by the availability of the metal, and with reduced availability of Mo, at low temperatures or in acidic environments, V replaces Mo giving rise to V-nitrogenases [7, 260, 263]. V-Nase similarly to Mo-Nase, contains a catalytic FeVco (FeV cofactor) a V, Fe, S polynuclear cluster including homocitrate and a P-cluster redox center. Despite genetic and biochemical similarity, the V-Nase simple substitution of Mo by V in the Mo-protein does not yield V-Nase. The two-component association drives catalysis with low-potential electrons from the central metabolism in an ATP mediated process represented in eq. 4 [264, 265]:

$$N_2 + 12e^- + 14\,H^+ + 40\,MgATP^{2-} + 40\,H_2O \rightarrow 2\,NH_4^+ + 3\,H_2 + 40\,MgADP^- + 40\,H_2PO_4^- \quad \text{(eq. 4)}$$

Electrons are delivered to the [4Fe-4S] cluster in the Fe protein component that binds ATP and associates with the N_2-reducing component. ATP is hydrolyzed and one electron is transferred *via* an [8Fe-7S] cluster to the FeVco where the substrate reduction takes place. Besides NH_4^+ ions, H_2 is also produced, thus nitrogenases also have hydrogenase activity.

The three isozymes (Mo-Nase, V-Nase and Fe-Nase) show quite different relative rates of H_2 formation and N_2 reduction [11, 266], with V-Nase being generally the less efficient of the series. Nevertheless, V-Nases are broadly distributed in the environment and are very important in terrestrial ecosystems as alternative biological nitrogen fixation systems under Mo limited conditions [267, 268]. These differences attracted interest in clarifying the structural/functional differences between the Mo- and V-Nase active sites [8]. Compared to FeMo cofactor (FeMoco), FeVco consists of a [V-7Fe-8S-C] cluster with a homocitrate bound to vanadium in which one sulfide is replaced by a bridging μ-1,3-carbonate (Fig. 7) [269].

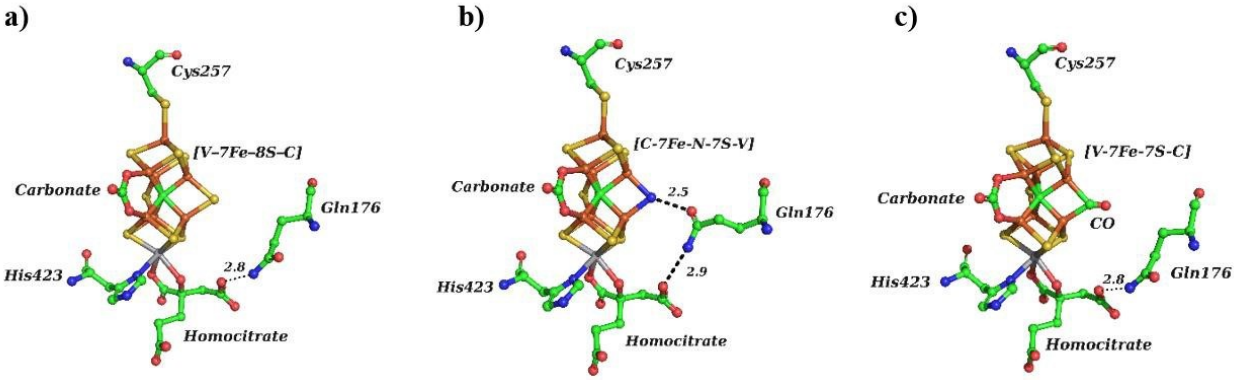

Fig. 7. Structural representation of the active site and FeVco of the V-Nase ($VnfD_2K_2G_2$) from *Azotobacter vinelandii*: a) in the resting state (PDB 5N6Y) [269]; b) in a non-resting state along the N_2 turnover displaying a μ_2-bridging ligand, identified as a N moiety between Fe2 and Fe6 after displacing S2B (PDB 6FEA) [270]; c) with a CO bound as bridging ligand to Fe2 and Fe6 (PDB 7ADR).

The catalytic FeVco is placed within the three domains of the VnfD subunit. As in its counterpart in Mo-Nase, it is linked to the protein by only two *coordinative* bonds, Fe1−Cys257 and V−His423. The homocitrate ligand coordinates V similarly to that reported for the Mo-Nase. A central carbide was clearly assigned [269], confirming previous X-ray emission spectroscopy reports [8]. Noteworthy, the exchange of Mo in FeMoco for V in FeVco yields minimal structural and bond distance changes, except an overall slightly elongated geometry [269]. However, the three mutations in VnfD subunit, 335T(I)GGP(L)RL(P)340, induce the opening of the pocket that can host an additional CO_3^{2-} ion in the FeVco [269].

The ability of V-nitrogenases to catalyze Haber-Bosch and Fischer-Tropsch-type reactions [271, 272] under ambient conditions and the fact that, in contrast with the industrial processes, the nitrogenase-catalytic cycle uses protons (H^+) instead of the expensive H_2, make these enzymes important subjects in small-molecule activation and in development of synthetic strategies based on biomimetic catalysts as cost-efficient systems to produce ammonia and hydrocarbons [146, 259]. Sippel *et al*. [270] presented a mechanistic discussion associated to the Thorneley-Lowe scheme [273], however the discussion of the details of the mechanism is out of the scope of this review.

One of the important catalytic differences between V- and Mo-Nases lies in their ability to reduce CO and CO_2; the V-Nase is more efficient and is able to reduce CO to hydrocarbons containing up to four carbon atoms, yielding methane (CH_4), ethane (C_2H_6), ethylene (C_2H_4), propane (C_3H_8), propylene (C_3H_6), butane (C_4H_{10}) and butene (C_4H_8) [272, 274-276]. The conversion of CO_2 to useful chemicals and fuels is an ongoing challenge to decrease the build-up of this greenhouse gas. Presently only nitrogenases are known to carry out the multielectron, multiproton reduction of CO_2 into hydrocarbons and among them, V-Nase, displaying the higher efficiency, has been the focus of extensive research [7, 9, 276-278].

Recently Rohde *et al*. [279] reported a structure with CO bound to the FeVco after catalytic turnover (Fig. 7, c). CO bridges iron atoms Fe2 and Fe6 in a μ_2-manner, replacing sulfide S2B, similarly to that observed with Mo-Nase [280]. The authors discussed the structural consequences of continued turnover when CO is removed, interpreted by the replacement of CO by OH^-, the movement of Gln176 and Lys361, the return of sulfide and the binding of two additional H_2O

molecules that are not present in the CO-bound state. A crystal structure of V-Nase, representing a reaction intermediate was reported, where one of the μ_2-sulphide ions of the active site (S2B) is replaced by a group, initially suggested to be NH^{2-} (Fig. 7, b). Benediktsson *et al*. [281], by a QM/MM strategy using CHARMM36 force-field and TPSSh functional to describe the MM and QM regions, respectively, concluded that it does not correspond to a N_2-derived reaction intermediate, but to an OH^--bound moiety [282]. More recently, Cao *et al*. [283] re-evaluated the structure taking the crystallographic raw data and, upon several QM/MM structural refinements using the standard Crystallography and NMR System (CNS) force-field to describe the MM r and TPSSh the QM region confirmed that the intermediate with OH^--bound better fits the crystal data [284]. This study also suggested that S2B reversibly dissociates from the active-site cluster, and that a flip of Gln176 may turn it to a position where it can form hydrogen bonds to the reaction intermediates [283]. In another QM/MM study (TPSSh/CHARMM36), Benediktsson *et al*. [285], taking advantage of the FeVco resting state X-Ray structures of V-Nase from *A. vinelandii* [269], confirmed the +III oxidation state, and concluded that V has less bonding interactions with Fe ions than Mo in FeMoco, these findings probably partly accounting for the different reactivity of FeVco and FeMoco.

V-Nase is substantially more active than Mo-Nase in the catalysis of the conversion of CO into hydrocarbons, but is less stable and efficient for the reduction of N_2 to NH_3. Harris *et al*. [11] reported a comparative study of CO reduction and inhibition of H^+ reduction under steady-state conditions for the three Mo-, V- and Fe-Nase isozymes. This study revealed that CO is a substrate of Fe-Nase and inhibitor of H^+ reduction, presenting a product profile and inhibition pattern distinct from those observed for Mo- and V-Nases [11]. They also emphasized that differences in the proteins around the active site in the three isozymes affect substrate reactivity. In particular, this is changed by the substitution of certain amino acids around the catalytic cofactor [11]. Clear evidence of an interstitial carbide in the FeVco of *A. vinelandii* V-Nase has been provided [8]. Although the FeV cofactor of V-Nase incorporates a homocitrate ligand and the central carbide [8], the distinct reactivity between FeVco and FeMoco suggests there are structural differences between them [10]. The studies also suggested that the interstitial carbide has a relevant role in substrate turnover [7, 280, 286]. In fact, it has a crucial role, both in location and function, and by orchestrating the restructuring events of the cofactor that underlie the unique reactivity of V-Nase towards CO [7].

5.2. Haloperoxidases

Vanadium-haloperoxidases (VHPOs) are a class of haloperoxidases containing vanadium at the active site [1]. VHPOs catalyze the $2e^-$ oxidation of halides by H_2O_2 (eq. 5). The hypohalous acids

(XOH) and XO^-, X_2, or X_3^- intermediates, generated during the turnover, react with low substrate specificity and non-enzymatically, with several organic entities (R-H) yielding halogenated compounds R-X (eq. 6).

$$H_2O_2 + X^- + H^+ \rightarrow XOH + H_2O \quad \text{(eq. 5)}$$

$$XOH + R\text{-}H \rightarrow R\text{-}X + H_2O \quad \text{(eq. 6)}$$

In the absence of RH (a nucleophilic acceptor), XOH may react with H_2O_2 resulting in the formation of singlet oxygen ($^1O_2$), eq. 7:

$$XOH + H_2O_2 \rightarrow {}^1O_2 + HX + H_2O \quad \text{(eq. 7)}$$

Vanadium-haloperoxidases are named in a manner depending on the most electronegative halide they can oxidize effectively: iodoperoxidases (VIPO), bromoperoxidases (VBrPO) and chloroperoxidases (VClPO). The discovery of VBrPO in 1984 [287] and the understanding of their relevance as major sources of halogenated organic natural products [4, 188, 288, 289], triggered significant interest in vanadium chemistry, and the prospective industrial applications of VBrPO and VClPO in halogenations of relevant organic compounds under mild conditions continue generating extensive interest. VHPOs have been addressed in previous reviews, namely from Wever [185, 289-293], Vilter [294], Rehder [4, 127], Crans *et al*. [1, 295], Licini *et al*. [296], Plass [297], Hartung [298], Visser [299, 300], Leblanc [2], and from several other authors [22, 186, 188], which we recommend for detailed information about this topic.

The first diffraction XRD structure of a V-chloroperoxidase was from the VClPO isolated from the fungus *Curvularia inaequalis* (*Ci*VClPO) [301]. Other structures from *Ci*VClPO, *Streptomyces* sp CNQ-525, and CNQ525, either in their apo- or peroxide-containing forms, were also determined [2, 22, 302]. XRD structures of VBrPOs isolated from brown and red algae were also solved, namely from *A. nodosum* (*An*VBrPO) [163], and from the red seaweeds *Coralina pilulifera* (*Cp*VBrPO) and *Coralina officinalis* [303, 304]. The V-containing active site shares structural analogies in all the species with vanadium(V) in a trigonal bipyramid coordination geometry, where His-N is in the apical position, one Ser-O^- is equatorially bound, and the remaining positions are occupied by 3 O-atoms (Fig. 8). In the native enzyme, the V is bound to two other O-atoms at 1.69 Å, one O-atom at 1.93 Å, and to an His-N donor at 2.02 Å. In the V-EXAFS measured for the native *An*VBrPO, the bond lengths determined are quite close to those from the XRD study. The reviews by Leblanc [2] and Costa Pessoa [22] give more structural and comparison details.

Noteworthy, although the characterized VHPOs share less than 30% sequence homology, their tertiary structure is quite similar, while the quaternary ones differ considerably. When V^{V} is substituted by V^{IV} their activity is almost totally lost. In the case of *An*VBrPO, ESEEM studies confirmed the equatorial coordination by His-N [121], and a recent docking/full DFT study reported the 3D structure unveiling a binding mode somewhat similar to the catalytic one (see Fig. 8), but with oxidovanadium(IV) in a square pyramidal arrangement with two His side-chains *trans* to each other coordinating vanadium equatorially, a Ser and a H_2O molecule completing the first coordination sphere [32, 268]. Variations of pH may change the V^{IV} binding mode.

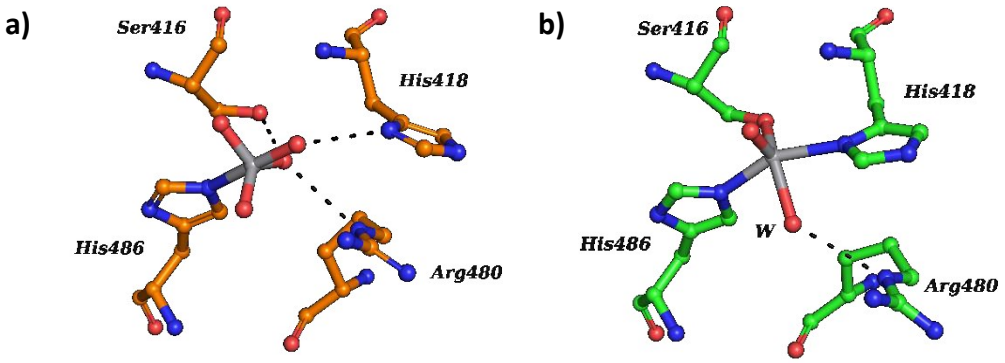

Fig. 8. Representation of the amino acids surrounding the active site of *An*VBrPO, depicting the main features of the binding of V^{V}, as determined by a) SC-XRD (PDB: 1QI9) [163], and b) of the DFT refined structure for the binding of V^{IV} [32]. *W* in b) represents a water molecule.

Mechanism of halide oxidation. Despite the very similar active sites of V-based haloperoxidases, their specificity toward halides differs. Several mutagenesis studies [189, 305-308] along with experimental [140, 309-311] and theoretical [140, 312-319] studies have been done disclosing the crucial role in specificity of the residues that belong to the second coordination sphere of V. These residues work somewhat concertedly, showing synergistic effects and all of them play important roles in the catalytic activity [185]. These issues were discussed by Wever [293]. Some details of the protonation states of the vanadate O-atoms were clarified in a magic angle spinning ^{51}V NMR spectroscopy (^{51}V MAS NMR) and by a DFT/B3LYP study − based on the comparison of experimental and simulated chemical shifts obtained from cluster models of the active site for 16 protonation states − on *Ci*VClPO, as well as on a triple mutant of this VClPO [140]. The results showed that the protonation states of the vanadate cofactor depend on pH, highlighting a resting state, at physiological pH, with the apical coordination of one water molecule and one hydroxide in the equatorial plane (Fig. 9). The distinct protonation behavior may be important to explain the large difference in the catalytic activities as a function of the pH.

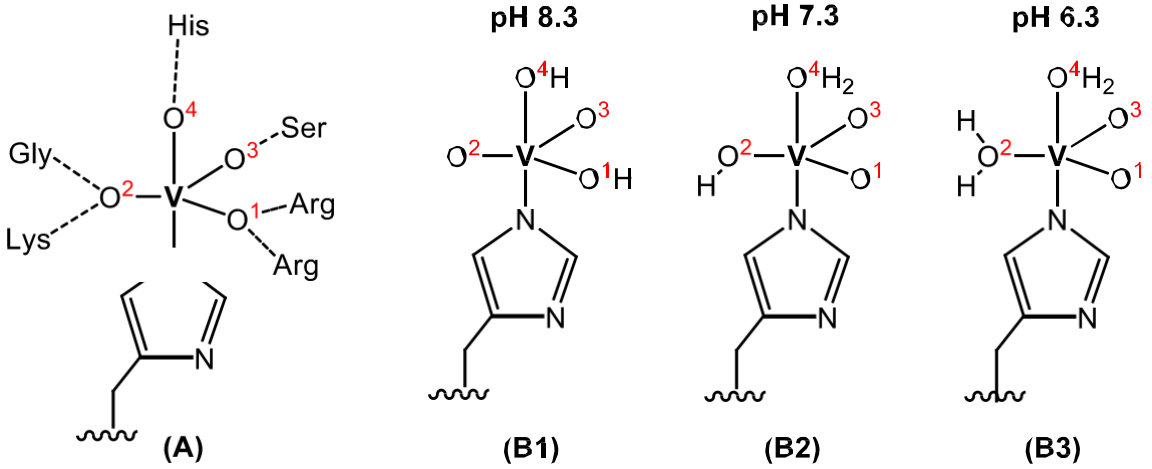

Fig. 9. (**A**) SC-XRD (PDB: 1IDQ) active site of the VClPO from *Ci*VClPO [302], showing the donor atoms of residues interacting with vanadate, and (**B1**, **B2**, **B3**) the proposed protonation states at several pH values obtained in the combined ^{51}V MAS NMR and DFT study of Gupta *et al*. [140].

Peroxido-vanadates are stronger oxidizing agents than vanadate and the peroxido intermediate of the *Ci*VClPO was also characterized by XRD analysis [302]. Upon binding of the peroxide, several changes occur in the H-bonding network and in the V coordination geometry. This is important but not yet fully clarified. While some authors suggest protonation of the peroxido O-atom and nucleophilic attack by halides at this O-atom [293], others do not assume protonation and/or that the attack is at the other peroxido O atom [186, 299, 314, 315, 320]. Other authors suggested mechanisms not involving side-on binding of the peroxido ligand [319].

Besides the type of binding of the peroxido ligand, there are several other relevant differences in the proposed mechanisms of catalytic action. For example, single-crystal XRD structures may differ from the actual structures 'in solution', and the vanadate in the resting state and/or when peroxido is bound may also be involved in several (de)protonation equilibria (e.g. Fig. 8), this possibly varying slightly from VIPO to VBrPO to VClPO. The same may occur with other intermediates involved in the mechanism. The whole enzyme also somewhat affects what happens, as well as the environment itself (pH, ionic strength, temperature).

Outlines of proposed catalytic steps of the oxidation of halides by VHPOs are depicted in Fig. 10. In all cases, the cycle starts with coordination of H_2O_2 to vanadium by substitution of a H_2O molecule, probably according to a dissociative mechanism. In path A, the halide X^- acts as a nucleophile towards the side-on peroxido ligand coming from the H_2O assisted deprotonation of the hydroperoxido intermediate forming a transient X-O bond [299, 300, 315, 321]. In path B, the nucleophilic attack of X^- occurs directly on the side-on hydroperoxido ligand entailing a concerted

O-O breaking and X-O bond forming [22, 293, 314, 315, 317, 321]. In path C, neither the formation of side-on hydroperoxido nor peroxido intermediates is assumed [319].

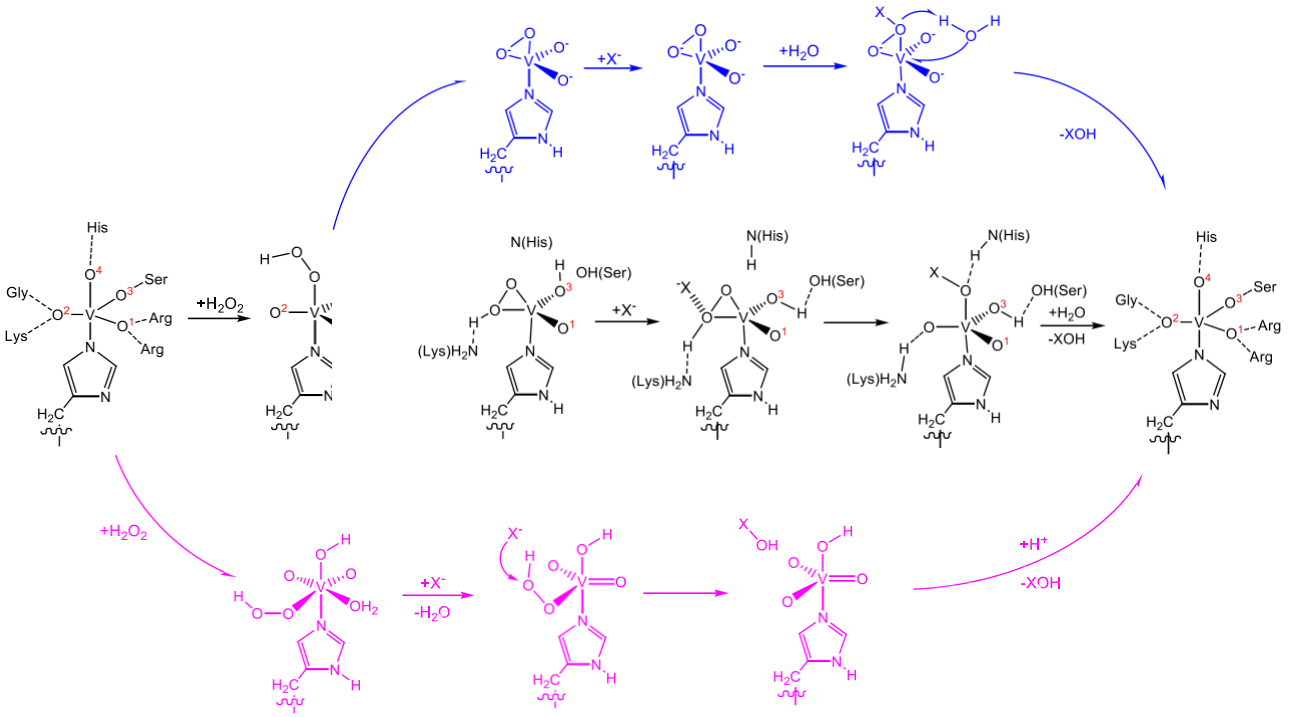

Fig. 10. Three outlines of proposed catalytic steps of the oxidation of halides by VHPOs: path A (blue), path B (black) and path C (purple). Details of protonation(s) and deprotonation(s) of vanadate O-atoms are not specified. The interested reader can refer to the original publications [22, 293, 299, 300, 314, 315, 317, 319, 321].

5.3. V-containing Nitrate Reductases

Nitrate reductases are enzymes catalyzing the $2e^-$ reduction of nitrate to nitrite (eq. 8), typically containing a Mo-pterin cofactor.

$$NO_3^- + 2e^- + 2H^+ \rightarrow NO_2^- + H_2O \qquad \text{(eq. 8)}$$

V-containing nitrate reductases were first isolated from *Pseudomonas isachenkovii* and *Thioalkalivibrio nitratireducens* bacteria [322, 323]. The corresponding enzyme is a homotetramer lacking the Mo-pterin cofactor and containing V and Fe in a molar ratio 1:3. In a previous review [22] we overviewed this topic, and Rehder critically discussed this subject [324]. We recommend those papers for more details.

As described by Rehder [324], in *P. isachenkovii*, grown in cultures containing lactate (lact) and V^V as electron donor and acceptor respectively, vanadium is stored by secretion of a 14 kDa protein

that, similarly to vanabins, binds up to 20 V ions per monomer [322]. Furthermore, the presence of periplasmatic V-containing nitrate reductase, indicates that V is used for *P. isachenkovii* dissimilatory functions. The enzyme primarily reduces vanadate(V) to $V^{IV}O(OH)_2$, with very low solubility at neutral pH values, employing molecular hydrogen and carbon monoxide as electron donors, eqs. 9 and 10 [4, 325].

$$H_2V^VO_4^- + 1/2\ H_2 + H^+ \rightarrow V^{IV}O(OH)_2\downarrow + H_2O \quad \text{(eq. 9)}$$

$$2\ H_2V^VO_4^- + CO + 2\ H^+ \rightarrow 2\ V^{IV}O(OH)_2\downarrow + CO_2 + H_2O \quad \text{(eq. 10)}$$

$$H_2V^VO_4^- + HCO_2^- + 2\ H^+ \rightarrow V^{III}(OH)_3 + CO_2 + H_2O \quad \text{(eq. 11)}$$

The reduction of V^V/V^{III} (eq. 11) was also observed for *P. isachenkovii* among other vanadate-respiring anaerobic bacteria from deep sea hydrothermal vents [326]. The use of vanadate(V) as an electron acceptor has been observed in a wide range of bacteria strains [4], as well as in mesophilic and thermophilic methanogenic archaea, namely *Methanothermobacter thermautotrophicus* [327].
The reduction of V^V to V^{IV} along the respiratory chain of specific bacteria strains can be promoted using lactate and formate or glycerol and formate as electron sources, as in the case of the Gram-negative soil bacterium *Shewanella oneidensis* and *Vibrio parahaemolyticus* , respectively [328], $V^{IV}O(OH)_2$ is produced and precipitates. In *S. oneidensis*, the $V^V \rightarrow V^{IV}$ reduction is catalyzed by a vanadate reductase, associated with the outer membrane. In the cytosolic membrane the flow of electrons for the $V^V \rightarrow V^{IV}$ reduction is such that they are finally transferred by cytochrome *c* type heme proteins to the outer membrane, and then to membrane-associated vanadate [4]. Many researchers have thus reported bio-reduction of vanadium by various microorganisms, mostly belonging to either the bacterial or the eukaryotic domain, e.g. [329-332]. The reduction of V^V to V^{IV}, and partly to V^{III} by prokarya probably contributes to the mineralization of soluble vanadate(V).
In a recent study [333], the bio-reduction of vanadate(V) coupled with anaerobic methane oxidation (the electron donor) and its connection to NO_3^- reduction was reported. V^{IV} was the main reduction product, and precipitated naturally in groundwater environment. Preliminary microbial community structure and metabolite analyses indicated that V^V was likely reduced via *Methylomonas* coupled with CH_4 oxidation, or through synergistic relationships between methane oxidizing bacteria and heterotrophic vanadate reducers. Methane was oxidized to CO_2, with volatile fatty acids serving as intermediates. The effectiveness of vanadate reduction was also demonstrated by *Lactococcus raffinolactis*, a Gram-positive bacterium belonging to the phylum Firmicutes. V^V is reduced to insoluble V^{IV}, being distributed both inside and outside the cells [331]. Nitrite reductase encoded by

gene *nirS* mainly catalyzes intracellular V^{V} reduction, so the processes occurring in this case somewhat differ.

Some species of *Thiobacillus*, widely distributed in environmental media, such as water, mud and soil [334], are denitrifiers with ability to oxidize Fe^{II} to Fe^{III}, S^{-II} to SO_4^{2-} and S^0, for reduction of NO_3^- [335, 336]. Heterotrophic V^{V} reducers (e.g., *Pseudomonas* and *Spirochaeta*) may achieve V^{V} elimination by using metabolic intermediates synthesized by autotrophic Fe^{II} oxidizers (e.g., *Thiobacillus*) and S^{-II} oxidizing genera (e.g., *Sulfuricurvum*). In a recent study [337], gene abundance and enzymatic activity tests confirmed that the nitrate reductase gene *napA* has a crucial function in the V^{V} reduction, Fe^{II} and S^{-II} donating the electrons. V^{V} is reduced to V^{IV}, while FeS in mackinawite are oxidized to Fe^{III} and SO_4^{2-}. This study demonstrated that mackinawite (FeS), a cheap, widely-distributed and natural reducing mineral, is an efficient and sustainable material for effective remediation of V^{V}-contaminated aquifers; the mackinawite-dependent V^{V} bio-reduction and denitrification may be described by the following reactions, eqs. 12 and 13 [337]:

$$9\ HV^{V}O_4^{2-} + FeS + 14\ H_2O \rightarrow Fe^{3+} + 9\ V^{IV}O(OH)_2\downarrow + SO_4^{2-} + 19\ OH^- \quad \text{(eq. 12)}$$

$$9\ NO_3^- + 5\ FeS + 7\ H_2O \rightarrow 5\ Fe^{3+} + 5\ SO_4^{2-} + 9/2\ N_2\uparrow + 14\ OH^- \quad \text{(eq. 13)}$$

Vanadate(V) being a contaminant in groundwater aquifers close to areas where vanadium mining and processing activities take or took place, some of the microbe-driven processes described above may prove useful in its remediation. However, in most cases, the actual protein systems involved are not yet known, or have not been adequately characterized.

5.4. Application of V-enzymes in synthesis

Due to the easy interconversion between the vanadium oxidation states +IV and +V, the wide variety of coordination numbers and geometries, the Lewis acid character of V-centers and their high affinity towards oxygen, V^{IV} and V^{V} complexes have been extensively used for oxidation catalysis using green oxidants of industrial interest such as H_2O_2 or O_2. The efficacy of VHPOs in various catalytic reactions [127, 338] further stimulated the search of V-based processes for organic transformations, either using enzyme promiscuity or *de novo* designed artificial enzymes [339-344]. Due to the retention of the oxidation state of vanadium in VHPOs during catalytic turnover, they do not suffer from oxidative inactivation [345]. VHPOs are also highly stable, tolerant to organic solvents and resistant to high temperatures [346, 347], making them valuable candidates for industrial synthesis of halogenated compounds. Another advantage of the use of VBrPO is that the formation from H_2O_2 and KBr of oxidized bromine species may be easily controlled. Due to these

advantages, a wide range of relevant Br- and Cl-containing organic compounds has been synthesized using bromoperoxidases and chloroperoxidases [298, 348, 349]. Interestingly, although VHPOs are generally considered to have low regio- and stereo-selectivity, some VHPOs have shown high selectivity, for example in halogenation of their indole substrates [6, 350].

Despite the advantages mentioned above, there are difficulties, particularly for VIPOs and VBrPOs, related to the enzymes' synthesis in a cheap and industrial scale way that have hampered their wider application. Many studies of halogenation of organic compounds by VHPOs have been reported and we only cite a few among the recent ones [4, 127, 185, 186, 298, 308, 338, 345, 351-354].

VHPOs also have ability to oxidize organic sulfides [355, 356], but sulfoxidations proceed much slower than brominations. Regarding enantioselective sulfoxidations, VBrPOs in the presence of H_2O_2 have been an option. Interestingly, depending on the particular VBrPO used (*Cp*VBrPO or *An*VBrPO) distinct enantiomers were obtained [185, 357]. By use of labelled H_2O_2, it was shown that the oxygens transferred to the sulfide yielding the chiral sulfoxide comes directly from the hydrogen peroxide. This selective O transfer proceeds upon binding of H_2O_2 at the active site of the VBrPO or very close to it [357].

Considering the structural analogy between phosphate and vanadate(V) and similarity of the active sites of VHPOs and phosphatases [1, 34, 304, 358, 359], pioneering results in the field of V-based artificial enzymes have been obtained by substitution of vanadate(V) at the active site of acid and phytase phosphatases, approaching haloperoxidases in the enantioselective sulfoxidation activity [340, 343, 360]. Sheldon *et al*., besides vanadate(V)-substituted acid phosphatases and phytases, have reported a wide array of artificial enzymes by incorporating V^V in sulfatase, phospholipase D, albumin, apo-ferritin and and aminoacylase [339-341]. The best results in terms of selectivity and turnover were reached for vanadate(V)-loaded *Aspergillus ficuum* phytase leading to sulfoxidation of sulfides with an enantiomeric excess up to 66% [361]. Up to now a unique example of *de novo* designed V-based artificial enzyme was reported by Ward *et al*., by including the $V^{IV}O^{2+}$ ion through a *non-covalent* approach into the biotin binding site of streptavidin. The resulting artificial enzyme showed complete conversions and up to 93% of enantiomeric excess in oxidation of aryl and alkyl sulfides using *t*-BuOOH as oxidant [342].

In conclusion, V-based enzymes have potential for industrial production of many fine chemicals under mild conditions. However, further improvements such as directed mutagenesis, rational design of *de novo* enzymes and engineering approaches using immobilized enzymes as well as spatially separated reaction compartments are still required for adequate industrial use [32, 352].

6. Vanadium binding to blood proteins

The interaction of VCs with the blood proteins plays an important role in their transport in the organism and pharmacological effects. The most relevant proteins for metal binding in the serum are human serum transferrin, human serum albumin and immunoglobulins (Ig), and the distribution of VCs among them and other bioligands depends on the stability of the chemical form of V-containing species. The HSA concentration is about 20 times higher than HTF, but vanadium has a higher affinity for transferrin. In the bloodstream, the uptake of VCs by red blood cells (RBC), where the vanadium species can interact with hemoglobin, is also possible.

6.1. Transferrins

Transferrins are glycoproteins with a single chain composed of *ca*. 700 amino acids, having a molecular mass of approximately 80 kDa [362]. Depending on the saturation degree, the forms of HTF are denoted as apo-HTF (without iron), monoferric HTF (Fe-HTF_C or Fe-HTF_N, where HTF_C and HTF_N are the sites in the *C*-terminal and *N*-terminal regions, respectively) and diferric HTF (Fe_2-HTF or holo-HTF). Transferrin concentration in the blood serum has a mean value of 29.9 μM [363]. Normally in plasma, only 30% of HTF sites bind Fe^{3+} with approximately 27% as Fe_2-HTF, 23% as Fe-HTF_N, 11% as Fe-HTF_C, and 39% as apo-HTF [364]; therefore, the concentration of available binding sites is *ca.* 34 μM. In higher animals, serum transferrin transports not only iron [365], but also other metal ions including vanadium in the oxidation states +III, +IV, and +V [22, 366].

HTF binds V in the two iron sites in the *C*-terminal and *N*-terminal regions with Asp63/Asp392, Tyr95/Tyr426, Tyr188/Tyr517 and His249/His585 coordination [22, 367]. Bi- or mono-dentate HCO_3^-/CO_3^{2-} ligand completes the coordination of V^{III} and V^{IV} (Fig. 3). The affinity order for the oxidation states is $V^{III} > V^{IV}O^{2+} > V^{V}$, in the presence of HCO_3^- and $V^{III} \sim V^{IV}O^{2+} > V^{V}$ in its absence [22]. (Hydrogen)carbonate can be substituted with other 'synergistic' anions [368, 369]. HCO_3^-/CO_3^{2-} is bidentate for V^{III}, monodentate for $V^{IV}O^{2+}$ and not coordinated for $V^{V}O_2^+$ ion [22, 367]. At pH 7.4 the value of log*K* for $(V^{III})_2$(HTF) is ~20 [370], logK_1 and logK_2 for $(V^{IV}O)$(HTF) and $(V^{IV}O)_2$(HTF) are in the range 13.0-13.4 and 11.8-12.5 [67, 371, 372], while those for (V^{V})(HTF) and $(V^{V})_2$(HTF) are 6.0-7.5 and 5.5-6.6 [128, 371, 373], respectively.

Upon coordination of V^{III}, very similar to that of Fe^{III}, the conformation of HTF becomes closed [30, 155, 156]. The closed conformation of $(V^{III})_2$(HTF) is possibly recognized by transferrin receptors of cells, thus the uptake of V^{III} may occur by receptor-mediated endocytosis [155, 156, 365, 374]. For many years there has been some debate in the literature whether or not $V^{IV,V}$ binding may cause the closure of the transferrin conformation. A combined voltammetric, spectrometric and

SAXS study, focusing on the interactions of $V^{IV}SO_4$ and $NaV^{V}O_3$ salts with apo- and holo-HTF was reported [173]. Upon binding of both V salts, the conformation of apo-HTF becomes partially closed, as inferred by the different SAXS parameters, but less than that observed for Fe^{III}. Moreover, while SAXS did not allow to substantiate the binding of $V^{IV}O^{2+}$ and V^{V} to holo-HTF, it revealed that its closed conformation was maintained [173]. Urea-PAGE experiments were carried out comparing the patterns obtained for solutions containing apo-HTF and V^{III}, V^{IV}, V^{V} or V^{III}/Fe^{III} salts. The results demonstrated that the binding patterns of $(V^{III})_2$(HTF), $(Fe^{III})_2$(HTF) and (V^{III}/Fe^{III})(HTF) were quite similar, indicating a closing of the HTF conformation under those conditions [156, 173]. In contrast, no bands (or weak ones) corresponding to closed conformation of the protein were found for the V^{IV}- and V^{V}-apo-HTF samples, as well as for systems containing apo-HTF and $V^{IV}O^{2+}$, $V^{IV}O$–ma, $V^{IV}O$–dhp, $V^{IV}O$–pic and $V^{IV}O$–dipic species [155], indicating that any conformation change eventually occurring does not resist the denaturing conditions of the Urea-PAGE experiments. Equivalent Urea-PAGE results were recently obtained by Levina *et al.* [30] for HTF samples containing V^{IV}- and V^{V}-salts.

It was demonstrated by EPR that when $V^{IV}O^{2+}$ is added at pH 7.4 to the system containing $(Fe^{III})_2$(HTF), in which the two iron sites are blocked, it can bind to another site named C, with $A_z(^{51}V)^{exptl} = 165.4\times10^{-4}$ cm^{-1} [375]. Taking into account the "additivity relationship" [95, 97], the binding of two His plus O donors from Asp/Glu or backbone CO was hypothesized [375]. Recent coordinative docking and DFT cluster studies, carried out following the protocol described in section 3, suggested three possible sites involving His and Asp/Glu residues: (His14, His289, Glu13; H_2O), (His25, His273; H_2O, OH^-) and (His473, Asp478; H_2O, H_2O) [24]. For all of them, the DFT values of ΔE_{bind} are negative, from -24.3 to -32.8 kcal/mol, and $A_z(^{51}V)^{calcd}$ values are very close to the experimental ones, in the range $(167.9\text{-}169.5)\times10^{-4}$ cm^{-1} (Table 1). All the sites are stabilized by hydrogen bonds with Thr17-OH (site C^1) and Lys280-NH_3^+ and Glu281-COO^- (C^2). The sites C^1 and C^2 are represented as examples in Fig. 11, a-b; notably the structures are similar to $V^{IV}O^{2+}$-substituted carboxypeptidase (two His and one Glu plus a water molecule [376]), and this is confirmed by comparison of $A_z(^{51}V)^{exptl}$ (165.4 for HTF vs. 165.9×10^{-4} cm^{-1} for $V^{IV}O^{2+}$–carboxypeptidase [376]). For solutions containing $(Fe^{III})_2$(HTF) and $V^{IV}O$–mhcpe, where Hmhcpe is 2-methyl-3*H*-5-hydroxy-6-carboxy-4-pyrimidinone ethyl ester, the EPR spectra were measured at 77 K and $A_z(^{51}V)^{exptl}$ was 168.2×10^{-4} cm^{-1} [377]. These data imply that the $V^{IV}O^{2+}$ ions and some $V^{IV}O$–L species may possibly be transported by transferrin even if Fe^{3+} and other metal ions are present, but whether efficient uptake of vanadium species attached to holo-HTF may indeed occur remains to be established.

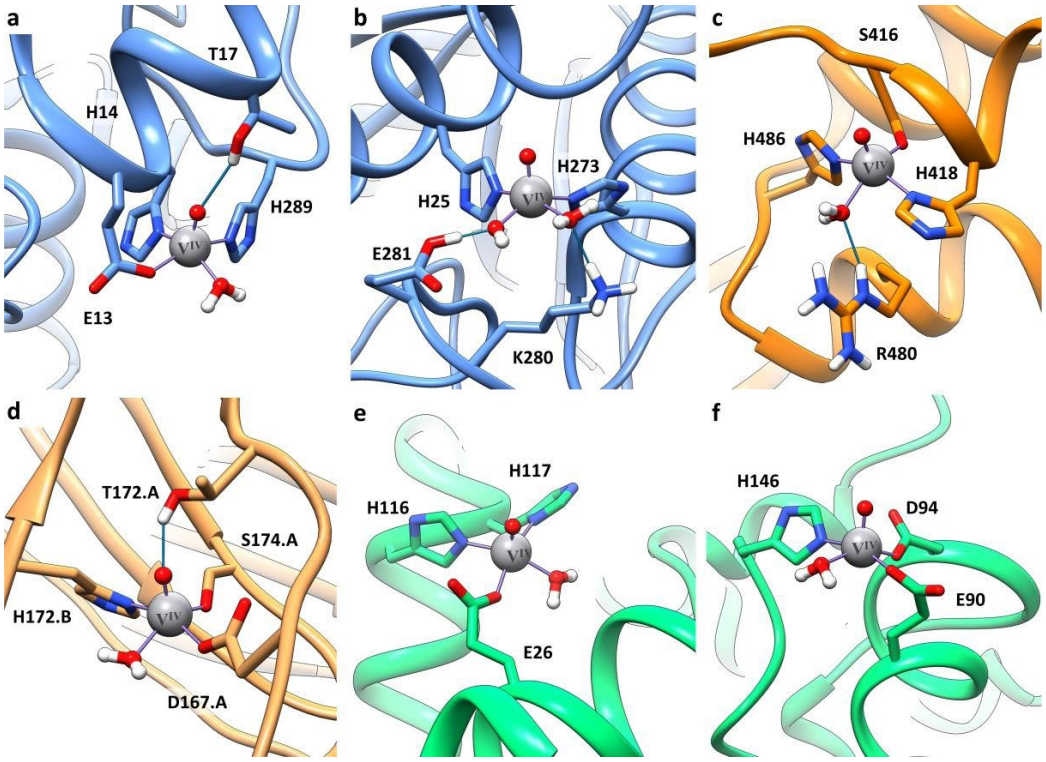

Fig. 11. Possible sites for binding of $V^{IV}O^{2+}$ to blood proteins: a-b) sites C^1 and C^2 of holo-HTF; c-d) sites 1 and 2 of IgG; e-f) sites β and γ of Hb. Adapted from ref. [24].

Table 1. Binding modes and energy and calculated and experimental $A_z(^{51}V)$ constants determined by computational methods for $V^{IV}O^{2+}$ binding to blood proteins.

Protein	Site	Donors [a]	F_{max} [b]	ΔE_{bind} [c]	$A_z(^{51}V)^{calcd}$ [d]	$A_z(^{51}V)^{exptl}$ [d,e]
HTF	C^1	**His14, His289, Glu13; H_2O**	66.0	-24.3	169.5	165.4
HTF	C^2	**His25, His273; H_2O, OH^-** [f]	38.8	-32.8	167.9	165.4
HTF	C^3	His473, Asp478; H_2O, H_2O [g]	37.6	-26.4	168.6	165.4
HSA	NTS-α	**His3, His9, Asp13, Asp255**	65.0	-31.7	163.7	162.9
HSA	NTS-β	His3, His9, Glu6; H_2O	54.7	-18.4	165.8	162.9
HSA	NTS-γ	His3, His9, Asp13; H_2O	53.0	-20.9	170.4	162.9
HSA	MBS_1	**His67, His247, Asp249; H_2O**	55.8	-26.2	165.2	166.4
HSA	MBS_2	**His67, His247, Asp249, Asn99-CO**	38.5	-32.9	169.5	166.4
IgG	1	**His172, Asp167, Ser174-O^-; H_2O**	75.0	-19.5	158.4	158.8
IgG	2	**His172, Asp167, Asp170, Asn138-NCO**	57.8	-31.8	165.8	163.6
IgG	3^1	**His189, Glu185, Glu185-CO; H_2O**	52.5	-26.2	171.0	167.4
IgG	3^2	**His460, Glu461, Asp399-CO; H_2O**	42.4	-23.5	172.3	167.4
Hb	β	**His146, Glu90, Asp94; H_2O**	40.2	-30.9	171.2	166.8
Hb	γ	**His116, His117, Glu26; H_2O**	61.3	-29.2	168.7	163.3

[a] The most plausible binding modes identified by docking and refined by QM are written in bold. [b] The value of GoldScore *Fitness* was obtained for the more stable pose of each *cluster*. [c] ΔE_{bind} in kcal/mol. [d] The absolute values of $A_z(^{51}V)$ are reported in 10^{-4} cm^{-1} units. [e] The values of $A_z(^{51}V)$ were calculated with DFT methods. [f] *cis* arrangement of H_2O and OH^- ligands. [g] *trans* arrangement of H_2O ligands.

Two alternative HTF binding modes were proposed for $V^{IV}O$–L complexes, with L being a bidentate monoanionic ligand: type 1 binding, possible for apo and holo forms, is based on the coordination of surface accessible residues of apo-HTF/holo-HTF as a *cis*-$V^{IV}OL_2$(apo-HTF/holo-HTF) moiety, and type 2 binding with a $V^{IV}OL^+$ moiety bound to free iron sites of apo-HTF [371, 375] (Fig. 12).

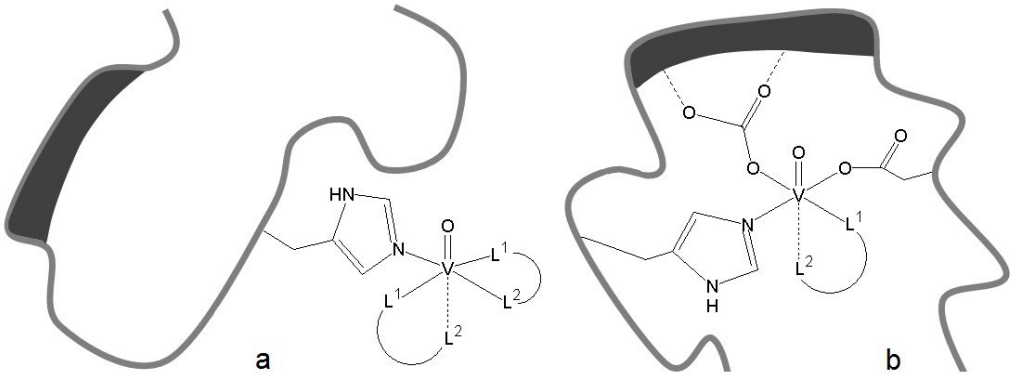

Fig. 12. Binding modes for $V^{IV}O$ complexes to HTF: (a) type 1 binding with the equatorial coordination of a His residue to *cis*-$V^{IV}OL_2$ moiety; (b) type 2 binding with $V^{IV}OL^+$ moiety in the Fe-binding site (the coordination of two among the residues Asp63, Tyr95, Tyr188, His249 is possible). L^1 and L^2 are the two donors of ligand L. Adapted from ref. [375].

By a combined CD and EPR study, the formation of $[V^{IV}O(L^1)$(apo-HTF)], $[(V^{IV}O)_2(L^1)$(apo-HTF)] and $[V^{IV}O(L^1)_2$(apo-HTF)] (L^1 = ma, dhp, mhcpe) was established and the conditional stability constants at pH 7.4 were calculated [67, 377]. Moreover, $[V^{IV}O(L^2)$(apo-HTF)], $[(V^{IV}O)_2(L^2)$(apo-HTF)] and $[(V^{IV}O)_2(L^2)_2$(apo-HTF)] (L^2 = lact, pic) and $[V^{IV}O$(cit)(apo-HTF)] (cit = citrate) were similarly studied [371]. In most of these species V^{IV} is coordinated to the residues belonging to the iron binding sites. The existence of type 2 binding is generally indicated by the strong CD bands recorded in the 400-900 nm range, only possible if at least two donor atoms from chiral moieties bind to V^{IV}. In the system with mhcpe, strong induced CD bands were detected in the 300-350 nm region, as well as modifications in the CD bands associated to Phe, and Trp bands of apo-HTF,

indicating that the $V^{IV}O$–mhcpe species binds in such a way that the ligand is closely surrounded by chiral residues [377].

The formation of $[V^{IV}OL_2]_n$–HTF adducts depends on the accessibility of coordinating side-chains on the protein surface. The comparison between $A_z(^{51}V)^{exptl}$ for $[V^{IV}OL_2]_n$–HTF and for $[V^{IV}OL_2(MeIm)]$ – with MeIm being 1-methylimidazole, a model for His-N coordination – indicates that the donors involved in V binding should belong to His residues [372, 378]. The possibility of formation of this type of $[V^{IV}OL_2]_n$–HTF adducts was verified by EPR and computational methods for the bis-chelated $V^{IV}O$ complex of nalidixato [379]. *Covalent* dockings into the *GoldScore* framework [43-45], revealed that apo-HTF has only His289 in the correct orientation to coordinate the *cis*-$[V^{IV}O(nal)_2]$ moiety (Fig. 13, a), while holo-HTF shows at least three His residues (His25, His349 and His606) (Fig. 13, b). Accessibility of the residues and strength of the secondary interactions (H-bonds and vdW contacts) are the key to explain the different complexing behavior of the surface histidine residues [379]. Overall, the adducts formed in solution can be described as $[VO(nal)_2]$–apo-HTF and $[VO(nal)_2]_3$–holo-HTF.

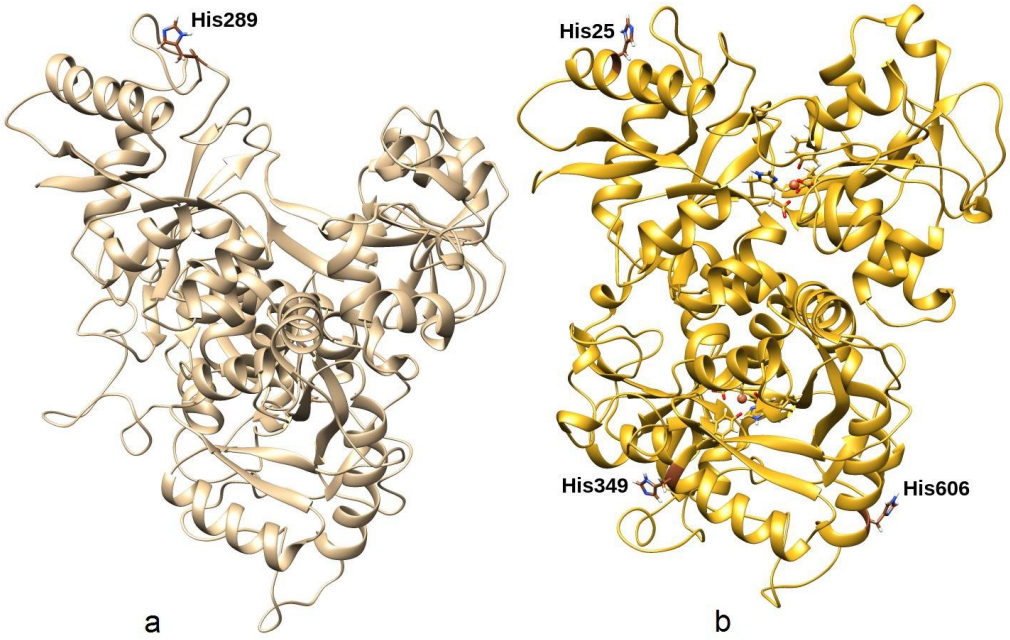

Fig. 13. The histidine residues involved in the *cis*-$VO(nal)_2$ moiety binding with: (a) apo-HTF and (b) holo-HTF. Adapted from ref. [379].

Partial hydrolysis of $[V^{IV}OL_2]$ may favor the formation of $[V^{IV}OL]$–HTF species. Kiss, Costa Pessoa and co-workers, through CD, EPR and other techniques demonstrated the formation of $[V^{IV}O(acac)]$–apo-HTF with the binding of $V^{IV}O(acac)^+$ to the Fe^{3+} sites and the involvement of Asp63, Tyr95 or His249 residues in a type 2 binding [68]. Type 2 binding was also demonstrated

for [V^{IV}OL]–apo-HTF (L = dhp, ma, pic, lactate, citrate and mhcpe) [67, 155, 371, 377], but without identifying the specific residues of the iron site involved.

Vanadate(V) binding to apo-HTF was studied by several techniques [22]. ^{51}V NMR spectroscopy, in particular, allowed the distinction of V^{V} bound to the two lobes of HTF [128, 130, 156]. In contrast with V^{III} and V^{IV}, V^{V} may bind HTF in the absence of any synergistic anion. Moreover, considerable amounts of V^{V} bound to HTF were found by both ^{51}V NMR and inductively coupled plasma spectroscopy (ICP) in solutions containing $(Fe^{III})_2$(HTF) and V^{V}-salts, indicating that part of V^{V} is bound to sites distinct from the iron binding ones [156]. Similar evidence was obtained by CD measurements in the Al^{III}/V^{V}/apo-HTF system, which suggested the co-existence of a V^{V}–HTF species and $(Al^{III})_2$(HTF) [156]. As mentioned above, while V^{V} binds to apo-HTF, the protein remaining in its open conformation, it can also bind to $(Fe^{III})_2$(HTF). Thus, besides uptake through anion channels, receptor-mediated endocytosis is also likely for the uptake of V^{V} by cells [156].

6.2. Albumins

Human serum albumin, the most abundant blood protein, has a mean concentration of 639.4 μM [363] and, with HTF, transports most essential metal ions and their compounds [380]. Moreover, HSA binds toxic metal ions, fatty acids (FAs), and endogenous and exogenous ligands [381]. The sites identified for the binding of medium- and long-chain FAs (from C10 to C18) with the highest affinity for HSA are FA2, FA4 and FA5, among the seven available ones (FA1-FA7) [255]. Human serum albumin contains several sites for metal ions: the *N*-terminal site (NTS), the preferential site for Cu^{2+} and Ni^{2+} ions [254, 255], the multi-metal binding site (MBS or site A), favored with Zn^{2+} and Cd^{2+}, plus unspecific sites B, the strongest for Co^{2+} and Mn^{2+} [255]. The involvement of Cys34, the only thiol group not involved in disulfide bridges, is limited to soft metal-containing species, for example gold and platinum compounds [382, 383].

Various studies were published about the interaction of $V^{IV}O^{2+}$ with HSA, with or without FAs (forms indicated here as HSA^{f} and HSA^{d}) [48, 66, 257, 371, 384-391]. With HSA^{f}, EPR spectroscopy suggested the presence, in an equimolar solution, of a dinuclear adduct in a triplet state (S = 1), $(V^{IV}O)_2{}^{D}(HSA^{f})$ where D stands for dinuclear, with a logβ value in the range 20.6-20.9 [372, 391]. When the $V^{IV}O^{2+}/HSA^{f}$ ratio is increased, one “strong” site (or VBS1) and several “weak” sites (VBS2) were proposed [384, 390, 391]; this multinuclear adduct, with S = 1/2 and the $V^{IV}O^{2+}$ ions not magnetically interacting, is indicated as $(V^{IV}O)_x{}^{M}(HSA^{f})$ where M means mononuclear [387-389, 391]. The mean value for the association constant of $(V^{IV}O)_x{}^{M}(HSA^{f})$ was calculated (logβ = 9.1) [372, 391]. EPR data indicated that the V coordination is not the same as for Cu^{2+} or Ni^{2+}, i.e. (NH_2, N^{-}, N^{-}, His-N) at the NTS [107].

EPR competition studies with Zn^{2+} and/or Ni^{2+} ions suggested a *primary* site located at the *N*-terminal site and a *secondary* one at multi-metal binding site; in fact, one equivalent of Cu^{2+} (or Ni^{2+}), that binds specifically at NTS, shifts $V^{IV}O^{2+}$ ion to the MBS [390, 391]. The two sites were characterized by an integrated spectroscopic/computational method based on: i) preliminary MD sampling of the structure of HSA using OpenMM engine [392] AMBER14SB force-field [393] used for standard atom types, while V bonds and angles force constants were DFT derived using MCPB.py [250] to identify stable conformations; ii) pattern recognition algorithms, using a preliminary version of BioMetAll [231] to find the motifs (His; His; Asp/Glu) pre-organized to bind $V^{IV}O^{2+}$; iii) docking simulations to obtain preliminary 3D structure; iv) full DFT/B3P86 cluster method to optimize the obtained structures; vi) calculation of the energy difference for the binding of $V^{IV}O^{2+}$ to HSA (ΔE_{bind}) and comparison of the predicted EPR parameters (at DFT/BHandHLYP level of theory) with the experimental values (Table 1) [107]. The results indicated that in the *N*-terminal region at least three binding modes are possible but the best one is (His3, His9, Asp13, Asp255), with ΔE_{bind} = -31.7 kcal/mol and $A_z(^{51}V)^{calcd}$ = 163.7×10^{-4} cm^{-1}, which agrees with $A_z(^{51}V)^{exptl}$ = 162.9×10^{-4} cm^{-1} (Fig. 14, b). Two potential $V^{IV}O^{2+}$ binding modes at the MBS site or site A with donors (His67, His247, Asp249; H_2O) and (His67, His247, Asn99-CO, Asp249) were revealed, with an equatorial position either occupied by a H_2O ligand or by the carbonyl-O of Asn99 (Fig. 14, a). These two sites, having comparable stability, should coincide with those named 'strong' by Chasteen [384] and VBS1 by Costa Pessoa [390].

The behavior of HSA^d and HSA^f significantly differs. In fact, FAs binding determines a rotation of subdomains IA and IIA and the dinuclear species $(V^{IV}O)_2{}^D(HSA^f)$ is formed, in which His67 and His247 cannot bind simultaneously the same metal ion, and a $\mu_{1,1}$-Asp249 bridges the two $V^{IV}O^{2+}$ ions with ferromagnetic coupling [107]. With HSA^f, the formation of mononuclear adducts at the MBS cannot take place due to the presence of FAs and the metal ions with a preference for this site (Zn^{2+} and Cd^{2+} besides $V^{IV}O^{2+}$) are forced to move to other available sites. In this case too, the combined spectroscopic and computational approach allowed to characterize four plausible binding modes, among which two are ferromagnetically coupled with $V^{IV}\cdots V^{IV}$ distances of 3.164 and 3.173 Å (Fig. 14, c), in good agreement with the distance obtained from the EPR data (~3.5 Å) [107].

The sites B, proposed previously in the literature, were not identified until a few months ago. They are *non-specific* and weaker than NTS and MBS [394-396], with the coordination of one His-N and one O-donor, like an Asp/Glu-COO^- or a carbonyl-O, and become populated with the increase of the $V^{IV}O^{2+}$/HSA ratio [107]. These sites, identified as 'weak' by Chasteen [384] and as VBS2 by Costa Pessoa [390], have $A_z(^{51}V)^{exptl}$ = 169.0×10^{-4} cm^{-1}. Probing with BioMetAll [231] the possible

sites with at least one His and one O donor with $V^{IV}O(H_2O)^{2+}$/$V^{IV}O(H_2O)_2^{2+}$ moieties, the adducts with the concomitant coordination of (His367, Glu313-CO), (His510, Asp512), (His338, Asp340), (His535, Glu531, Asn503-CO), (His288, Glu153), and (His128, Glu131) were identified, most of them found also in the XRD structure for Zn^{2+} ion [397].

Finally, sites C have only O-donors, from Asp/Glu-COO^- or backbone carbonyl-O, and are occupied only at acid pH [107].

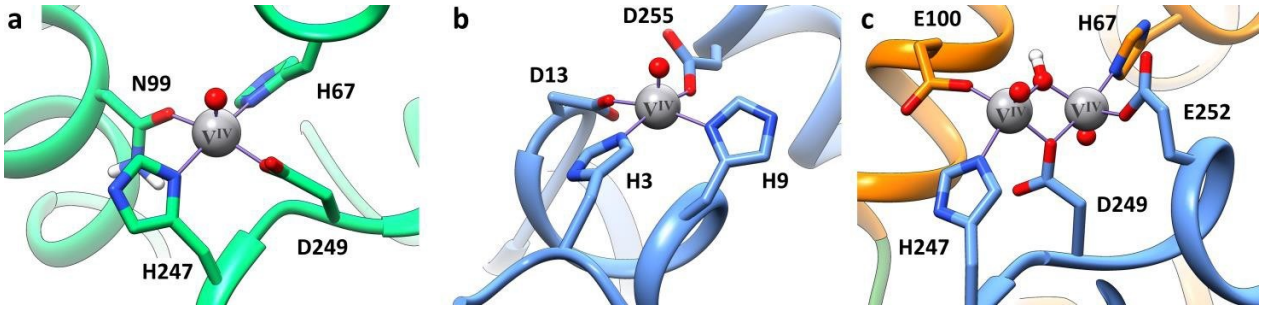

Fig. 14. Binding of $V^{IV}O^{2+}$ ion to HSA: a) MBS site of HSA^d; b) NTS site; c) dinuclear species $(V^{IV}O)^D_2(HSA^f)$ at the subdomain IA/IIA interface of HSA^f. The subdomains IA and IIA are shown in blue and orange, respectively. Adapted from ref. [107].

The binding properties of animal albumins may differ. The coordination of bovine serum albumin (BSA) is similar to that of HSA [390]. Instead, the presence of Tyr3 in place of His3 makes NTS unavailable for the metal coordination in porcine serum albumin (PSA), forcing vanadium to interact with the MBS [107]. Accordingly, the CD (and EPR) spectra somewhat differ for solutions containing $V^{IV}O^{2+}$ and HSA or BSA, or containing PSA [390]. When one equivalent of Zn^{2+} is added to these systems, it removes quantitatively $V^{IV}O^{2+}$ from MBS, since zinc is bound more strongly to PSA when compared to HSA and BSA [390, 398].

The interaction of V^V with HSA is weak and probably involves only surface carboxylic functions. ^{51}V NMR spectroscopy, fluorimetry and ultrafiltration experiments confirmed the weak interaction [128, 399]. Using ^1H STD NMR and docking studies it was shown that $[V^VO_2(dhp)(OH)(H_2O)]^-$ and $[V^VO_2(ma)_2]^-$ bind to HSA, preferentially at the drug site 1, named also Sudlow's site I or warfarin site [138]; more information on this site can be found in ref. [255].

HSA can interact with *cis*-$V^{IV}OL_2$ or $V^{IV}OL^+$ moieties, with accessible residues and His binding being favored. When the hydrolysis gives $[V^{IV}OL(H_2O)_2]^+$, two adjacent equatorial sites become available (Fig. 6, e). The CD spectra recorded for $[V^{IV}OL_2]$-protein systems in the visible range are typically much stronger for apo-HFT than for albumins, suggesting that the formation of $[V^{IV}OL]$–albumin species, where V^{IV} is bound to more than one residue (thus giving higher induction of

chirality), is less plausible than $[V^{IV}OL_2]$–albumin (with V^{IV} bound to only one amino acid residue). The sites involved in the binding could be the same found by dockings for $V^{IV}O^{2+}$ ion with concomitant (His-N, Asp/Glu-COO) coordination (see above). In studies of solutions containing HSA and several $[V^{IV}OL_2]$ complexes (L = ma, dhp, pic, hpno, where hpno is the deprotonated 2-hydroxypyridine-*N*-oxide), in most cases $[V^{IV}OL_2]$–HSA are formed, and the conditional formation constants at pH = 7.4 were calculated. Only for pic both $[V^{IV}OL_2]$–HSA and $[V^{IV}OL]$–HSA were found. The stability constant was also determined for 1-methylimidazole (MeIm), which was similar as that for HSA [372]. This is confirmed by the coincidence of $A_z(^{51}V)^{exptl}$ for several $[V^{IV}OL_2]_n$–HSA adducts and $[V^{IV}OL_2(MeIm)]$ [372, 378, 391]. For *cis*-$[V^{IV}O(nal)_2]$, the most exposed residues are His105, His367 and His510 [379].

Several studies on the binding of potentially therapeutic VCs to BSA have been published in the last ten years, some of them using fluorescence measurements. Both V^{IV} and V^{V} complexes were examined. Here we are providing only a part of the references [39, 58, 60-64, 68, 72-88]. 3D fluorescence has also been used to gain further insight into these systems [60, 64]. Fluorescence emission properties of BSA are provided mainly by two Trp residues: Trp134, on the surface of domain IA, and Trp212, located in the hydrophobic pocket of domain IIB, which dominates the emission [70]. Recently also HSA was evaluated in studies based on the same principles [400]. The conditional association constants *K*, calculated from fluorescence quenching data, go from 10^2 to 10^{12} and the number *n* of sites is in the range ~0-3 (see eq. 2). The major limitation and errors associated with these measurements is that the fluorescence is generally attributed to the parent species dissolved in solution, e.g. a $[V^{IV}OL_2]$ complex, while – as highlighted by some of us [31, 39, 68] – several species could be formed after biotransformation and simultaneously contribute to the experimental emission. For example, in the case of $[V^{IV}O(phen)_2]^{2+}$, it was shown that in the typical conditions used to measure the fluorescence spectra (albumin and complex concentrations below 20 μM), the added $[V^{IV}O(phen)_2]^{2+}$ does not exist and $V^{IV}O^{2+}$ is mostly hydrolyzed or bound to albumin [31, 39].

BSA is contained in fetal bovine serum (FBS), used in mammalian cell culture media for cytotoxicity studies. Typically 10% FBS is used, corresponding to BSA *ca*. 40 μM [37, 401]. This protein may act as a ligand to V^{IV}, totally or partly displacing L upon adding a $[V^{IV}OL_2]$ complex to the cell media. Recently, the stability in cell culture media was examined and the cytotoxicity determined for several human cancer cell lines at different incubation times for $[V^{IV}O(phen)_2(SO_4)]$, $[V^{IV}O(Me_2phen)_2(SO_4)]$ (Metvan, with Me_2phen = 4,7-dimethyl-1,10-phenanthroline), and $[V^{IV}O(amphen)_2(SO_4)]$ (amphen = 5-amino-1,10-phenanthroline). It was found that $V^{IV}O^{2+}$ primarily binds to BSA, while only at V concentrations higher than ~40 μM, when BSA is not

enough to strongly bind the $V^{IV}O^{2+}$ ions, $V^{IV}O$–phen species become relevant [39]. For these and many other $V^{IV}O$ systems, a significant amount of VCs decompose, particularly at low concentrations, and V^{IV} may also undergo oxidation to V^{V}, with the additional consequence that a part of the ligands are free in solution. Therefore, we highlight that the mechanism of cytotoxic action cannot be proposed without taking into consideration the speciation taking place, as a mixture of several V-containing species could be present [31, 39].

6.3. Immonuglobulins

Immunoglobulins are glycoproteins which react with an immune response to foreign pathogens present in an organism and are grouped into the classes IgA, IgD, IgE, IgG and IgM. 75% of immunoglobulins is represented by IgG, a "Y"-shaped protein with a mass of *ca*. 150 kDa and a mean concentration in blood of 101.0 μM [363]. Therefore, they can contribute to the transport of vanadium in the serum together with HTF and HSA. The binding of $V^{IV}O^{2+}$ to IgG was demonstrated [402]: EPR spectra indicate that $V^{IV}O^{2+}$ ion distributes among three donor sites characterized by $A_z(^{51}V)^{exptl}$ of 158.8×10^{-4} cm^{-1} (site 1), 163.6×10^{-4} cm^{-1} (site 2) and 167.4×10^{-4} cm^{-1} (site 3) [402]. The high $A_z(^{51}V)$ for sites 2 and 3 suggests the coordination of one His-N plus a number of Asp/Glu-COO^{-}, while the low value for site 1 indicates the presence of strong donors, like Tyr-O^{-}, Ser/Thr-O^{-} or Cys-S^{-}. Ser and Thr residues are present on the protein surface, mainly in the fragment antigen binding region (Fab, located on the arms of the "Y"), where their number is much higher than Tyr and Cys [403].

The identification of the binding sites was obtained only recently using the computational procedure described in section 3 [23]. Docking analysis allowed predicting four potential sites with three donors, located mainly at the interface C_H1/C_L region of the Fab domain. The values of F_{max} are very high, while ΔE_{bind} are negative and $A_z(^{51}V)^{calcd}$ are comparable to the experimental values. Site 3 can be explained with the two docking solutions found at the C_L chain of the Fab region or at the C_H3 of the fragment crystallizable region (Fc), i.e. the base of the "Y" involved in modulating immune cell activity. The binding site consists of one His-N, one Glu-COO^{-} and one Asp/Glu-CO, and a H_2O ligand in the remaining equatorial plane. The coordination mode is (His189, Glu185, Glu185-CO; H_2O) or (His460, Glu461, Asp399-CO; H_2O) and is indicated with 3^1 and 3^2 in Table 1.

Sites 1 and 2 are not independent (Table 1). Site 2 is based on the *coordinative* binding (His172, Asp167, Asp170, Asn138-NCO) with Ser174 and Thr172 involved in a H-bond with V=O (Fig. 11, c). Site 1 is generated from site 2 upon the deprotonation of Ser174 with alcoholate-O^{-} which replaces Asp170-COO^{-} (Fig. 11, d). The binding of Ser174-O^{-} accounts for $A_z(^{51}V)^{exptl}$ lower than

160×10^{-4} cm^{-1}, an unusually low value for a V-protein (see section 2.4). At pH 7.4, sites 1 and 2 are in equilibrium and both occupied.

The formation of $[V^{IV}OL_2]_n$–IgG adducts was detected by EPR spectroscopy, at mM concentrations, for *cis*-octahedral species of maltolate, ethylmaltolate, kojate (koj), picolinate and dhp [378, 402, 404]. In these systems, the binding should occur again in non-specific manner through histidine residues accessible on the protein surface, and their number *n* determines how many $V^{IV}OL_2$ moieties are bound to the protein. The number of exposed His residues for IgG is 16 [403]. The non-specific His binding was confirmed by comparison of the stability constants of $[V^{IV}OL_2]_n$–IgG, determined by EPR, with that of the model complex *cis*-$[V^{IV}OL_2(MeIm)]$, determined by pH-potentiometry. For example, logβ is 19.6 for $[V^{IV}O(ma)_2]_n$–IgG (19.12 for $[V^{IV}O(ma)_2(MeIm)]$), 19.8 for $[V^{IV}O(ema)_2]_n$–IgG (19.32 for $[V^{IV}O(ema)_2(MeIm)]$), and 17.6 for $[V^{IV}O(koj)_2]_n$–IgG (17.40 for $[V^{IV}O(koj)_2(MeIm)]$) [378, 404]. At concentrations in the range of μM, hydrolysis could give also $[V^{IV}OL(H_2O)_2]^+$, whose interaction with IgG should result in the formation of adducts with composition $[V^{IV}OL]_n$–IgG (see Fig. 6, e).

6.4. Hemoglobin

The iron containing protein hemoglobin (Hb) transports molecular oxygen in all the vertebrates [363]. For humans, Hb is a tetramer which consists of two α and two β subunits, structurally similar; each one is composed of 141 and 146 amino acid residues, respectively. In the red blood cells (RBC), Hb has a concentration of 5.3 mM [363]. The uptake by red blood cells was substantiated for several vanadium complexes [405-411], and in the cytosol a significant fraction of V species interacts with hemoglobin [40, 412-415]. This can completely or in part inactivate the V drugs, except when these are expelled from RBC before reaching the target organs. Experimental studies show that, inside the erythrocytes, $V^{IV}O^{2+}$ ion is primarily bound to Hb. EPR spectra at pH 7.4 allowed to demonstrate the presence of two sites, with $A_z(^{51}V)^{exptl}$ of 163.3×10^{-4} cm^{-1} (site γ) and 166.8×10^{-4} cm^{-1} (site β) [412]. Applying the "additivity relationship" [95, 97], the binding of two Asp/Glu and one His, respectively, was inferred. Through an integrated docking/DFT/QM approach, the most plausible binding regions were explored, ΔE_{bind} computed, and spin Hamiltonian EPR parameters were calculated for the coordination sites [23]. The results suggested that Hb has two potential sites (Table 1 and Fig. 11, e-f): the first site is based on the coordination mode (His116, His117, Glu26; H_2O) and the second one on (His146, Glu90, Asp94; H_2O). These sites were named γ (two His-N coordinated to V) and β (one His-N). Notably, for site γ, three different positions of the V=O bond with respect to the side-chain donors were predicted. The bond distances of the QM refinement for the two sites are in the range 2.06-2-16 Å (V–N_{His}), 1.94-1.99 Å (V–

$O_{Asp/Glu}$), 2.08-2.09 Å ($V–O_{water}$), coherent with those expected for vanadium complexes [57]. The values of ΔE_{bind} for the formation of the two adducts suggested that the stability of the sites β and γ is similar (-30.9 and -29.2 kcal/mol), in good agreement with the comparable EPR intensity detected at pH 7.4. Furthermore, the order of $A_z(^{51}V)^{calcd}$, γ < β, is in line with the experimental data.
When red blood cells are incubated with $[V^{IV}OL_2]$ compounds with potential pharmacological activity, $V^{IV}O^{2+}$ ions distribute among $(V^{IV}O)(Hb^{\beta})$ and $(V^{IV}O)(Hb^{\gamma})$, mixed species with composition $V^{IV}O–bL$ (bL indicates a bioligand, in this case from cytosol of RBCs) and adducts as $V^{IV}O–L–Hb$. At high concentrations (> 100 μM), when $[V^{IV}OL_2]$ survives in part in solution, *cis*-VOL_2 moieties can bind through the equatorial site with accessible His residues, 26 for Hb [416] (Fig. 6, c). When the geometry of $[VOL_2]$ is square pyramidal, as for acetylacetonate, the interaction is weak or negligible in the apical position (Fig. 6, d). When its concentration is low (1-50 μM), the relative amount of VOL^+ fragments increases and the coordination mode is that of the adducts represented by the structures e (bidentate ligands) or f (tridentate ligands) in Fig. 6.
When RBC are incubated with $[V^{V}O_2L_2]$ complexes, for example formed by dhp or pic derivatives, reduction occurs inside the cytosol and $V^{IV}O^{2+}$ ion interacts with Hb and bLs [417]. Among the possible reductants, L-ascorbic acid is more effective than GSH and NADH [417, 418]. The formation of $(V^{IV}O)(Hb^{\beta})$, $(V^{IV}O)(Hb^{\gamma})$, $V^{IV}O–bL$, $[V^{IV}O(pic/dhp)]_n–Hb$ and $[V^{IV}O(pic/dhp)_2]_n–Hb$ was demonstrated by EPR spectroscopy. Interestingly, another mixed species with possible formula *cis*-$V^{IV}O(pic/dhp)_2(RS^{–})$ was detected, but up to now it is not clear if the $S^{–}$ donors come from GSH or another thiol or from a membrane protein [417].

7. Vanadium binding to other physiologically relevant proteins

Lysozyme, myoglobin, ubiquitin and cytochrome *c* (Cyt) have been recently examined, both for their physiological role and as models to study the binding of VCs to proteins. In fact, the moderate size, small number of binding sites, high conformational stability and commercial availability with high purity make them ideal systems to study by instrumental and computational techniques [32, 51]. Other examples, namely chymotrypsin, have been also characterized over the years [243].

7.1. Lysozyme

Lysozyme (Lyz) is an antimicrobial enzyme, with 129 amino acids, structurally stable and suitable for spectroscopic, spectrometric and structural studies [419, 420]. It contains a single histidine (His15) plus various carboxylate donors which may interact with metal species [51].

The interaction of any VC with a protein depends on the geometry and thermodynamic stability of the latter, and the existence of suitably positioned donor atoms in the biomolecule. For *cis*-$[V^{IV}O(pic)_2(H_2O)]$ the formation of an adduct was demonstrated through XRD characterization, with *cis*-$V^{IV}O(pic)_2$ moiety coordinated by the side-chain carboxylate group of Asp52 [69] (Fig. 6, c). This coordination mode was rationalized by *coordinative* docking performed by Gold software, QM/MM calculations and NCI analysis [45]. Briefly, after exploring the protein space with pattern recognition algorithm set for searching putative binding regions, docking simulations were carried out with the updated *GoldScore* SF [43-45] using the full DFT/B3P86 optimized structures of the Δ and Λ isomers of *OC*-6-$V^{IV}O(pic)_2(H_2O)$ complex and replacing the H_2O ligand by a fictitious hydrogen for *coordinative* docking assays. The enantiomeric selectivity of this binding site was examined, showing that only *OC*-6-23-Δ can effectively bind to Asp52 side-chain carboxylate. The preference for Asp52-COO^- over His15-N was confirmed, by demonstrating that the latter residue is not sufficiently exposed on the protein surface. Therefore, other factors, besides the basicity, determine the formation of the metal adduct (section 4). Similar results were obtained in aqueous solution for maltolate. The $A_z(^{51}V)^{exptl}$ value of *cis*-$V^{IV}O(ma)_2$-Lyz (167.6×10^{-4} cm^{-1}), halfway between *cis*-$[V^{IV}O(ma)_2(H_2O)]$ (170.8×10^{-4} cm^{-1}) and *cis*-$[V^{IV}O(ma)_2(MeIm)]$ (164.6×10^{-4} cm^{-1}), suggests that Lyz binds V^{IV} with a O-carboxylate donor from an Asp/Glu, and not with a His residue [45]. Dockings found that the two side-chains involved in the metal binding could be Asp52 or Glu35, even though for steric reasons the simultaneous coordination of Asp52 and Glu35 to the moiety $V^{IV}O(ma)_2$ is not possible.

To assess whether there are other sites in addition to Asp52, ESI-MS and EPR data were recently collected on the system containing the equilibrium mixture $[V^{IV}O(nal)_2]/[V^{IV}O(nal)_2(H_2O)]$ and lysozyme at various molar ratios, and integrated with a computational methodology (sections 3 and 4). The results indicated that at least two *cis*-$V^{IV}O(nal)_2$ moieties, with an equatorial accessible site, interact through a *coordinative* binding. The most plausible candidates for the *covalent* interaction are Asp52 and Asp87, which bind preferentially the moieties *OC*-6-32-Λ and *OC*-6-34-Λ. Among them, Asp52 has the highest affinity, confirming the results obtained with picolinate [25]. When the ratio is higher than 2, two-three additional fragments can interact in a *non-covalent* manner with non-specific sites; the square planar species *SPY*-5-13 and *SPY*-5-12 interact more favorably, compared to *OC*-6 isomers, due to an increased stabilization by a H-bond network with Tyr, Arg, Lys and Ser residues (see Fig. 5) [25].

EPR spectra of the system with *cis*-$[V^{IV}O(hqs)_2(H_2O)]^{2-}$ confirmed that His15 is not involved in the coordination of *cis*-$V^{IV}OL_2$ moieties and that H_2O ligand is replaced by Asp and Glu residues to give $[V^{IV}O(hqs)_2]_n$–Lyz, with n = 1-2 [179].

The coordination behavior changes significantly for [$V^{IV}OL(H_2O)$] complexes formed by tridentate (O^-, N, O^-) aroylhydrazone ligands. Differently from *cis*-octahedral species, the most stable adducts are formed after the coordination of His15, which replaces the water ligand. This was explained assuming that His15 is not completely exposed on the surface of the protein and the steric hindrance of the second anionic ligand with equatorial-axial arrangement in *cis*-$V^{IV}OL_2$ hinders the interaction with vanadium. Instead, the $V^{IV}OL$ fragments of tridentate ligands are less hindered and the approach of His15 is possible [42]. The coordination is shown in Fig. 6, f.

When the geometry of $V^{IV}O$ complex is square planar the interaction in the apical site may be weak or absent (adduct d of Fig. 6). Computational approaches (docking and DFT) established that only the *non-covalent* binding should be considered for [$V^{IV}O(acac)_2$]. In the site with highest affinity a H-bond between the V=O and Trp63-NH, and a weak axial contact of carbonyl-O of Ala107 with V were predicted. Notably, a competition between these two contacts is expected: when the strength of the axial interaction with Ala107 increases, the strength of the contact of V=O with Trp63 decreases and *vice versa* [99, 177]. Two stable binding modes were obtained by DFT: in the first mode V=O···HN–Trp63 is 2.029 Å and V···OCN–Ala107 is 3.370 Å (Fig. 15, a), while in the second one V=O···HN–Trp63 is 1.644 Å and V···OCN–Ala107 is 3.875 Å (Fig. 15, b) [177].

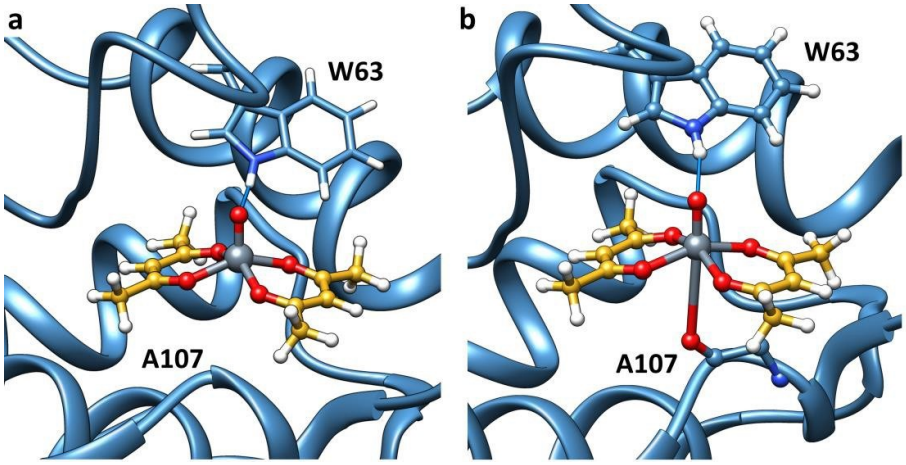

Fig. 15. Most stable sites predicted by docking methods for the *non-covalent* binding of [$V^{IV}O(acac)_2$] to Lyz: (a) V=O···HN–Trp63 = 1.644 Å and V···OCN–Ala107 = 3.875 Å (residue not shown); (b) V=O···HN–Trp63 = 2.029 Å and V···OCN–Ala107 = 3.370 Å. The H-bond with Trp63 is indicated with the full blue line. The one letter code for amino acids was used. Adapted from ref. [177].

The strength of the *non-covalent* binding on the protein surface has been monitored by EPR spectroscopy at room temperature for the [$V^{IV}OL_2$] complexes of flavonoids [99]. Molecular

dockings studies assessed that the strength and type of interaction is determined by OH or CO groups on the flavonoid structure that form H-bonds with the polar groups of the protein. The regions of the Lyz surface with stronger interactions are close to the active site, i.e. the large cleft where the bacterial carbohydrate chain binding takes place [421, 422]. On the basis of the docking results, only polar residues are involved in the interactions, in particular Arg, Trp, Ser, Asn, Gln, Asp and Glu [99]. The order of binding strength, obtained by a combined approach of spectroscopic and computational methods, is: $[V^{IV}O(que)_2]^{2-}$ (3 OH and 1 CO free groups) ~ $[V^{IV}O(mor)_2]$ (4 OH) > $[V^{IV}O(7,8\text{-dhf})_2]^{2-}$ (1 CO) > $[V^{IV}O(chr)_2]$ (1 OH) ~ $[V^{IV}O(5\text{-hf})_2]$ (0 groups), where que indicates quercetin, mor morine, 7,8-dhf 7,8-dihydroxyflavone, 5-hf 5-hydroxyflavone, and chr chrysin. For $[V^{IV}O(chr)_2]$ and $[V^{IV}O(5\text{-hf})_2]$ the transition from a *rigid limit* to an *isotropic* spectrum occurs [99]. Therefore, in these systems, a dynamical equilibrium between different binding sites with $V^{IV}O$–flavonoid species is reached, involving both bound (giving a *rigid limit* EPR experimental spectrum) and unbound V-moieties (which, being free to rotate, give a *slow tumbling* or an *isotropic* spectrum).

Non covalent binding was demonstrated for $[V^{V}O_2L]^-$ and non-oxido $[V^{IV}L_2]$ complexes formed by tridentate (O^-, N, O^-) aroylhydrazones incorporating naphthalene moieties. The interaction is stabilized by various H-bonds, namely between NH of Trp62 and Trp63, NH_2 of Arg112, CO of Asn109, and COO^- of Asp52 with the phenolic function of the ligand. Interestingly, only the hydroxo derivative with a non-coordinating OH group on the phenyl ring, and not that with NH_2, form strong H-bonds with lysozyme [42].

ESI-MS spectra of the systems with maltol, acetylacetone, picolinic acid and dhp, with a V concentration is in the range 15-150 μM and pH values in the range 5-6, indicated that the formation of $[V^{IV}OL]_n$–Lyz adducts is preferred with ma and acac, and that these coexist with $[V^{IV}OL_2]_n$–Lyz in the systems with pic and dhp. Considering the distribution of $V^{IV}O$ species determined by the stability constants, the formation of $[V^{IV}OL_2]$ species is favored at 15 μM with pic and dhp, while with maltol and acetylacetone $[V^{IV}OL(H_2O)_2]^+$ is the major species in solution. When the VCs concentration is 150 μM, the amount of $[V^{IV}OL_2]$ increases in comparison with $[V^{IV}OL]^+$, and both $[V^{IV}OL_2]$–Lyz and $\{[V^{IV}OL] + [V^{IV}OL_2]\}$–Lyz adducts were detected in the mass spectra.

For $[V^{IV}OL]_n$–Lyz adducts, the interaction with two equatorial and one apical site, is possible of (Fig. 6, e). With $V^{IV}O(acac)^+$, the *in silico* predictions indicated that four sites are available. Among the residues 44-52, one or two $V^{IV}O(acac)^+$ can bind to sites named **A** with (NCO, COO^-) coordination and affinity order (Asn46, Asp48) > (Asn46, Asp52) ~ (Asn44, Asp52) [177]. Another site (**B**) is present in the *N*-terminal region with the coordination of His15 and a H_2O molecule plus

a H-bond between V=O and Thr89. The third and fourth sites are weaker and are based on the coordination of (Asp18, Asn19) (site **C**) and (Asp119, Gln121) (site **D**) [177].

$[V^{V}O_2(acac)_2]^-$ is stable only at high V concentration (around some mM), but not when it is in the order of μM. Therefore, in the ESI spectrum of $[V^{V}O_2(acac)_2]^-$ and Lyz, recorded with protein concentrations from 5 to 50 μM, a series of signals of the adducts formed by 1, 2 and 3 $V^{V}O_2^+$ ions were detected, and dockings suggested three sites with a distorted trigonal bipyramidal environment with (Asn46, Asp52, Asn59), (His15, Asp87; H_2O) and (Asp18, Asn 19; H_2O) coordination [177].

7.2. Myoglobin

Myoglobin (Mb) is a protein, present in heart and skeletal muscles with O_2 storage function. It is a polypeptide with 153 amino acids and a heme moiety, and accounts for 5-10% of all the cytoplasm proteins found in the muscle cells [363, 423]. At physiological conditions, 70% of Mb is constituted by eight alpha helices (A-H) which generate a globular structure with heme group inserted in a cleft at helices C-F [424].

EPR results suggested that $V^{IV}O^{2+}$ interacts with at least two sites with $A_z(^{51}V)^{exptl}$ of 163.8×10^{-4} cm^{-1} and 167.0×10^{-4} cm^{-1} [178]. In analogy with Hb [412, 425], they were named γ (2 His bound to V^{IV}) and β (1 His). The γ site shows the coordination (His24, His119, Asp20; H_2O) with a square pyramidal structure. For site β there are two possibilities (β_1 and β_2): the first has the donor set (His82, Glu83, Asp141; H_2O), while the second (His81, Glu83, Gly80-CO; H_2O). The values of ΔE_{bind} obtained by DFT cluster method are -31.7 kcal/mol for γ, -31.9 kcal/mol for β_1, and -29.1 kcal/mol for β_2. The order of binding affinity for the three sites is $\gamma \sim \beta_1 > \beta_2$, thus sites γ and β_1 will populate before β_2 [178].

The binding of $[V^{IV}OL_2]$ complexes depends on the ligand features. With a moderate strong ligand, such as dhp, adducts $[V^{IV}O(dhp)]$–Mb, $\{[V^{IV}O(dhp)] + [V^{IV}O(dhp)_2]\}$–Mb, $[V^{IV}O(dhp)_2]_n$–Mb with n = 1-2 were observed by ESI-MS and EPR. EPR measurements were recorded as a function of $[V^{IV}O(dhp)_2]$/Mb to evaluate the number of $V^{IV}O(dhp)_2$ moieties interacting with the protein. From Fig. 16 it emerges that, up to the ratio 2, the resonances of the adducts $[V^{IV}O(dhp)_2]_n$–Mb (**II**), analogous to the model *cis*-$[VO(dhp)_2(MeIm)]$ (**III**), are detected, suggesting the coordination of two His-N. When more than two equivalents are added to the solution, the *cis*-$V^{IV}O(dhp)_2$ moiety does not find other His residues suitable for metal coordination and the bis-complexes $[V^{IV}O(dhp)_2]$ (**Ia**) and *cis*-$[V^{IV}O(dhp)_2(H_2O)]$ (**Ib**) are formed [178].

After exploring the protein space searching for putative binding regions, *coordinative* docking simulations were carried out on the Δ and Λ isomers *OC*-6 and A and C of *SPY*-5. The results established that, among the potential donors His81, His113, His116, and His119, only His81 and

His113 are accessible for *cis*-$V^{IV}O(dhp)_2$ fragment with F_{max} = 45.3-49.4, in agreement with EPR data. For the $V^{IV}O(dhp)^+$ moiety, favored at low V concentration, three sites were found with the following affinity order: (His24, His119) > (His82, Asp141) > (Glu83, Asp141), Fig. 17.

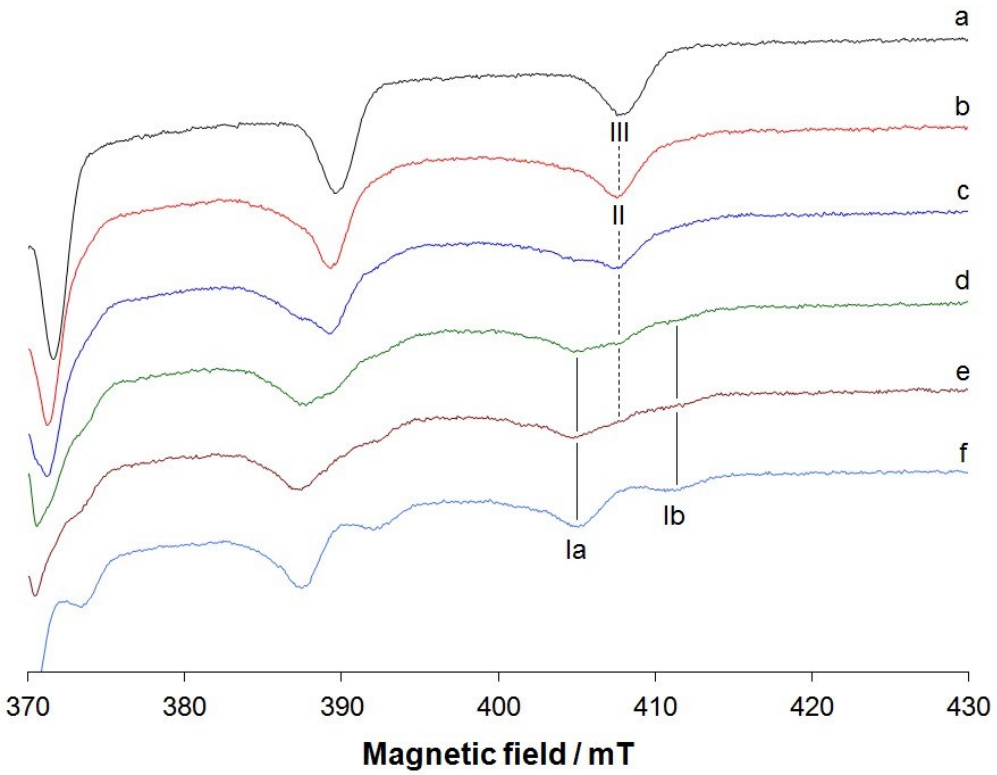

Fig. 16. High field region of the X-band anisotropic EPR spectra recorded at 120 K on the systems containing: a) $V^{IV}O^{2+}$/dhp/MeIm 1/2/4; b) $V^{IV}O^{2+}$/dhp/Mb 1/2/1; c) $V^{IV}O^{2+}$/dhp/Mb 2/4/1; d) $V^{IV}O^{2+}$/dhp/Mb 4/8/1; e) $V^{IV}O^{2+}$/dhp/Mb 6/12/1; f) $V^{IV}O^{2+}$/dhp 1/2. $V^{IV}O^{2+}$ concentration 1.0×10^{-3} M. The M_I = 7/2 resonances of $[V^{IV}O(dhp)_2]_n$–Mb are indicated with **III** and dotted line, of the model *cis*-$[V^{IV}O(dhp)_2(MeIm)]$ with **II** and of the bis-complexes $[V^{IV}O(dhp)_2]$ and *cis*-$[V^{IV}O(dhp)_2(H_2O)]$ with **Ia** and **Ib** and full lines. Adapted from ref. [178].

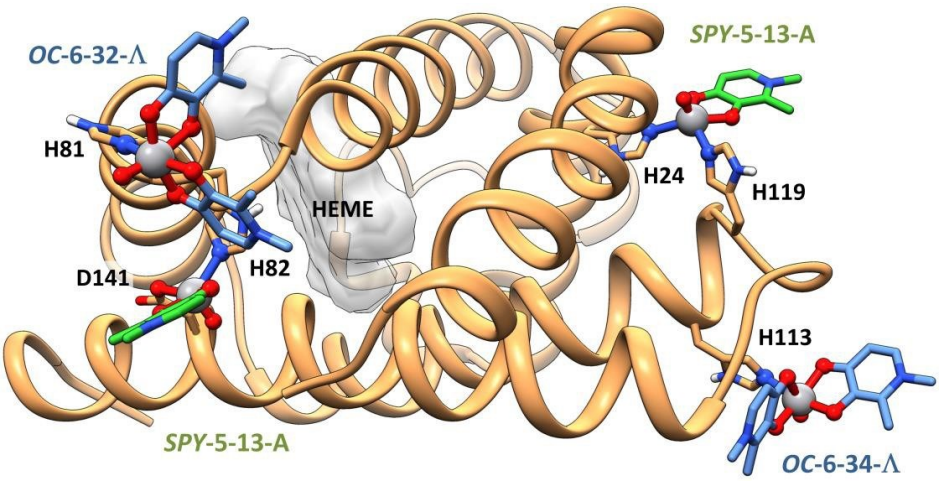

Fig. 17. Most stable coordination sites predicted by docking methods for the interaction of *cis*-$V^{IV}O(dhp)_2$ moiety with Mb at His 81 and His113, and of $V^{IV}O(dhp)^+$ with (His24, His119) and (His82, Asp141) couples of donors. The one letter code for amino acids was used. Reproduced from ref. [32] by permission of The Royal Society of Chemistry.

In contrast, when *cis*-$V^{IV}O(mim)_2$ moiety is examined, all four His residues could interact with V. The reason is in the formation of several H-bonds between the free amino group of L-mimosinate and polar residues of Mb (in particular, Lys79 and Glu83), not expected for *cis*-$V^{IV}O(dhp)_2$. Notably, His113, His116, and His119 were considered the candidates for the binding to Mb of the cisplatin and transplatin hydrolysized products, *cis*-$[Pt^{II}(NH_3)_2(H_2O)_2]$ and *trans*-$[Pt^{II}(NH_3)_2(H_2O)_2]$ [426, 427].

With weaker ligands, like maltolato and acetylacetonato, the hydrolysis favors the interaction of the $V^{IV}OL^+$ moiety. At pH 4.8 the two sites assessed by computational methods, are (Glu83, Asp141) and (Glu105, Asp109), which replace the H_2O molecules coordinated in two contiguous equatorial positions (Fig. 6, e). At pH 6.2, with the deprotonation of His, two other binding modes were identified: (His82, Asp141) which derives from that at lower pH after replacement of Glu83 with His82, and (His24, His119), see Fig. 17 for the position of these couples. So, three potential sites for $V^{IV}OL^+$ emerge: (Glu83; Asp141)/(His82; Asp141), not independent between each other, (Glu105; Asp109) and (His24; His119).

A general picture of the Mb binding sites is given in Fig. 18, where the residues involved in the interaction with *cis*-$V^{IV}OL_2$, $V^{IV}OL^+$ or $V^{IV}O^{2+}$ are explicitly represented. Comparing the data obtained by spectrometric/spectroscopic/computational approaches, it results that the number of *cis*-$V^{IV}OL_2$ moieties able to interact with Mb is larger than $V^{IV}OL^+$ or $V^{IV}O^{2+}$, since His residues bind independently as long as they are exposed on the protein surface. In contrast, only three binding sites are possible for the interaction of $V^{IV}OL^+$ or $V^{IV}O^{2+}$ because two or three neighbouring residues must interact simultaneously with vanadium.

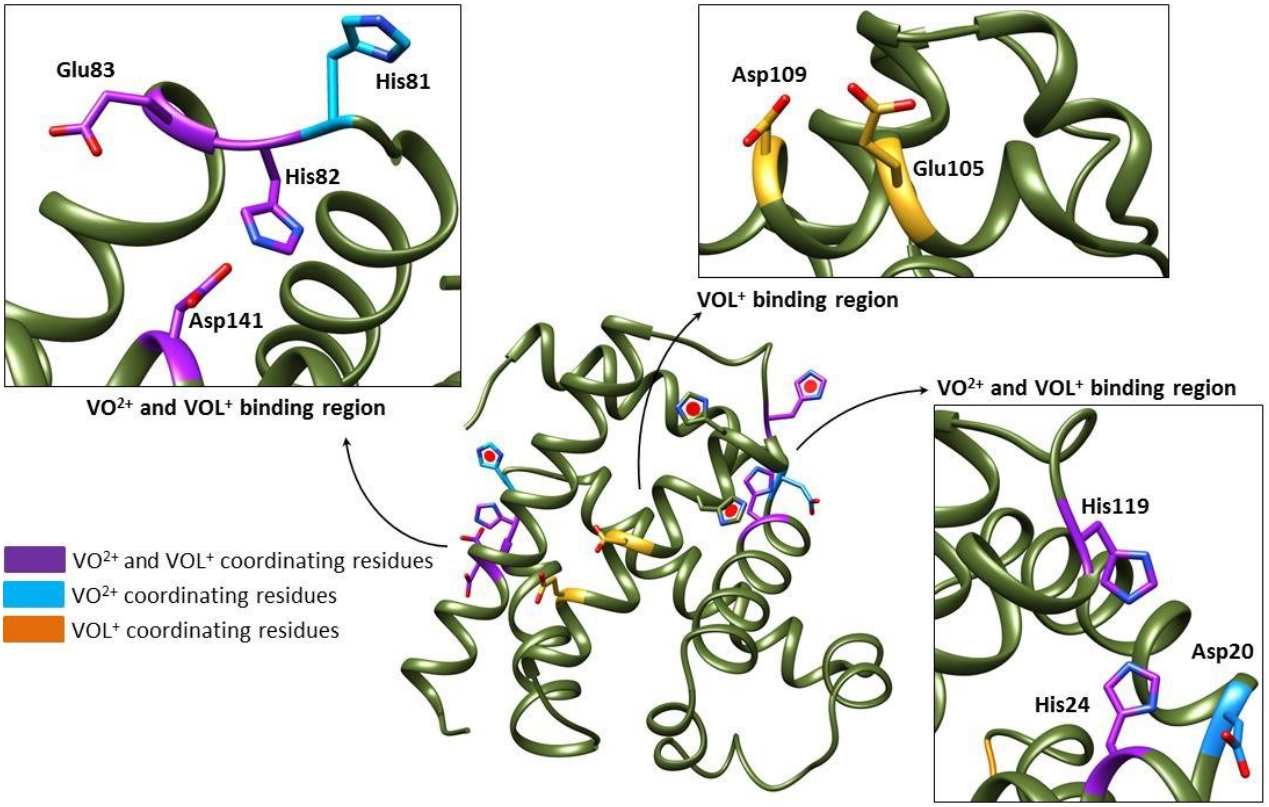

Fig. 18. Representation of Mb binding sites. The residues involved in the coordination are explicitly shown. The histidine residues that bind *cis*-$V^{IV}OL_2$ are depicted with the red disks. Reproduced from ref. [178] by permission of The Royal Society of Chemistry.

7.3. Ubiquitin

Ubiquitin (Ub) is a protein with 76 amino acids and a molecular mass of 8.5 kDa. Ub is involved in the ubiquitination, a post translational modification with a regulatory role in the cellular processes [428]. It contains a low number of metal binding sites, among them the *N*-terminal methionine (Met1), one histidine (His68) and various carboxylate O-donors [50].

For $V^{IV}O^{2+}$ ions, EPR and docking results suggested the presence of three binding sites (named **1**, **2** and **3**). Integrating the spectroscopic information in the computational framework, sites **1** and **2** were identified with (Glu16, Glu18) and (Glu24, Asp52), while that indicated with **3** includes His68 plus the backbone O-carbonyls of Thr7 and Leu69. The same sites were ascertained for vanadium(V), for which ESI-MS proved that three $V^{V}O_2^{+}$ ions can interact with the protein; sites **1** and **2** are characterized by a distorted trigonal bipyramidal environment around V^{V}, while **3** involves the coordination of His68, stabilized by a V^{V}=O···H_3N^{+}–Lys6 H-bond (Fig. 19) [177]. These adducts become important when the V-based drug concentration reaches very low values, around few μM; for example, with $[V^{V}O_2(acac)_2]^{-}$ hydrolytic processes favor the dissociation of the complex with formation of $[V^{V}O_2]_3$–Ub adducts [177].

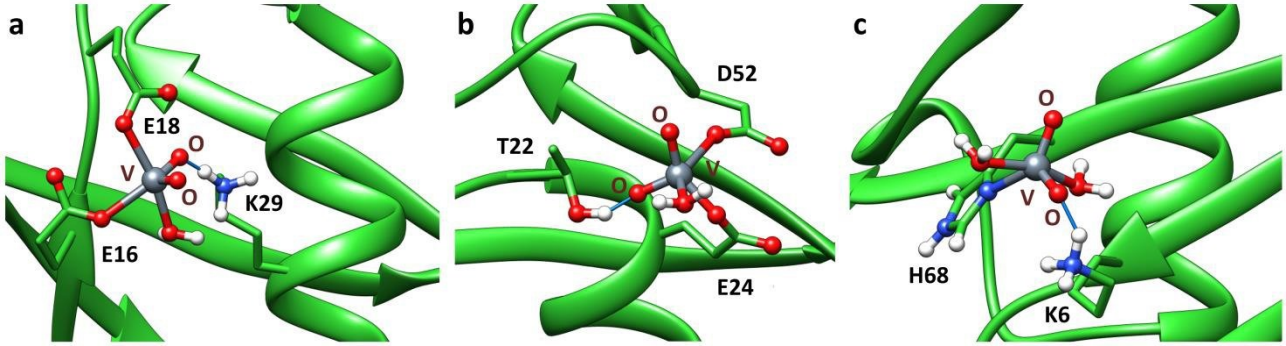

Fig. 19. Most stable adducts predicted by docking calculations for the binding of $V^{V}O_2^{+}$ to Ub (a-c). The H-bonds are indicated with the full blue lines. The one letter code for amino acids was used. Adapted from ref. [177].

As pointed out above, the interaction of $V^{IV}OL_2$ complexes also depends on the favored geometry in aqueous solution. For *cis*-octahedral complexes, as *cis*-$[V^{IV}O(ma)_2(H_2O)]$, the interaction occurs after the replacement of the equatorial H_2O. Notably, the isomers have different affinity for Ub, which is highest for *OC*-6-23-Δ, *OC*-6-23-Λ and *OC*-6-32-Δ. The relative binding affinity is Asp21 >> Glu18 > His68 >> Glu16, but Asp21 and Glu18 cannot bind two *cis*-$V^{IV}OL_2$ moieties at the same time (Fig. 20, a-c). Therefore, the formation of $[V^{IV}O(ma)_2]_3$–Ub, indicated by the ESI-MS data, can be rationalized with the coordination of three *cis*-$V^{IV}O(ma)_2$ moieties to Asp21 or Glu18, His 68 and Glu16 [180].

The study of the interaction of *cis*-$[V^{IV}O(hqs)_2(H_2O)]^{2-}$ with Ub allowed to identify other available residues for the binding to V with the series Glu18 ~ Asp39 ~ Asp52 >> His68 ~ Asp58 > Glu16 ~ Glu24 ~ Glu51 > Asp21 [179]. The stabilization through H-bonds between sulfonate moieties and neighboring residues, accounts for this order.

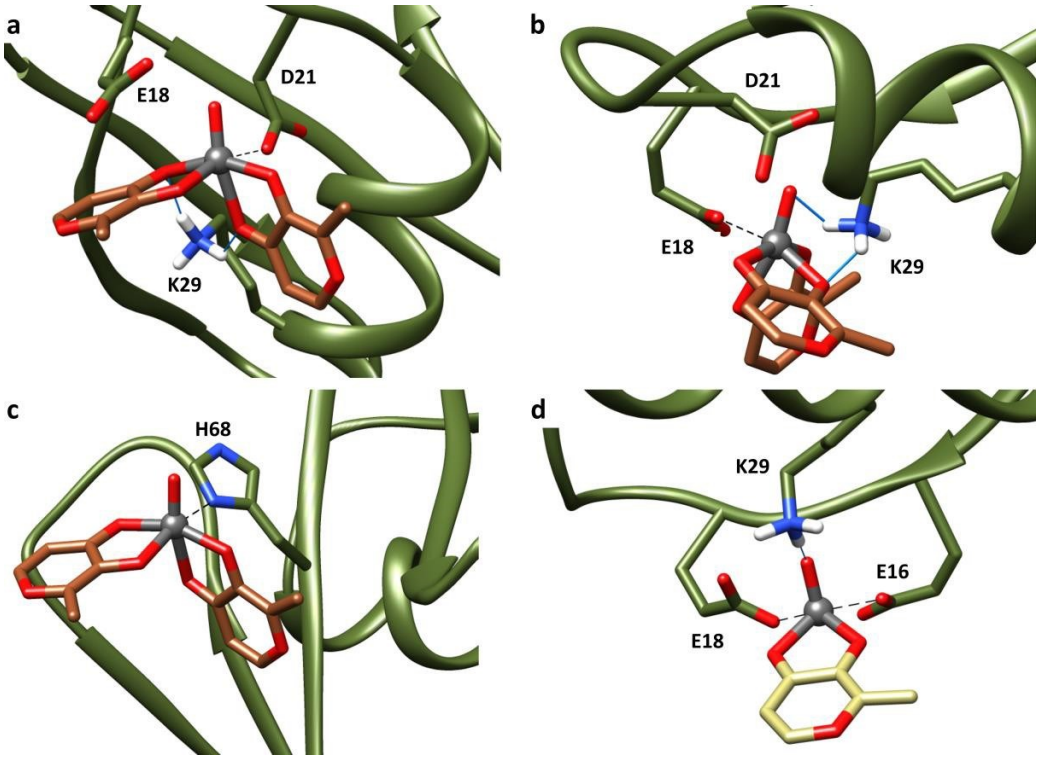

Fig. 20. Most stable structures obtained with docking calculations for the binding of *cis*-$V^{IV}O(ma)_2$ and $V^{IV}O(ma)^+$ to Ub: a) *OC*-23-Δ-$V^{IV}O(ma)_2$ to Asp21; b) *OC*-23-Δ-$V^{IV}O(ma)_2$ to Glu18; c) *OC*-23-Δ-$V^{IV}O(ma)_2$ to His68; d) *SPY*-5-13-C-$V^{IV}O(ma)^+$ to (Glu16, Glu18). The H-bonds are indicated with the full blue lines. The one letter code for amino acids was used. Adapted from ref. [180].

When the complexes exist in solution only as square pyramidal species, as in the case of $[V^{IV}O(acac)_2]$, the binding is generally driven by *non-covalent* interaction with possible assistance of weak coordination in the axial position (Fig. 6, d). The strongest H-bonds are formed between the V=O and side-chain $NH/NH_2/NH_3^+$ groups of Arg42, Gln49, Lys6, His68, Arg54 and Arg72.
Decreasing the metal concentration, $V^{IV}OL^+$ fragments can be formed, which have two available equatorial positions. ESI-MS spectra of the system with ma, acac and koj, revealed the formation of $[V^{IV}OL]_n$–Ub adducts, with n = 1-3 [180]. The residues involved in the V coordination were identified using the computational methods as described for lysozyme (section 7.1) and assuming the existence of two major sites. One is (Glu 16, Glu18; site **1**) or (Glu18, Asp21; site **1'**), the two options being mutually exclusive (Fig. 20, d). The second involves the equatorial binding of non-independent sites (Glu24, Asp52; **2**) or (Glu51, Asp52; **2'**) [177, 180]. The monodentate coordination of His68, eventually assisted by CO groups of the backbone, is also possible.
Besides the availability of suitably positioned donor atoms, the stability of the adducts $[V^{IV}OL_2]_n$–Ub and $[V^{IV}OL]_n$–Ub may be associated to the stability of the bis-complex $V^{IV}OL_2$ in aqueous solution; with intermediate strength ligands L (for example, ma, koj and acac) the formation of

$V^{IV}OL^{+}$ moiety is favored at low concentrations, while with stronger L (dhp and mim), $V^{IV}OL_2$ can survive in solution, and the VOL_2 fragment can interact with the protein.

7.3. Cytochrome c

Cytochrome *c* (Cyt) is a heme-protein composed of 104 amino acids [176]. Located in the mitochondrial membrane, it has electron carrier function and when released into the cytoplasm stimulates apoptosis [429]. Cyt has several available aspartate, glutamate, and histidine correctly oriented on its surface for metal coordination.

ESI-MS data were reported for $[V^{IV}O(nal)_2]$, square pyramidal, and *cis*-$[V^{IV}O(nal)_2(H_2O)]$, octahedral, in equilibrium in aqueous solution [25]. The spectra showed five adducts that correspond to $[V^{IV}O(nal)_2]_n$–Cyt with n =1-5. EPR spectra recorded with ratio 2/1 suggested that two $V^{IV}O(nal)_2$ equivalents bind to Cyt, while for higher excesses were detected the resonances of the free complexes $[V^{IV}O(nal)_2]$/*cis*-$[V^{IV}O(nal)_2(H_2O)]$, which could interact with the protein surface. Therefore, the spectrometric and spectroscopic data allowed to demonstrate that two *cis*-$V^{IV}O(nal)_2$ moieties interact through *coordinative* binding with the COO^{-} group of Asp or Glu residues, while three equivalents are bound in a *non-covalent* manner [25]. Computational methods methods established that the *covalent* binding involves preferentially isomers *OC*-6-24-Δ (Glu21) and *OC*-6-23-Λ (Glu90), while non-specific *non-covalent* interactions are expected when *OC*-6-32-Λ, *OC*-6-23-Δ and *OC*-6-24-Λ interact with the residues Gln16, Lys72 (*OC*-6-32-Λ), Lys13, Lys86, Lys87 (*OC*-6-23-Δ) and Lys55 (*OC*-6-24-Λ) (Fig. 21).

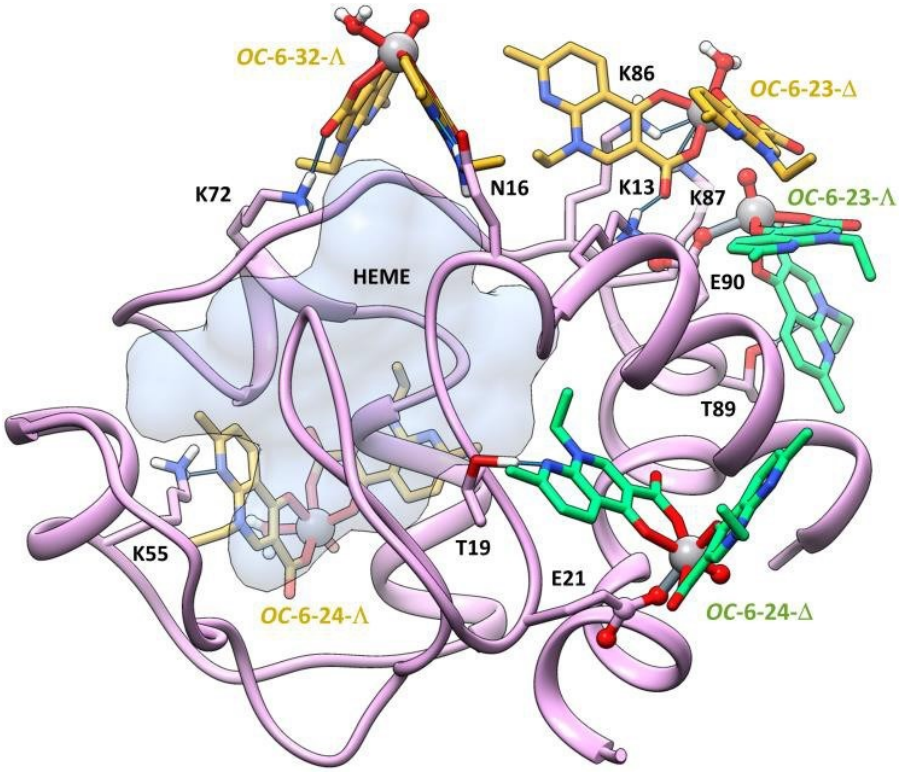

Fig. 21. Coordination sites for the binding of $V^{IV}O(nal)_2$ moiety to Cyt forming the *covalent* adduct $[V^{IV}O(nal)_2]_2$–Cyt (in green), and representation of the first cluster for the *non-covalent* interaction of *OC*-6-23-Δ, *OC*-6-32-Λ and *OC*-6-24-Λ-$[V^{IV}O(nal)_2(H_2O)]$ (in yellow). The one letter code for amino acids was used. Reproduced from ref. [25] by permission of The Royal Society of Chemistry.

8. Binding to Polyoxidovanadates

Decavanadate is a polyoxidovanadate (POV) with general formula $H_xV_{10}O_{28}^{(6-x)-}$ with x = 0-3. It is the vanadium(V) oligomer that predominates in V^V solutions at concentrations above ~1 mM and pH range 2-6. V_{10} gives rise to three ^{51}V NMR resonance peaks, due to different environments of its vanadium atoms, whereas by UV-Vis spectroscopy specific absorptions at 360 and 400 nm are revealed. Environmental changes around V_{10} influence its symmetry reflecting the possibility to monitor either protonation and coordination, or interaction with proteins that result in ^{51}V NMR peak shifts and broadening, respectively.

Considering that in aqueous solution decavanadate is in equilibrium with monovanadate and other V^V-hydrolytic species, care must be taken to assign the biological action to V_{10}; in fact, it was demonstrated that the pharmacological effects of solutions containing V_{10} are often due to other oligomers or monomeric vanadate (V_1) [430, 431].

Since V_{10} can persist under physiological conditions in extracellular and intracellular fluids, also because of its kinetic inertness, many studies on the biological activity of V_{10} have been reported

(for reviews see e.g. [430, 432-434]), including how biological activity of V_{10} compares to V_1. Most data point to decavanadates' biological relevance arising from their ability to bind to proteins. There are numerous studies on the inhibition ability of V_{10} on different types of enzymes, from kinases to glucosidases, and the interested readers are referred to ref. [435]. It was proposed that the antitumor activity of decavanadates is in part related to their enzyme inhibition activity toward phosphatases, kinases, and P-type ATPases (Adenosine Triphosphatases). Recently Aureliano *et al.* showed that several POVs are able to inhibit *Escherichia coli* growth, and the antibacterial activity displayed a reverse correlation to the Ca^{2+}-ATPase activity [436]. V_{10} showed the ability to mineralize inside protein cages of virions [437], moreover V/W and Ti/W mixed Keggin derivatives[1] demonstrated anti-RNA virus activities against dengue, influenza, parainfluenza, respiratory syncytial distemper, and HIV viruses [438]. The viral glycoproteins gp120 [439] and antibody CD4 [440] have been reported as specific targets for POVs, suggesting the virus-cell host binding inhibition is the base of their antiviral mechanism of action [441].

Several X-ray crystallographic structures of V_{10} bound to proteins have been reported over the last years, namely *Francisella tularensis* acid phosphatase A [442], nucleoside triphosphate diphosphohydrolase1 [443, 444], activated receptor tyrosine kinase [445], and human transient receptor potential melastatin 4 (TRPM4) channel [210]. The latter is a Ca^{2+}-dependent cation channel permeable to both Na^+ and K^+. The cryo-EM structure of a human TRPM4 channel bound to Ca^{2+} and V_{10} unveils a unique architecture, paving the way for V_{10} modulation and selectivity on TRPM family [210] (section 2.14).

From a molecular perspective the binding of V_{10} is mainly driven by *non-covalent* electrostatic interactions in positively charged regions with Arg and Lys side-chains. Other secondary interactions such as direct and water- or cation-mediated H-bonds through Ser, Tyr, Asp and Glu, as well as vdW contacts, can further stabilize the adducts. Both *specific* and surface *non-specific* binding regions have been detected depending on the electrostatic charge, shape and volume of the protein regions. Moreover, environmental characteristic such as pH and ionic strength can alter the equilibria between the different binding sites [446].

Rompel *et al*. studied the interaction of free V_{10} and a $V_{10}Co$ complex in which V_{10} is present as ligand, $[(2\text{-hepH})_2[\{Co(H_2O)_5\}_2V_{10}O_{28}]\cdot 4H_2O$ ($V_{10}Co$), with 2-hep = 2-hydroxyethylpyridine], with lysozyme, thaumatin, proteinase K, as well as HSA and HTF. ^{51}V NMR spectroscopy was used to study both species under conditions mimicking protein crystallization [134]. Using linewidths at half-height as a measure of the interaction strength, they observed that V_{10} and $V_{10}Co$ are able to

[1] A Keggin structure is an anion with a general formula $[XM_{12}O_{40}]^{n-}$, where X is a heteroatom and M is the a metal (generally V, Mo, and W). A Keggin structure has 5 isomers, named α, β, γ, δ, and ε.

efficiently bind to thaumatin, while $V_{10}Co$ binds to proteinase K and V_{10} to Lyz. V_{10} interacts with both transferrin and albumin, while $V_{10}Co$ exhibits high affinity to transferrin but shows no interaction with albumin. Although some hypotheses suggest the competition between Co^{II} centers and V_{10} toward HSA specific sites, the molecular reasons behind these differences are far from be clarified.

Decavanadate binds to various proteins that regulate the muscle contraction, such as myosin, actin and Ca^{2+}-ATPase [447-453]. The interaction of V_{10} with sarcoplasmic reticulum calcium-ATPase is known from 1980s [454, 455]. It was demonstrated that V_{10} has an inhibitory effect higher than V_1 and induces significant changes both in the structure and function of these enzymes [456]. The inhibition of myosin occurs throughout the binding in a different site from that of ATP, accounting for the non-competitivity with this latter and actin; in particular, only V_{10} and not V_1 inhibits myosin ATPase activity stimulated by actin [451]. The interaction region could be the phosphate-binding domain, in the proximity of the so-called "back-door" site [432].

Aureliano *et al*. assessed the interaction of V_{10} with actin with EXAFS and XANES [167]. They observed that the binding of V_{10} to globular actin (G-actin) entails a protein conformational rearrangement favoring the exposition and oxidation of specific Cys residues and concomitant vanadium reduction. The interaction of V_{10} with the protein was proposed to occur at the ATP binding site, since the effects were almost totally reversed by the addition of ATP. Additionally, weak interaction of V_{10} with F-actin, the polymerized form, takes place through a mechanism different from that observed for G-actin. Recently Sciortino *et al*. rationalized these experimental data through docking and MD simulations [457]. A first blind docking exploration using Gold software and updated version of *GoldScore*, accounting for vanadium parametrization, unveiled four possible binding regions rich of polar and positive residues for V_{10} binding. A subsequent MD sampling of the docking adducts was carried out using OpenMM engine [392] (AMBER14SB force-field [393] for standard residues and DFT-derived via MCPB.py [250] V-bond force constants) and MM derived binding free energy simulations (molecular mechanics-generalized Born surface area, MM-GBSA [458]. This approach allowed to characterize three main binding sites, α, β and γ, being the site α, where the hydrolysis of ATP takes place, the most affine to V_{10}. However, further dockings and MD simulations unveiled that V_{10} in presence of ATP moves from its primary binding site toward the weaker site β. This study also explained the binding inhibition exerted by the nucleotide toward V_{10}. On this basis, the cysteine oxidation observed in the V_{10}/G-actin system was also explained considering that the reduction product, $V^{IV}O^{2+}$, is found at the catalytic site α, rationalizing the V_{10} and $V^{IV}O^{2+}$ competition with ATP for the nucleotide binding site, as determined through EPR spectroscopy (Fig. 22). The most plausible binding

mode identified by docking for $V^{IV}O^{2+}$, (His161, Asp154; H_2O; H_2O), is located into the catalytic cleft of G-actin, excluding the simultaneous binding of $V^{IV}O^{2+}$ and Ca^{2+}-ATP which results hindered by electrostatic repulsion and steric clashes. Moreover, parallel studies using the isostructural decaniobate (Nb_{10}) unveiled that, for this species, the inhibition effect is negligible, site β being its primary binding site [457].

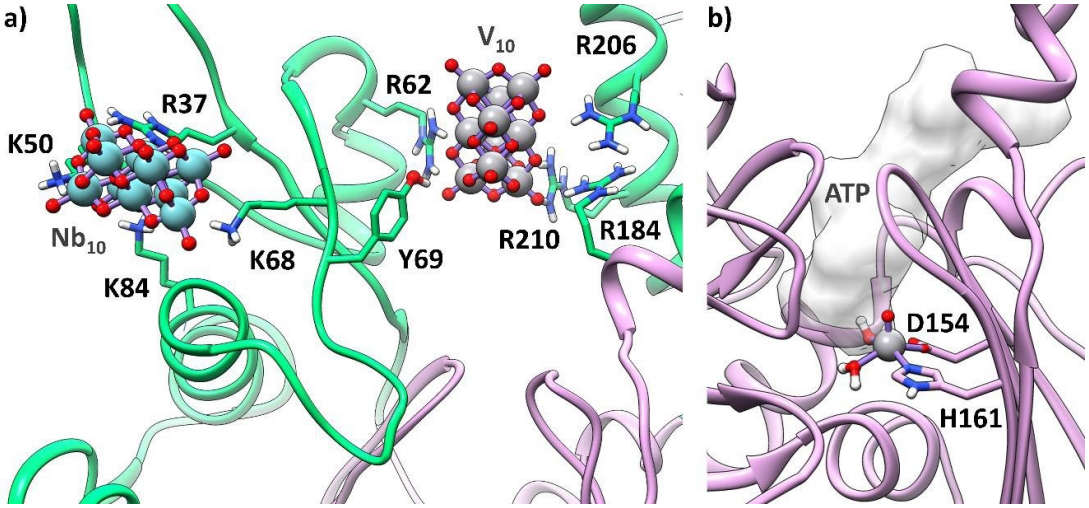

Fig. 22. Computational characterized most stable G-actin binding sites for: a) V_{10} at the catalytic cleft (site α), Nb_{10} at the I/II subdomain interface; b) $V^{IV}O^{2+}$ at the nucleotide binding region. The ATP surface is also shown.

PV_{14}, a hetero-polyoxidovanadate with a trans-bicapped α-Keggin structure with formula $H_xPV_{14}O_{42}^{(9-x)-}$, was characterized in the solid state and aqueous solution [459, 460]. It inhibits P-type ATPases more effectively than V_{10}. For example, IC_{50} for the inhibition of Ca^{2+}-ATPase is 5.4 μM *vs*. 15 μM of decavanadate, which is more active than V_1 (IC_{50} = 80 μM) [460].

Crans *et al.* recently discussed the role of vanadium as indirect activator of a G protein-coupled receptor – the luteinizing hormone receptor (LHR) – able to initiate the signaling transduction in the presence of some VCs [461]. Upon activation, G proteins transduce extracellular signals from membrane receptors to the cell interior by signaling pathways, and are responsible for many physiological responses related to metabolism and other physiologic processes [462, 463]. V_1, V_{10} and mixed valence heteropolyoxidovanadates V_{14} and V_{15} were able to directly decrease the lipid membrane packing, and indirectly drive aggregation of LHR, increasing signal transduction in Chinese hamster ovary cells [463]. However, the effects were only observed in cells in which LHR protein density is low. ^{51}V NMR and EPR spectroscopies were used in speciation and stability studies in cell media. All POVs were able to initiate signaling, with V_{10} and V_{15} showing the

highest activity on cellular functions, while mononuclear vanadate, V_1, resulted substantially less active.

Crans *et al.* also compared the effect of decavanadate and oxidovanadates on the growth of two mycobacterial species, *Mycobacterium smegmatis* and *Mycobacterium tuberculosis*, since these are particularly resistant to hydrophilic drug penetration, and considered also the speciation of the compounds in growth media and in the biological context of the cells. Results showed an inhibition potential higher by a factor of 100 for V_{10}, when compared to V_1, in terms of concentration and a factor of 10 in terms of concentration of V-atoms, for both mycobacterial strains. Speciation studies and ^{51}V NMR spectra substantiated that the growth effects observed were not due to V_1 formed from hydrolyzed V_{10} [135].

Jones *et al.* studied the inhibition of *Leishmania tarentolae* secreted acid phosphatases (SAP), related to the survival of the *Leishmaniasis* parasite, by V_1 and V_{10}. They observed that V_{10} is a better inhibitor of SAP, especially at low substrate:inhibitor ratios, and highlighted the importance of considering the speciation taking place in solution [464].

9. Pharmacological implications of vanadium-protein binding

VCs can be potentially used as therapeutic agents in a great range of medical conditions, but the most explored applications are as insulin-enhancing, anti-cancer and anti-parasitic drugs [22]. Throughout this and previously published reviews, it became clear that vanadium ions and complexes have propensity to interact with proteins. However, apart from effects derived from the high resemblance between vanadate(V) and phosphate, and its consequent interference in phosphate-dependent enzymes and the transport of VCs in blood, not much has been discussed associated with binding of V-species to proteins. Much beyond the putative inhibition of the protein/enzyme, this binding may significantly alter the properties of the original complex which is certainly relevant for its biological action.

Most of the experimental confirmation of V-protein interactions came from spectroscopic data of $[V^{IV}OL_2]$ or V^V complexes measured with vanadium concentrations in the range 50-200 μM, but more recently ESI-MS and MALDI-MS results, obtained with lower concentrations (10-40 μM), provided further insights closer to biological conditions. Namely, EPR signals in serum samples incubated with pharmacological active $[V^{IV}OL_2]$ species at ~90 μM could be attributed to $(V^{IV}O)(HTF)/(V^{IV}O)_2(HTF)$ and $[V^{IV}OL_2]$–Protein adducts [41], but $V^{IV}O$–L–HTF adducts were clearly detected by CD spectroscopy (strong bands in the 300-400 nm region were observed) in similar conditions for L = mhcpe, ma and dhp [377].

Insulin-enhancing VCs have been considered as prospective oral drugs to treat type 2 diabetic patients. Once a particular VC, for example a $[V^{IV}OL_2]$ complex, is orally taken, it comes into contact with saliva and then with the gastrointestinal tract. Due to the propensity of vanadium to exchange ligands with those present in the biological media, the orally administered $[V^{IV}OL_2]$ will be involved in a complex speciation. In the acidic pH of the stomach, in the presence or absence of food, there may be a mixture of V^{V}, $V^{IV}O$ and V^{III} species [465], that may or may not contain the ligand L. In the intestine, it is not easily predicted if V–L species exist; this depends on too many factors, but most probably the separate uptake of vanadium and L takes place. V^{IV} may precipitate as $V^{IV}O(OH)_2$, which may be excreted with the faeces, and the relative amount that passes into the blood will depend on the original ligand, L, as well as on the presence of endogenous bioligands and others coming from food [465]. Therefore, if it is desirable to use oral administration, some type of encapsulation should be used to control the delivery of the active species and/or improve its bio-availability [466].

In blood serum, V^{III} has a very high affinity for HTF, closing its conformation, and cell uptake by endocytosis is plausible [69]. Among transport proteins, $V^{IV}O^{2+}$ has particular affinity to HTF. Thus, most $V^{IV}O^{2+}$ species bind HTF as $(V^{IV}O)(HTF)/(V^{IV}O)_2(HTF)$, but a part of it could form mixed ligand species with ligands L and bioligands (bL), such as citrate, lactate, oxalate, amino acids, ascorbate, ATP, GSH, etc., with composition $V^{IV}O–L–bL$, as it was demonstrated for the antitumor Metvan that forms stable ternary complexes $[V^{IV}O)(citrH_{-1})(Me_2phen)]^{2-}$ ranging from 50 to 100 μM [40]; their uptake by cells occurs mainly by passive diffusion. Vanadate(V) may enter cells by anion channels. $V^{IV}O^{2+}$ and vanadate(V) may also bind to holo-HTF, endocytosis being plausible, but this uptake mechanism was never confirmed. A recent *in vitro* study suggested that cellular uptake of VCs is decreased upon HTF binding and that this could inhibit, rather than promote, their biological activity [30]. Potential V^{IV}- or V^{V}-based drugs should be stable enough to survive in the serum and enter intact into the cells and release the active species only in the cytosol [30]. In this respect, the stability and lipophilicity of the $[VOL_2]$ complexes are relevant factors for their biological action. Vanadium also enters red blood cells and binds Hb, this possibly corresponding to a significant proportion of the total vanadium in blood [412, 415, 417, 425, 467]. *In vitro* studies indicated that, once uptaken by erythrocytes, it does not return to the serum [412, 415], but it is not clear if the same happens *in vivo*. Overall, most of VCs do not enter cells in the form of the orally taken $[V^{IV}OL_2]$ complex and only for strong ligands V–L species can be uptaken by cells.

Inside cells the antidiabetic action of V is possibly also connected to the ability of VCs to vary their oxidation state and exchange ligands with those present in the biological media, namely proteins.

Reactive oxygen species being available, $V^{IV}O^{2+}$ may be oxidized to vanadate(V) forming $H_2VO_4^-/HVO_4^{2-}$ [468], well known for similarities with phosphate anions [22]. Thus, inside cells many of the effects may be traced back to the phosphate/vanadate antagonism, and many phosphate-regulated enzymatic processes may be altered. Besides phosphatases, kinases and phosphorylases, also glucose-6-phosphate dehydrogenase, nucleoside triphosphate diphosphohydrolases, phosphodiesterases, phosphoglucomutases, and ATPases may be affected [4, 19, 22, 27, 33, 34, 462, 468, 469].

Several mechanisms were suggested for the action of insulin-enhancing VCs. Upon binding of Cys side-chains at the active sites of protein tyrosine phosphatase (PTP) enzymes, vanadate(V) may block the access of phosphate (phosphorylated tyrosine residues) to proteins, namely insulin receptors (IR), to be dephosphorylated by PTPs, such as PTP-1B [33, 34]. This may imply that specific tyrosine side groups of the intracellular β subunit of the transmembrane insulin receptor (IR-β) remain phosphorylated. This entails vanadate(V)-induced upstream signaling, one of the consequences being multi-step processes activating the glucose transporter [4, 22, 33, 468]. Recently, it was proposed that also $[V^{IV}O(OH)_3]^-$, that correspond to $[H_3V^{IV}O_4]^-$, may contribute to the insulin-enhancing action, being structurally similar to $[V^VO_2(OH)_2]^-$, i.e. $[H_2V^VO_4]^-$ [1, 374, 468, 470]. However, other enzymes such as phosphatases and kinases may also be targets of vanadium action: for example, transmembrane IR is a protein tyrosine kinase (PTK) complex which triggers a series of signaling processes that result in the uptake of glucose. VCs may therefore modulate signaling pathways and/or transcription factors. During evolution, Nature established a network of kinases and phosphatases in the presence of very low concentrations of intracellular V, but, when the supply of vanadium increases, a great number of signaling changes will take place [33].

The difficulties in understanding the vanadium speciation upon oral administration of VCs, yielding uncertain ADMET (Absorption, Distribution Metabolism, Excretion, Toxicity) properties, the multitude of effects of V inside cells, the narrow therapeutic window and the toxicity risks associated with the requirement of long-term administration, are all factors which might make doubtful the use of VCs for oral treatment of diabetes in the future, unless a particularly effective VC and/or encapsulation and/or nanomaterial based platforms will be applied, allowing the use of very low V doses.

Many other therapeutic applications of VCs have been suggested, namely in the treatment of cancer and parasitic diseases [5, 21, 22, 26, 28, 471, 472], and interactions with proteins could be related to several of the suggested mechanisms of action. Among the antitumor action of VCs, the increased ROS generation, which may disturb cellular metabolism and lead to damage to lysosomes and

mitochondria has been suggested [473]. It has been pointed out that other mechanisms involve inhibition of phosphatase and metalloproteinase activity, or *via* MAPK cascades (ERK and p38) [474], sometimes with induction of G2/M phase arrest [21, 475, 476], as well as inhibition of neutral endopeptidase activity [477]. As expected, the effects of VCs depend on many factors, namely on type of cells, type of vanadium compound and the administered dose. One of the important proteins is p53: in p53-defective cells, enhanced by ROS, apoptosis is favored by VCs which inhibit the cell cycle [478]. However, in p53-functional cells, apoptosis may be inhibited by VCs due to their interference on the phosphorylation of p53 [479]. In most studies, changes of the coordination mode by exchange of labile water molecules and ligands were considered to have important cooperative effects on the antitumor activity. The MAPK/ERK and PI3K/AKT signaling pathways are activated by vanadate(V) and $[V^{IV}O(acac)_2]$; the fact that the activation may be counteracted or inhibited by the antioxidant *N*-acetylcysteine (NAC) [476] suggested that it is mainly vanadate(V) which is interfering with the activity of the enzymes. However, this is not completely clear because inside cells V^V is partly reduced to V^{IV} and the effects of NAC could be explained with its radical scavenging effect of ROS formed by vanadium(IV) in Fenton-like reactions [480]. This indicates that, under physiological conditions, a mixture of species could be responsible of the biological effects, and this has been confirmed recently for V^{IV}/V^V complexes with potential antitumor activity [42].

VCs have been also suggested to have a relevant anti-parasitic action namely, but not exclusively, against trypanosomiasis, amoebiasis, and leishmaniasis through distinct modes of action including the binding of VCs to the DNA [22] and the inhibition of the activity of phosphatases such as the acid phosphatase SAcP [481, 482].

The examples described in this work demonstrate that the interaction of VCs with proteins is a crucial factor in their therapeutic action, but many aspects related to this topic, *e.g.* how membrane or cytosolic proteins are affected as well as how they can change their conformation and/or lose their function upon binding, remain unknown. Related to these aspects is the correct identification of the active complex or complexes, a crucial finding to be clarified to boost the design of more active V drugs and the possible clinical tests by the pharmaceutical companies.

10. Challenges and future directions

As mentioned in section 5, vanadium haloperoxidases have potential for industrial production of many fine chemicals under mild conditions. In fact, numerous proposals on the use of VClPOs as antiseptic agents have been patented [483], while applications of VBrPOs have been significantly

less discussed in the literature. Moreover, many studies were also carried out using VHPOs in brominations and sulfoxidations. A future widespread industrial use of VHPOs still depends on the findings from complementary fields such as molecular biology (e.g., more efficient variants for a given optimal pH) and bioengineering (e.g., immobilized enzymes and spatially separated reaction compartments). Most of the reported methodologies require improvements to reach preparative scale, but the feasibility of the processes has been demonstrated, thus opening ways for the development of new sustainable procedures using aqueous and/or alternative solvents.

The ability of V-nitrogenases, besides catalyzing the reduction of N_2, to reduce CO and CO_2, also opens perspectives to further investigate their use for the conversion of these gases into hydrocarbons, in ambient conditions [276]. This may ultimately allow the production of hydrocarbon fuels from CO and CO_2 at an industrial scale. Thus, challenges are to solve issues to make the processes with V-Nases economically viable and provide bases for efficient hydrogenation of CO_2 to produce hydrocarbon products, thus helping to mitigate the increase of this gas in the atmosphere.

Vanadium groundwater contamination due to geological weathering of V-containing minerals and from vanadium mining and processing activities became an environmental concern, that demands new remediation methods [333]. Purification of vanadium-contaminated groundwater is essential to protect public health and the environment, and microorganisms containing nitrate reductases able to reduce V^V to insoluble V^{IV} may be promising in this respect. However, adequate characterization of microbial communities, functional genes involved, and suitable electron donors are still required to develop new and microbiologically safe processes for the remediation of vanadate-contaminated aquifers.

Regarding therapeutic applications, as emphasized by Crans [471], more studies are required before vanadium-based anticancer or antiparasitic agents, as well as for other therapeutic uses, will be ready for use in the clinic. The extensive reactivity of VCs in biological media and the associated toxicity has hindered their use in clinical practice. Therefore, it seems essential that future drug development should include strategies to overcome these obstacles. One such strategy was suggested by Levina *et al*. [484] by which VCs were used in intratumoral injections offering two simultaneous advantages: not only the cancer cells are attacked instantly after the VCs administration but also their metabolites are not so harmful when released from the tumoral environment into the blood stream.

One way to overcome the requirement of the full speciation up to the uptake in cells, as well as the off-target toxicity of ligands and vanadium itself, is to use formulation strategies, packaging VCs into nanoparticles or nanocomposites. In this context, cancer is an obvious area for the use of

nanocarriers, for example using the enhanced permeability and retention effect (EPR effect) in solid tumours, thus allowing active targeted delivery to cells [485]. By decreasing off-target systemic toxicity of V, one could better overcome vanadium interference with PTPs. Encapsulation of VCs when ligands are cytotoxic, also means that their side-reactions during circulation can be reduced, thus further concentrating the amount of active complex that reaches the target tissue. In this way, the design of bi-potential vanadium complexes whereby cells would be subjected to both the anticancer effects of the PTP-inhibitory vanadate action plus the cytotoxic action of the ligands, could generate additive or synergistic anticancer effects [34].

Other strategies have been developed by the group of Crans, namely the use of oncolytic viruses and their potential for treating cancer [486]: both *in vitro* and *ex vivo* experiments have demonstrated that the valuable medicinal action of such viruses is remarkably improved when coupled with the effects of VCs acting as PTP inhibitors. This new type of tumor-reducing effect of VCs offers new perspectives in the development of improved immunotherapeutic strategies against cancer.

Globally, from the biological perspective, VCs are widely known as putative drug agents in a great variety of conditions. However, it is also known that their therapeutic use implies to perfectly unveil the answers to several biological questions including their transport, protein-ligand interactions, pharmacokinetics and pharmacodynamics (see section 9). Many advances have been made but, as this work emphasized, vanadium has a high propensity to interact with proteins, and little attention has been given, for example to the roles of membrane and cytosol proteins, whose functions may be affected by the presence of vanadium species. Moreover, binding to proteins is not necessarily an advantage but can result in the deactivation of the vanadium-based drug, and in the inhibition of the uptake into cells and/or release of the active species. For example, noteworthy amounts of the pharmacologically active VCs could be retained in the erythrocytes, and therefore deactivated, upon binding to hemoglobin that forms stable adducts, hindering the excretion and the transport towards the target organs.

A methodology that remains underexplored in studies of therapeutic use of vanadium is proteomics. These studies may be complex, even when the topic of search is restricted, but phosphorylations and ubiquitinations are typical modifications that VCs may affect. The great development in technologies such as mass spectrometry-based methods and micro arrays hopefully will enhance the large-scale study of proteins upon contact of cells with VCs.

Acknowledgements

This work was supported by: Centro de Química Estrutural which is financed by national funds from *Fundação para a Ciência e Tecnologia* (FCT), projects UIDB/00100/2020 and UIDP/00100/2020 and *Programa Operacional Regional de Lisboa 2020*; the Applied Molecular Biosciences Unit (UCIBIO) which is financed by National Funds from FCT (UIDP/04378/2020 and UIDB/04378/2020); Regione Autonoma della Sardegna (grant RASSR79857) and Fondazione di Sardegna (grant 2017). G.S. also thanks Spanish MINECO' Juan de la Cierva program, FJC2019-039135- I.

List of Abbreviations

ABC transporter - ATP-binding cassette transporter

Hacac - acetylacetone

ADMET - Absorption, Distribution, Metabolism, Excretion, Toxicity

ADP - Adenosine Diphosphate

amphen - 5-amino-1,10-phenanthroline

*An*VBPO - vanadium bromoperoxidase from *A. nodosum*

apo-HTF – human serum apo-transferrin

ArMs - Artificial Metalloenzymes

ATP - Adenosine Triphosphate

ATPase - Adenosine Triphosphatase

A_z - hyperfine coupling constant, z component

$A_z(^{51}V)^{exptl}$ - experimental A_z

$A_z(^{51}V)^{calcd}$ - calculated A_z

BEOV - Bis(ethylmaltolato)oxidovanadium(IV)

bL - bioligand

BMOV - bis(maltolato)oxidovanadium(IV)

BSA - Bovine Serum Albumin

CD - Circular Dichroism

Chr - chrysin

Cit - citrate

*Ci*VClPO - vanadium chloroperoxidase from *Curvularia inaequalis*

CNS - Crystallography & NMR System

COSMO - COnductor-like Screening MOdel

*Cp*VBrPO - vanadium bromoperoxidase from *Coralina pilulifera*

cryo-EM - cryogenic Electron Microscopy

CV - Cyclic Voltammetry

Cyt - cytochrome *c*

δ - NMR chemical shift

ΔE_{bind} - energy difference for the binding of $V^{IV}O^{2+}$ to a protein site

DFT - Density Functional Theory 7,8-

dhf - 7,8-dihydroxyflavone

Hdhp - 3-hydroxy-1,2-dimethyl-4-pyridinone

H_2dipic - 2,6-dipicolinic acid

DPV - Differential Pulse Voltammetry

DSC - Differential Scanning Calorimetry

Hema - ethylmaltol

ENDOR - Electron-Nuclear Double Resonance

EPR - Electron Paramagnetic Resonance

EPR effect - Enhanced Permeability and Retention effect

ESEEM - Electron Spin Echo Envelope Modulation

ESI - Electro Spray Ionization

EXAFS - Extended X-ray Absorption Fine Structure Spectroscopy

Fab - Fragment antigen binding region (of IgG)

FBS - fetal bovine serum

Fc - Fragment crystallizable region (of IgG)

Fe_2-HTF - diferric human serum transferrin (or holo-HTF)

Fe-HTF_C - monoferric human serum transferrin, with Fe bound at C-terminal region

Fe-HTF_N - monoferric human serum transferrin, with Fe bound at N-terminal region

FeMoco - FeMo cofactor

Fe-Nase - Fe-nitrogenase

FeVco - FeV cofactor

^{1}H STD NMR - ^{1}H Saturation Transfer Difference NMR

Hb - hemoglobin

H-bond - Hydrogen bond

2-hep - 2-hydroxyethylpyridine

5-hf - 5-hydroxyflavone

HFC - Hyperfine Coupling

HFEPR - High-Field Electron Paramagnetic Resonance

H_2hqs - 8-hydroxyquinoline-5-sulfonic acid

H_3hidpa - *N*-hydroxyimino-2,2′-diisopropionic acid

holo-HTF - Human holo-serum Transferrin

Hpno - 2-hydroxypyridine-*N*-oxide

HSA - Human Serum Albumin

HSA^f - fatted Human Serum Albumin

HSA^d - defatted Human Serum Albumin

HTF - Human Serum Transferrin

ICP - Inductively coupled plasma

Ig - immunoglobulin

IGPD - imidazoleglycerol-phosphatase dehydratase

IMAC - Immobilized Metal-Affinity Chromatography

IR - Insulin Receptor

IR-β - intracellular β subunit of the transmembrane insulin receptor

Isapn - oxindolimine

ITC - Isothermal Titration Calorimetry

J - coupling constant (NMR)

K_{ass} - equilibrium association constant

K_{dis} - equilibrium dissociation constant

K_q - bimolecular quenching constant

K_{SV} - Stern-Volmer quenching constant

Hkoj - kojic acid

lact - lactate

LHR - Luteinizing Hormone Receptor

LLCT - Ligand-to-Ligand Charge Transfer

LMCT - Ligand-to-Metal Charge Transfer

LMPTP - Low-Molecular-mass Protein Tyrosine Phosphatase

Lyz - lysozyme

Hma - maltol

MAD - Mean Absolute Deviation

MALDI - Matrix-Assisted Laser Desorption/Ionization

MALDI-TOF - MALDI time of flight

MAPD - Mean Absolute Percent Deviation

MAPK/ERK - Mitogen-Activated Protein Kinases/Extracellular Signal-Regulated Kinases

MAS - Magical angle spinning

Mb - myoglobin

MBS - Multi-metal Binding Site (of human serum albumin)

MD - Molecular Dynamics

MeIm - 1-methylimidazole

Me_2phen - 4,7-dimethyl-1,10-phenanthroline

Metvan - $[V^{IV}O(Me_2phen)_2(SO_4)]$

Hmhcpe - 2-methyl-3*H*-5-hydroxy-6-carboxy-4-pyrimidinone ethyl ester

mim - L-mimosinato

MLCT - metal-to-ligand charge transfer

MM-GBSA - molecular mechanics-generalized Born surface area Mo-

Nase - Mo-nitrogenase

mor - morin

MS - Mass Spectrometry

MST - MicroScale Thermophoresis

NAC - *N*-acetylcysteine

nal - nalidixato

Nb_{10} - decaniobate

NCIPlot - Non Covalent Interaction Plot

NTPDase - Nucleoside Triphosphate Diphosphohydrolase

NTS - *N*-terminal site (of human serum albumin)

OVA - ovalbumin

PAGE - polyacrylamide gel electrophoresis

PI3K/AKT - Phosphatidylinositol-3-Kinase/Protein Kinase B

PCM - Polarizable Continuum Model

PD - percent deviation

PDB - Protein Data Bank

phen = 1,10-phenanthroline

Hpic = picolinic acid

H_2pip - pipemidic acid

POV - polyoxidovanadate

PTK - protein tyrosine kinase

PTP - protein tyrosine phosphatase

PSA - porcine serum albumin

que - quercetin

QM - Quantum Mechanical

QM/MM - Quantum Mechanical/Molecular Mechanical

RBC - red blood cells

ROS - Reactive Oxygen Species

SAP - secreted acid phosphatases

SAXS - Small-angle X-ray scattering

SCRF - Self-Consistent Reaction Field

SDS-PAGE - sodium dodecyl sulfate-polyacrylamide gel electrophoresis

SEC - size-exclusion chromatography

SF - Scoring Functions

SHE - standard hydrogen electrode

SHFC - superhyperfine coupling

SMD - Solvation Model Based on Density

SO - spin-orbit term

SOMO - singly occupied molecular orbital

TauD - α-ketoglutarate-dependent taurine dioxygenase

TD-DFT - Time-dependent density-functional theory

TRPM4 - human transient receptor potential melastatin 4

Try - trypsin

τ_0 - lifetime of the fluorophore in the absence of quencher

Ub - ubiquitin

Urea-PAGE - urea polyacrylamide gel electrophoresis

UV-Vis - electronic absorption spectroscopy

V_1 - monovanadate

V_{10} - decavanadate

VBrPO - vanadium bromoperoxidase

VClPO - vanadium chloroperoxidase

VCs - vanadium complexes (or compounds)

vdW - van der Waals

VHPO - vanadium-haloperoxidase

VIPO - vanadium iodoperoxidase V-

Nase - V-nitrogenase

XANES - X-ray Absorption Near Edge Structure

XAS - X-ray absorption spectroscopy

XRD - X-ray diffraction

ZFS - the zero-field splitting

References

[1] D.C. Crans, J.J. Smee, E. Gaidamauskas, L. Yang, Chem. Rev. 104 (2004) 849-902.

[2] C. Leblanc, H. Vilter, J.B. Fournier, L. Delage, P. Potin, E. Rebuffet, G. Michel, P.L. Solari, M.C. Feiters, M. Czjzek, Coord. Chem. Rev. 301-302 (2015) 134-146.

[3] C.C. McLauchlan, B.J. Peters, G.R. Willsky, D.C. Crans, Coord. Chem. Rev. 301 (2015) 163-199.

[4] D. Rehder, Metallomics 7 (2015) 730-742.

[5] A. Ścibior, Ł. Pietrzyk, Z. Plewa, A. Skiba, J. Trace Elem. Med. Biol. 61 (2020) 126508.

[6] J.M. Winter, B.S. Moore, J. Biol. Chem. 284 (2009) 18577-18581.

[7] A.W. Fay, M.A. Blank, C.C. Lee, Y. Hu, K.O. Hodgson, B. Hedman, M.W. Ribbe, J. Am. Chem. Soc. 132 (2010) 12612–12618.

[8] J.A. Rees, R. Bjornsson, J. Schlesier, D. Sippel, O. Einsle, S. DeBeer, Angew. Chem. Int. Ed. 54 (2015) 13249-13252.

[9] Y.L. Hu, M.W. Ribbe, Angew. Chem. Int. Ed. 55 (2016) 8216-8226.

[10] D. Sippel, J. Schlesier, M. Rohde, C. Trncik, L. Decamps, I. Djurdjevic, T. Spatzal, S.L.A. Andrade, O. Einsle, J. Biol. Inorg. Chem. 22 (2017) 161–168.

[11] D.F. Harris, E. Jimenez-Vicente, Z.-Y. Yang, B.M. Hoffman, D.R. Dean, L.C. Seefeldt, J. Inorg. Biochem. 213 (2020) 111278.

[12] T. Ueki, H. Michibata, Coord. Chem. Rev. 255 (2011) 2249–2257.

[13] T. Ueki, N. Yamaguchi, Romaidi, Y. Isago, H. Tanahashi, Coord. Chem. Rev. (2015) 300-308.

[14] D. Fattorini, F. Regoli, Hyper-accumulation of vanadium in polychaetes, in: H. Michibata (Ed.) Vanadium: Biochemical and Molecular Biological Approaches, Springer, Dordrecht, 2012, pp. 73-92.

[15] J.A.L. Silva, J.J.R.F. Silva, A.J.L. Pombeiro, Amavadine, a Vanadium Compound in Amanita Fungi, in: H. Michibata (Ed.) Vanadium. Biochemical and Molecular Biological Approaches, Springer, Dordrecht, 2012, pp. 35-49.

[16] M.A.A.F.C.T. Carrondo, M.T.L.S. Duarte, J. Costa Pessoa, J.A.L. Silva, J.J.R. Fraústo da Silva, M.C.T.A. Vaz, L.F. Vilas Boas, J. Chem. Soc. Chem. Commun. (1988) 1158-1159.

[17] R.E. Berry, E.M. Armstrong, R.L. Beddoes, D. Collison, S.N. Ertok, M. Helliwell, C.D. Garner, Angew. Chem., Int. Ed. 38 (1999) 795−797.
[18] K. Schwarz, D.B. Milne, Science 174 (1971) 426-428.
[19] J. Costa Pessoa, S. Etcheverry, D. Gambino, Coord. Chem. Rev. 301 (2015) 24-48.
[20] N.D. Chasteen, Vanadium-Protein Interactions, in: H. Sigel, Sigel, A. (Ed.) Met. Ions Biol. Syst., Marcel Dekker, Inc., New York, 1995, pp. 231-247.
[21] J. Korbecki, I. Baranowska-Bosiacka, I. Gutowska, D. Chlubek, Acta Chim. Pol. 59 (2012) 195-200.
[22] J. Costa Pessoa, E. Garribba, M.F.A. Santos, T. Santos-Silva, Coord. Chem. Rev. 301 (2015) 49-86.
[23] G. Sciortino, E. Garribba, Chem. Commun. 56 (2020) 12218-12221.
[24] V. Ugone, D. Sanna, G. Sciortino, D.C. Crans, E. Garribba, Inorg. Chem. 59 (2020) 9739-9755.
[25] V. Ugone, D. Sanna, S. Ruggiu, G. Sciortino, E. Garribba, Inorg. Chem. Front. 8 (2021) 1189-1196.
[26] E. Kioseoglou, S. Petanidis, C. Gabriel, A. Salifoglou, Coord. Chem. Rev. 301-302 (2015) 87-105.
[27] S. Treviño, A. Díaz, E. Sánchez-Lara, B.L. Sanchez-Gaytan, J.M. Perez-Aguilar, E. González-Vergara, Biol. Trace Elem. Res. 188 (2019) 68-98.
[28] D.C. Crans, H. LaRee, G. Cardiff, B.I. Posner, Developing Vanadium as an Antidiabetic or Anticancer Drug: A Clinical and Historical Perspective in: P.L. Carver (Ed.) Essential Metals in Medicine: Therapeutic Use and Toxicity of Metal Ions in the Clinic, De Gruyter GmbH, Berlin, 2019, pp. 203-230.
[29] D. Rehder, Future Med. Chem. 8 (2016) 325-338.
[30] A. Levina, P.A. Lay, Inorg. Chem. 59 (2020) 16143-16153.
[31] J. Costa Pessoa, I. Correia, Inorganics 9 (2021) 17.
[32] G. Sciortino, J.-D. Maréchal, E. Garribba, Inorg. Chem. Front. 8 (2021) 1951-1974.
[33] T. Scior, J.A. Guevara-Garcia, Q.T. Do, P. Bernard, S. Laufer, Curr. Med. Chem. 23 (2016) 2874-2891.
[34] E. Irving, A.W. Stoker, Molecules 22 (2017) 2269.
[35] L.C. Cantley, J.H. Ferguson, K. Kustin, J. Am. Chem Soc. 100 (1978) 5210-5212.
[36] L.C. Cantley, L.G. Cantley, L. Josephson, J. Biol. Chem. 253 (1978) 7361-7368.
[37] A. Levina, D.C. Crans, P.A. Lay, Coord. Chem. Rev. 352 (2017) 473-498.
[38] A. Levina, P.A. Lay, Chem. Asian J. 12 (2017) 1692-1699.

[39] P. Nunes, I. Correia, I. Cavaco, F. Marques, T. Pinheiro, F. Avecilla, J. Costa Pessoa, J. Inorg. Biochem. 217 (2021) 111350.
[40] D. Sanna, V. Ugone, G. Micera, P. Buglyo, L. Biro, E. Garribba, Dalton Trans. 46 (2017) 8950-8967.
[41] D. Sanna, V. Ugone, M. Serra, E. Garribba, J. Inorg. Biochem. 173 (2017) 52-65.
[42] A. Banerjee, S.P. Dash, M. Mohanty, G. Sahu, G. Sciortino, E. Garribba, M.F.N.N. Carvalho, F. Marques, J. Costa Pessoa, W. Kaminsky, K. Brzezinski, R. Dinda, Inorg. Chem. 59 (2020) 14042-14057.
[43] G. Sciortino, J. Rodriguez-Guerra Pedregal, A. Lledos, E. Garribba, J.D. Marechal, J. Comput. Chem. 39 (2018) 42-51.
[44] G. Sciortino, E. Garribba, J.-D. Maréchal, Inorg. Chem. 58 (2019) 294-306.
[45] G. Sciortino, D. Sanna, V. Ugone, G. Micera, A. Lledós, J.-D. Maréchal, E. Garribba, Inorg. Chem. 56 (2017) 12938-12951.
[46] G. Heinemann, W. Vogt, Clin. Chem. 42 (1996) 1275-1282.
[47] K.H. Thompson, J. Lichter, C. LeBel, M.C. Scaife, J.H. McNeill, C. Orvig, J. Inorg. Biochem. 103 (2009) 554-558.
[48] G.R. Willsky, A.B. Goldfine, P.J. Kostyniak, J.H. McNeill, L.Q. Yang, H.R. Khan, D.C. Crans, J. Inorg. Biochem. 85 (2001) 33-42.
[49] K.H. Thompson, B.D. Liboiron, Y. Sun, K.D. Bellman, I.A. Setyawati, B.O. Patrick, V. Karunaratne, G. Rawji, J. Wheeler, K. Sutton, S. Bhanot, C. Cassidy, J.H. McNeill, V.G. Yuen, C. Orvig, J. Biol. Inorg. Chem. 8 (2003) 66-74.
[50] C.G. Hartinger, M. Groessl, S.M. Meier, A. Casini, P.J. Dyson, Chem. Soc. Rev. 42 (2013) 6186-6199.
[51] M. Wenzel, A. Casini, Coord. Chem. Rev. 352 (2017) 432-460.
[52] C.A. Smith, E.W. Ainscough, A.M. Brodie, J. Chem. Soc., Dalton Trans. (1995) 1121-1126.
[53] C.J. Ballhausen, H.B. Gray, Inorg. Chem. 1 (1962) 111-122.
[54] E. Garribba, G. Micera, A. Panzanelli, D. Sanna, Inorg. Chem. 42 (2003) 3981-3987.
[55] E. Lodyga-Chruscinska, D. Sanna, E. Garribba, G. Micera, Dalton Trans. (2008) 4903-4916.
[56] G. Micera, E. Garribba, Eur. J. Inorg. Chem. (2011) 3768-3780.
[57] L.F. Vilas Boas, J. Costa Pessoa, Vanadium, in: G. Wilkinson, R.D. Gillard, J.A. McCleverty (Eds.), Comprehensive Coordination Chemistry, Pergamon Press, Oxford, 1987, Vol. 3, pp. 453-583.
[58] A. Mathavan, A. Ramdass, S. Rajagopal, J. Fluoresc. 25 (2015) 1141–1149.
[59] J.R. Lakowicz, Principles of fluorescence spectroscopy, 3rd ed., Springer, Boston, MA, 2006.

[60] M. Kongot, N. Dohare, D.S. Reddy, N. Pereira, R. Patel, M. Subramanian, A. Kumar, J. Trace Elem. Med. Biol. 51 (2019) 176-190.
[61] Q.-. Guo, L. Li, J. Dong, H. Liu, T. Xu, J. Li, Spectroch. Acta A, Molec. Biomol. Spectr. 106 (2013) 155-162.
[62] S.D. Kurbah, A. Kumar, I. Syiemlieh, R.A. Lal, Inorg. Chem. Commun. 86 (2017) 6-9.
[63] D. Biswal, N.R. Pramanik, S. Chakrabarti, M.G.B. Drew, K. Acharyad, S. Chandra, Dalton Trans. 46 (2017) 16682-16702.
[64] J.E. Parente, L.G. Naso, K. Jori, C.A. Franca, A.M.C. Ferreira, P.A.M. Williams, E.G. Ferrer, New J. Chem. 43 (2019) 17603-17619.
[65] J. Costa Pessoa, I. Correia, G. Goncalves, A.I. Tomaz, J. Arg. Chem. Soc. 97 (2009) 151-165.
[66] T. Kiss, T. Jakusch, D. Hollender, A. Dornyei, E.A. Enyedy, J. Costa Pessoa, H. Sakurai, A. Sanz-Medel, Coord. Chem. Rev. 252 (2008) 1153-1162.
[67] T. Jakusch, D. Hollender, E.A. Enyedy, C.S. Gonzalez, M. Montes-Bayon, A. Sanz-Medel, J. Costa Pessoa, I. Tomaz, T. Kiss, Dalton Trans. (2009) 2428-2437.
[68] I. Correia, I. Chorna, I. Cavaco, S. Roy, M.L. Kuznetsov, N. Ribeiro, G. Justino, F. Marques, T. Santos-Silva, M.F.A. Santos, H.M. Santos, J.L. Capelo, J. Doutch, J. Costa Pessoa, Chem. Asian J. 12 (2017) 2062-2084.
[69] M.F.A. Santos, I. Correia, A.R. Oliveira, E. Garribba, J. Costa Pessoa, T. Santos-Silva, Eur. J. Inorg. Chem. (2014) 3293-3297.
[70] F. Macii, T. Biver, J. Inorg. Biochem. 216 (2021) 111305.
[71] M. van de Weert, L. Stella, J. Mol. Struct. 998 (2011) 144-150.
[72] N.H. Khan, N. Pandya, N.C. Maity, M. Kumar, R.M. Patel, R.I. Kureshy, S.H.R. Abdi, S. Mishra, S. Das, H.C. Bajaj, Eur. J. Med. Chem. 46 (2011) 5074-5085.
[73] V. Gomathi Sankareswari, D. Vinod, A. Mahalakshmi, M. Alamelu, G. Kumaresan, R. Ramaraj, S. Rajagopal, Dalton Trans. 43 (2014) 3260-3272.
[74] S. Zhai, Q. Guo, J. Dong, T. Xu, L. Li, Transition Met. Chem. (London) 39 (2014) 271-280.
[75] M. Mohamadi, S.Y. Ebrahimipour, M. Torkzadeh-Mahani, S. Foro, A. Akbari, RSC Adv. 5 (2015) 101063-101075.
[76] S.P. Dash, A.K. Panda, S. Dhaka, S. Pasayat, A. Biswas, M.R. Maurya, P.K. Majhi, A. Crochet, R. Dinda, Dalton Trans. 45 (2016) 18292-18307.
[77] L.G. Naso, L. Lezama, M. Valcarcel, C. Salado, P. Villacé, D. Kortazar, E.G. Ferrer, P.A.M. Williams, J. Inorg. Biochem. 157 (2016) 80-93.
[78] M.A. Neelakantan, C. Balakrishnan, V. Selvarani, M. Theetharappan, Appl. Organomet. Chem. 32 (2018) e4125.

[79] K. Savithri, H.D. Revanasiddappa, Bioinorg. Chem. Appl. 2018 (2018) 2452869.
[80] A. Banerjee, S.P. Dash, M. Mohanty, D. Sanna, G. Sciortino, V. Ugone, E. Garribba, H. Reuter, W. Kaminsky, R. Dinda, J. Inorg. Biochem. 199 (2019) 110786.
[81] D. Biswal, N.R. Pramanik, M.G.B. Drew, N. Jangra, M.R. Maurya, M. Kundu, P.C. Sil, S. Chakrabarti, New J. Chem. 43 (2019) 17783.
[82] O.A. Chaves, M.C.C. Oliveira, C.M.C. Salles, F.M. Martins, B.A. Iglesias, D.F. Back, J. Inorg. Biochem. 200 (2019) 110800.
[83] S. Lima, A. Banerjee, M. Mohanty, G. Sahu, C. Kausar, S.K. Patra, E. Garribba, W. Kaminsky, R. Dinda, New J. Chem. 43 (2019) 17711-17725.
[84] G. Scalese, I. Machado, I. Correia, J. Costa Pessoa, L. Bilbao, L. Pérez-Diaz, D. Gambino, New J. Chem. 43 (2019) 17756-17773.
[85] J. Shi, Y. Wei, Y. Zhang, J. Tang, H. Bian, Q. Yu, F. Huang, Polyhedron 162 (2019) 81-90.
[86] R. Kalantari, Z. Asadi, J. Mol. Struct. 1219 (2020) 128664.
[87] D. Sharma, H.D. Revanasiddappa, B. Jayalakshmi, Egypt. J. Basic Appl. Sci. 7 (2020) 323-341.
[88] B.A. Hamid, M. Maryam, K.F.-P. Soudeh, R.H. Mohammad, A. Danial, H.N. Mohammad, M. Mehdi, Anti-Cancer Agents Med. Chem. 21 (2021) 630-639.
[89] M. Brustolon, E. Giamello, Electron Paramgnetic Resonance. A Practitioner's Toolkit, John Wiley & Sons, Inc., Hoboken, New Jersey, 2009.
[90] M. Drescher, G. Jeschke, EPR Spectroscopy. Applications in Chemistry and Biology, Springer-Verlag, Berlin, Germany, 2012.
[91] F.E. Mabbs, D. Collison, Electron Paramagnetic Resonance of d Transition Metal Compounds, Elsevier Science Publishers B.V., Amsterdam, 1992.
[92] M.M. Roessler, E. Salvadori, Chem. Soc. Rev. 47 (2018) 2534-2553.
[93] J.A. Weil, J.R. Bolton, Electron Paramagnetic Resonance: Elementary Theory and Practical Applications, 2nd Ed., John Wiley & Sons, Inc., Hoboken, New Jersey, 2007.
[94] D. Goldfarb, S. Stoll, EPR Spectroscopy: Fundamentals and Methods, John Wiley & Sons, Inc., Chichester, UK, 2018.
[95] D.N. Chasteen, Vanadyl(IV) EPR Spin Probe. Inorganic and Biochemical Aspects, in: L.J. Berliner, J. Reuben (Eds.) Biological Magnetic Resonance, Springer US, Boston, MA, 1981, pp. 53-119.
[96] J.K. Money, K. Folting, J.C. Huffman, D. Collison, J. Temperley, F.E. Mabbs, G. Christou, Inorg. Chem. 25 (1986) 4583-4589.
[97] T.S. Smith, R. LoBrutto, V.L. Pecoraro, Coord. Chem. Rev. 228 (2002) 1-18.

[98] D. Sanna, G. Sciortino, V. Ugone, G. Micera, E. Garribba, Inorg. Chem. 55 (2016) 7373-7387.
[99] G. Sciortino, D. Sanna, V. Ugone, A. Lledós, J.-D. Maréchal, E. Garribba, Inorg. Chem. 57 (2018) 4456-4469.
[100] D. Sanna, V. Ugone, G. Micera, E. Garribba, Dalton Trans. 41 (2012) 7304-7318.
[101] R.F. Campbell, J.H. Freed, J. Phys. Chem. 84 (1980) 2668-2680.
[102] M.L. Munzarová, M. Kaupp, J. Phys. Chem. B 105 (2001) 12644-12652.
[103] F. Neese, J. Chem. Phys. 118 (2003) 3939-3948.
[104] A.C. Saladino, S.C. Larsen, J. Phys. Chem. A 107 (2003) 1872-1878.
[105] C.P. Aznar, Y. Deligiannakis, E.J. Tolis, T.A. Kabanos, M. Brynda, R.D. Britt, J. Phys. Chem. A 108 (2004) 4310-4321.
[106] S. Gorelsky, G. Micera, E. Garribba, Chem. A Eur. J. 16 (2010) 8167-8180.
[107] G. Sciortino, D. Sanna, G. Lubinu, J.D. Marechal, E. Garribba, Chem. A Eur. J. 26 (2020) 11316-11326.
[108] P.L.W. Tregenna-Piggott, H. Weihe, J. Bendix, A.-L. Barra, H.-U. Güdel, Inorg. Chem. 38 (1999) 5928-5929.
[109] J. Krzystek, A.T. Fiedler, J.J. Sokol, A. Ozarowski, S.A. Zvyagin, T.C. Brunold, J.R. Long, L.-C. Brunel, J. Telser, Inorg. Chem. 43 (2004) 5645-5658.
[110] J. Krzystek, A. Ozarowski, J. Telser, D.C. Crans, Coord. Chem. Rev. 301-302 (2015) 123-133.
[111] K. Fukui, H. Ohya-Nishiguchi, H. Kamada, Inorg. Chem. 36 (1997) 5518-5529.
[112] F. Kouichi, O.-N. Hiroaki, K. Hitoshi, I. Masamoto, X. Yuanzhi, Bull. Chem. Soc. Jpn. 71 (1998) 2787-2796.
[113] D.M. Murphy, R.D. Farley, Chem. Soc. Rev. 35 (2006) 249-268.
[114] A. Schweiger, Angew. Chem., Int. Ed. Engl. 30 (1991) 265-292.
[115] Y. Deligiannakis, M. Louloudi, N. Hadjiliadis, Coord. Chem. Rev. 204 (2000) 1-112.
[116] R. Bogumil, J. Hüttermann, R. Kappl, R. Stabler, C. Sudfeldt, H. Witzel, Eur. J. Biochem. 196 (1991) 305-312.
[117] J. Petersen, T.R. Hawkes, D.J. Lowe, J. Inorg. Biochem. 80 (2000) 161-168.
[118] S.C. Larsen, N.D. Chasteen, Hyperfine and Quadrupolar Interactions in Vanadyl Proteins and Model Complexes: Theory and Experiment, in: G. Hanson, L. Berliner (Eds.) Metals in Biology: Applications of High-Resolution EPR to Metalloenzymes, Springer New York, New York, NY, 2010, pp. 371-409.
[119] R. LoBrutto, B.J. Hamstra, G.J. Colpas, V.L. Pecoraro, W.D. Frasch, J. Am. Chem. Soc. 120 (1998) 4410-4416.

[120] S.S. Eaton, J. Dubach, K.M. More, G.R. Eaton, G. Thurman, D.R. Ambruso, J. Biol. Chem. 264 (1989) 4776-4781.
[121] E. de Boer, C.P. Keijzers, A.A.K. Klaassen, E.J. Reijerse, D. Collison, C.D. Garner, R. Wever, FEBS Lett. 235 (1988) 93-97.
[122] K. Fukui, T. Ueki, H. Ohya, H. Michibata, J. Am. Chem. Soc. 125 (2003) 6352-6353.
[123] A.L.P. Houseman, R. LoBrutto, W.D. Frasch, Biochemistry 34 (1995) 3277-3285.
[124] R.S. Macomber, A Complete Introduction to Modern NMR Spectroscopy, John Wiley & Sons, Inc. , 1998.
[125] J. Keeler, Understanding NMR Spectroscopy, 1st Ed., Wiley, 2002.
[126] N.J. Bunce, J. Chem. Educ. 64 (1987) 907-914.
[127] D. Rehder, Bioinorganic Vanadium Chemistry, John Wiley & Sons, Ltd., Chichester, 2008.
[128] T. Jakusch, A. Dean, T. Oncsik, A.C. Bényei, V. Di Marco, T. Kiss, Dalton Trans. 39 (2010) 212-220.
[129] A. Butler, H. Eckert, M.J. Danzitz, J. Am. Chem. Soc. 109 (1987) 1864-1865.
[130] A. Butler, H. Eckert, J. Am. Chem. Soc. 111 (1989) 2802-2809.
[131] B. Borah, C. Chen, W. Egan, M. Miller, A. Wlodawer, J.S. Cohen, Biochemistry 24 (1985) 2058-2067.
[132] H. Vilter, D. Rehder, Inorg. Chim. Acta 136 (1987) L7-L10.
[133] D. Rehder, T. Polenova, M. Bühl, Vanadium-51 NMR, in: G.A. Webb (Ed.) Annu. Rep. NMR Spectrosc., Elsevier, Amsterdam, 2007, pp. 49-114.
[134] L. Krivosudsky, A. Roller, A. Rompel, New J. Chem. 43 (2019) 17863-17871.
[135] N. Samart, Z. Arhouma, S. Kumar, H.A. Murakami, D.C. Crick, D.C. Crans, Front. Chem. 6 (2018) 519.
[136] M. Hadžibrahimović, D. Sužnjević, P. F., T. Cvetić Antić, M. Žižić, J. Zakrzewska, M. Živić, Antonie Van Leeuwenhoek 110 (2017) 365-373.
[137] M. Žižić, Z. Miladinović, M. Stanić, M. Hadžibrahimović, M. Živić, J. Zakrzewska, Res. Microbiol. (2016) 521-528.
[138] D.M. Dias, J.P.G.L.M. Rodrigues, N.S. Domingues, A.M.J.J. Bonvin, M.M.C.A. Castro, Eur. J. Inorg. Chem. (2013) 4619-4627.
[139] M.P. Waller, M. Bühl, K.R. Geethalakshmi, D. Wang, W. Thiel, Chem. Eur J. 13 (2007) 4723-4732.
[140] R. Gupta, G. Hou, R. Renirie, R. Wever, T. Polenova, J. Am. Chem. Soc. 137 (2015) 5618-5628.

[141] D. Lacabanne, T. Wiegand, N. Wili, M.I. Kozlova, R. Cadalbert, D. Klose, A.Y. Mulkidjanian, B.H. Meier, A. Böckmann, Molecules 25 (2020) 5268.
[142] P.R. Srinivas, Introduction to Protein Electrophoresis, in: B.T. Kurien, R.H. Scofield (Eds.) Electrophoretic Separation of Proteins – Methods in Molecular Biology, Humana Press, 2019, pp. 23-29.
[143] C. Arndt, S. Koristka, A. Feldmann, M. Bachmann, Native Polyacrylamide Gels, in: B.T. Kurien, R.H. Scofield (Eds.) Electrophoretic Separation of Proteins – Methods in Molecular Biology, Humana Press, 2019, pp. 87-91.
[144] S.R. Gallagher, Curr. Protoc. Protein Sci. 68 (2012) 10.11.11-10.11.44.
[145] S. Liu, Z. Li, B. Yu, S. Wang, Y. Shen, H. Cong, Adv. Colloid Interf. Sci. 284 (2020) 102254.
[146] M.P. Newcomb, C.C. Lee, K. Tanifuji, A.J. Jasniewski, J. Liedtke, M.W. Ribbe, Y. Hu, ChemBioChem 21 (2020) 1742-1748.
[147] M.A. Gunasinghe, A.T. Kim, S.M. Kim, Appl. Biochem. Biotechn. 189 (2019) 49-64.
[148] T. Ueki, T. Nakagawa, H. Michibata, J. Inorg. Biochem. 116 (2012) 70-76.
[149] B.V. Hong, J.H. Lee, R.H. Rice, Peer J. 8 (2020) e9504.
[150] U.J. Kim, B.H. Lee, K.H. Lee, Brain Res. 1719 (2019) 133-139.
[151] A.R. Otrelo-Cardoso, R.R. Nair, M.A.S. Correia, R.S.C. Cordeiro, A. Panjkovich, D.I. Svergun, T. Santos-Silva, M.G. Rivas, Scient. Reports 7 (2017) 5798.
[152] J. Ramos, J. Muthukumaran, F. Freire, J. Paquete-Ferreira, A.R. Otrelo-Cardoso, D. Svergun, A. Panjkovich, T. Santos-Silva, Int. J. Molec. Sci. 20 (2019) 860.
[153] M.H. Nagaoka, Y. Yamazaki, T. Maitani, Biochem. Biophys. Res. Commun. 296 (2002) 1207-1214.
[154] S.L. Byrne, A.B. Mason, J. Biol. Inorg. Chem. 14 (2009) 771-781.
[155] S. Mehtab, G. Goncalves, S. Roy, A.I. Tomaz, T. Santos-Silva, M.F. Santos, M.J. Romao, T. Jakusch, T. Kiss, J. Costa Pessoa, J. Inorg. Biochem. 121 (2013) 187-195.
[156] J. Costa Pessoa, G. Gonçalves, S. Roy, I. Correia, S. Mehtab, M.F.A. Santos, T. Santos-Silva, Inorg. Chim. Acta 420 (2014) 60-68.
[157] J. Yano, V.K. Yachandra, Photosynt. Res. 102 (2009) 241.
[158] P. Zimmermann, S. Peredkov, P.M. Abdala, S. DeBeer, M. Tromp, C. Müller, J.A. van Bokhoven, Coord. Chem. Rev. 423 (2020) 213466.
[159] P. Behrens, XANES, EXAFS and Related Techniques, in: H.G. Karge, J. Weitkamp (Eds.) Characterization I. Molecular Sieves – Science and Technology, vol 4., Springer Berlin Heidelberg, Berlin, Heidelberg, 2004, pp. 427-466.

[160] J.J. Rehr, A.L. Ankudinov, Coord. Chem. Rev. 249 (2005) 131-140.
[161] G. Bunker, Introduction to XAFS: A Practical Guide to X-ray Absorption Fine Structure Spectroscopy, Cambridge University Press, Cambridge, 2010.
[162] J. Hormes, U. Kuetgens, R. Chauvistre, W. Schreiber, N. Anders, H. Vilter, D. Rehder, C. Weidemann, Biochim. Biophys. Acta (BBA) - Prot. Struct. Molec. Enzymol. 956 (1988) 293-299.
[163] M. Weyand, H. Hecht, M. Kiess, M. Liaud, H. Vilter, D. Schomburg, J. Mol. Biol. 293 (1999) 595-611.
[164] C. Weidemann, D. Rehder, U. Kuetgens, J. Hormes, H. Vilter, Chem. Phys. 136 (1989) 405-412.
[165] R. Renirie, J.M. Charnock, C.D. Garner, R. Wever, J. Inorg. Biochem. 104 (2010) 657-664.
[166] A. Levina, A.I. McLeod, P.A. Lay, Chem. A Eur. J. 20 (2014) 12056-12060.
[167] M.P.M. Marques, D. Gianolio, S. Ramos, L.A.E. Batista de Carvalho, M. Aureliano, Inorg. Chem. 56 (2017) 10893-10903.
[168] C.D. Garner, P. Baugh, D. Collison, E.S. Davies, A. Dinsmore, J.A. Joule, E. Pidcock, C. Wilson, Pure Appl. Chem. 69 (1997) 2205-2212.
[169] D.I. Svergun, Biol. Chem. 391 (2010) 737-743.
[170] T.W. Gräwerty, D.I. Svergun, J. Mol. Biol. 432 (2020) 3078-3092.
[171] S.D. Vela, D.I. Svergun, Curr. Res. Struct. Biol. 2 (2020) 164-170.
[172] P. Chen, P. Masiewicz, K. Perez, J. Hennig, IUCr Journal 7 (2020) 644-655.
[173] C.G. Azevedo, I. Correia, M.M.C. dos Santos, M.F.A. Santos, T. Santos-Silva, J. Doutch, L. Fernandes, H.M. Santos, J.L. Capelo, J. Costa Pessoa, J. Inorg. Biochem. 180 (2018) 211-221.
[174] L. Messori, A. Merlino, Chem. Commun. 53 (2017) 11622-11633.
[175] T. Pivetta, V. Lallai, E. Valletta, F. Trudu, F. Isaia, D. Perra, E. Pinna, A. Pani, J. Inorg. Biochem. 151 (2015) 107-114.
[176] T. Jakusch, T. Kiss, Coord. Chem. Rev. 351 (2017) 118-126.
[177] G. Sciortino, V. Ugone, D. Sanna, G. Lubinu, S. Ruggiu, J.-D. Maréchal, E. Garribba, Front. Chem. 8 (2020) 345.
[178] G. Sciortino, D. Sanna, V. Ugone, J.D. Marechal, E. Garribba, Inorg. Chem. Front. 6 (2019) 1561-1578.
[179] G. Sciortino, D. Sanna, V. Ugone, J.-D. Maréchal, M. Alemany-Chavarria, E. Garribba, New J. Chem. 43 (2019) 17647-17660.
[180] V. Ugone, D. Sanna, G. Sciortino, J.D. Marechal, E. Garribba, Inorg. Chem. 58 (2019) 8064-8078.
[181] P. Galloni, V. Conte, B. Floris, Coord. Chem. Rev. 301 (2015) 240-299.

[182] W.R. Harris, C.J. Carrano, J. Inorg. Biochem. 22 (1984) 201-218.
[183] B.R. Lydon, C.C. Lee, K. Tanifuji, N.S. Sickerman, M.P. Newcomb, Y. Hu, M.W. Ribbe, J.Y. Yang, ChemBioChem 21 (2020) 1773-1778.
[184] J. Hon, M.S. Hwang, M.A. Charnetzki, I.J. Rashed, P.B. Brady, S. Quillin, M.W. Makinen, J. Biol. Inorg. Chem. 22 (2017) 1267-1279.
[185] R. Wever, B.E. Krenn, R. Renirie, Meth. Enzymol. 605 (2018) 141-201.
[186] S.M.K. McKinnie, Z.D. Miles, B.S. Moore, Meth. Enzymol. 604 (2018) 405-424.
[187] A.V. Fejzagić, S. Myllek, F. Hogenkamp, J. Greb, J. Pietruszka, T. Classen, ChemistryOpen 9 (2020) 959-966.
[188] T. Punitha, S.M. Phang, J.C. Juan, J. Beardall, Mar Biotech. 20 (2018) 282-303.
[189] J.-B. Fournier, E. Rebuffet, L. Delage, R. Grijol, L. Meslet-Cladière, J. Rzonca, P. Potin, G. Michel, M. Czjzek, C. Leblanc, Appl. Env. Microbiol. 80 (2014) 7561-7573.
[190] V. Lemesheva, C. Birkemeyer, D. Garbary, E. Tarakhovskaya, Eur. J. Phycol. 55 (2020) 275-284.
[191] C.A. Brautigam, H. Zhao, C. Vargas, S. Keller, P. Schuck, Nat. Protoc. 11 (2016) 882-894.
[192] L. Baranauskiene, T.C. Kuo, W.-Y. Chen, D. Matulis, Curr. Opin. Biotechn. 55 (2019) 9-15.
[193] H. Su, Y. Xu, Front. Pharmacol. 9 (2018) 1133.
[194] F. Bou-Abdallah, T.R. Giffune, Biochim. Bioph. Acta-Gen. Subj. 1860 (2016) 879-891.
[195] J.M. Messmore, R.T. Raines, Arch. Biochem. Bioph. 381 (2000) 25-30.
[196] A.-K. Bordbar, A.L. Creagh, F. Mohammadi, C.A. Haynes, C. Orvig, J. Inorg. Biochem. 103 (2009) 643-647.
[197] J.P. Gaffney, A.M. Valentine, Biochemistry 48 (2009) 11609-11611.
[198] S.M. Stanford, A. Aleshin, V. Zhang, R.J. Ardecky, M.P. Hedrick, J. Zou, S. Ganji, M.R. Bliss, F. Yamamoto, A.A. Bobkov, J. Kiselar, Y. Liu, G.W. Cadwell, Khare, J. Yu, A. Barquilla, T.D.Y. Chung, T. Mustelin, S. Schenk, L.A. Bankston, R.C. Liddington, A.B. Pinkerton, N. Bottini, Nature Biochem. Biol. 13 (2017) 624-632.
[199] M. Asmari, R. Ratih, H.A. Alhazmi, S.E. Deeb, Methods 146 (2018) 107-119.
[200] E. Nogales, Nature Meth. 13 (2016) 24-27.
[201] M. Carroni, H.R. Saibil, Methods 95 (2016) 78-85.
[202] J.-P. Renaud, A. Chari, C. Ciferri, W.-t. Liu, H.-W. Rémigy, H. Stark, C. Wiesmann, Nature Rev. Drug Discov. 17 (2018) 471-492.
[203] A. Brown, S. Shao, Ribosomes and cryo-EM: a duet, 2018, 52, 1-7, Curr. Opin. Struct. Biol. 52 (2018) 1-7.
[204] J. Hanske, Y. Sadian, C.W. Müller, Curr. Opin. Struct. Biol. 52 (2018) 8-15.

[205] M.C. Puljung, J. Gen. Physiol. 150 (2018) 653-669.
[206] C. Xu, W.J. Rice, W. He, D.L. Stokes, J. Mol. Biol. 316 (2002) 201-211.
[207] W. Mi, Y. Li, S.H. Yoon, R.K. Ernst, T. Walz, M. Liao, Nature 549 (2017) 233-237.
[208] Y. Li, B.J. Orlando, M. Liao, Nature 567 (2019) 486-490.
[209] S. Hofmann, D. Januliene, A.R. Mehdipour, C. Thomas, E. Stefan, S. Brüchert, B.T. Kuhn, E.R. Geertsma, G. Hummer, R. Tampé, A. Moeller, Nature 580 (2019) 580-583.
[210] P.A. Winkler, Y. Huang, W. Sun, J. Du, W. Lu, Nature 552 (2017) 200-204.
[211] C. Fan, J.T. Kaiser, D.C. Rees, Proc. the Nat. Acad. Sci. USA 117 (2020) 19228-19236.
[212] Y. Zhang, Q. Fan, X. Chi, Q. Zhou, Y. Li, Cell Discov. 6 (2020) 86.
[213] G. Micera, E. Garribba, Eur. J. Inorg. Chem. (2010) 4697-4710.
[214] G. Micera, E. Garribba, J. Comput. Chem. 32 (2011) 2822-2835.
[215] D. Sanna, V. Pecoraro, G. Micera, E. Garribba, J. Biol. Inorg. Chem. 17 (2012) 773-790.
[216] S. Kundu, D. Mondal, K. Bhattacharya, A. Endo, D. Sanna, E. Garribba, M. Chaudhury, Inorg. Chem. 54 (2015) 6203-6215.
[217] G. Sciortino, J.-D. Maréchal, E. Garribba, Inorg. Chem. Front. 8 (2021) 1951-1974.
[218] G. Micera, E. Garribba, Int. J. Quantum Chem. 112 (2012) 2486-2498.
[219] D. Sanna, V. Ugone, G. Sciortino, B.F. Parker, Z. Zhang, C.J. Leggett, J. Arnold, L. Rao, E. Garribba, Eur. J. Inorg. Chem. 2018 (2018) 1805-1816.
[220] S.P. Dash, S. Majumder, A. Banerjee, M.F.N.N. Carvalho, P. Adão, J. Costa Pessoa, K. Brzezinski, E. Garribba, H. Reuter, R. Dinda, Inorg. Chem. 55 (2016) 1165-1182.
[221] A.C. Saladino, S.C. Larsen, J. Phys. Chem. A 106 (2002) 10444-10451.
[222] L. Alonso-Cotchico, J. Rodríguez-Guerra, A. Lledós, J.-D. Maréchal, Acc. Chem. Res. 53 (2020) 896-905.
[223] V. Muñoz Robles, E. Ortega-Carrasco, L. Alonso-Cotchico, J. Rodriguez-Guerra, A. Lledós, J.-D. Maréchal, ACS Catalysis 5 (2015) 2469-2480.
[224] P.E.M. Siegbahn, F. Himo, Wiley Interdiscip. Rev. Comput. Mol. Sci. 1 (2011) 323-336.
[225] J.N. Harvey, F. Himo, F. Maseras, L. Perrin, ACS Catalysis 9 (2019) 6803-6813.
[226] S. Miertuš, J. Tomasi, Chem. Phys. 65 (1982) 239-245.
[227] R. Cammi, J. Tomasi, J. Comput. Chem. 16 (1995) 1449-1458.
[228] J. Tomasi, B. Mennucci, R. Cammi, Chem. Rev. 105 (2005) 2999-3094.
[229] A.V. Marenich, C.J. Cramer, D.G. Truhlar, J. Phys. Chem. B 113 (2009) 6378-6396.
[230] A. Klamt, G. Schüürmann, J. Chem. Soc., Perkin Trans. 2 (1993) 799-805.
[231] J.-E. Sánchez-Aparicio, L. Tiessler-Sala, L. Velasco-Carneros, L. Roldán-Martín, G. Sciortino, J.-D. Maréchal, J. Chem. Inf. Model. 61 (2021) 311-323.

[232] G.L. Warren, C.W. Andrews, A.-M. Capelli, B. Clarke, J. LaLonde, M.H. Lambert, M. Lindvall, N. Nevins, S.F. Semus, S. Senger, G. Tedesco, I.D. Wall, J.M. Woolven, C.E. Peishoff, M.S. Head, J. Med. Chem. 49 (2006) 5912-5931.
[233] M. Xuan-Yu, Z. Hong-Xing, M. Mihaly, C. Meng, Curr. Comput.-Aided Drug Des. 7 (2011) 146-157.
[234] I.A. Guedes, C.S. de Magalhães, L.E. Dardenne, Biophys. Rev. 6 (2014) 75-87.
[235] E. Yuriev, J. Holien, P.A. Ramsland, J. Mol. Recognit. 28 (2015) 581-604.
[236] M. Akhter, JSM Chem. 4 (2016) 1025.
[237] S. Agarwal, R. Mehrotra, JSM Chem. 4 (2016) 1024.
[238] G. Wang, W. Zhu, Future Med. Chem. 8 (2016) 1707-1710.
[239] Z. Wang, Y. Kang, D. Li, H. Sun, X. Dong, X. Yao, L. Xu, S. Chang, Y. Li, T. Hou, J. Phys. Chem. B 122 (2018) 2544-2555.
[240] Z. Wang, H. Sun, X. Yao, D. Li, L. Xu, Y. Li, S. Tian, T. Hou, Phys. Chem. Chem. Phys. 18 (2016) 12964-12975.
[241] G.B. Akcapinar, O.U. Sezerman, Biosci. Rep. 37 (2017) BSR20160179.
[242] G. Jones, P. Willett, R.C. Glen, J. Mol. Biol. 245 (1995) 43-53.
[243] A. Moulin, J.H. Bell, R.F. Pratt, D. Ringe, Biochemistry 46 (2007) 5982-5990.
[244] T.A.S. Brandão, A.C. Hengge, S.J. Johnson, J. Biol. Chem. 285 (2010) 15874-15883.
[245] K.M. Holtz, B. Stec, E.R. Kantrowitz, J. Biol. Chem. 274 (1999) 8351-8354.
[246] Y. Lindqvist, G. Schneider, P. Vihko, Eur. J. Biochem. 221 (1994) 139-142.
[247] K.M. Davis, M. Altmyer, R.J. Martinie, I. Schaperdoth, C. Krebs, J.M. Bollinger, A.K. Boal, Biochemistry 58 (2019) 4218-4223.
[248] J. Rittle, M.J. Field, M.T. Green, F.A. Tezcan, Nature Chem. 11 (2019) 434-441.
[249] J.M. Seminario, Int. J. Quantum Chem. 60 (1996) 1271-1277.
[250] P. Li, K.M. Merz, J. Chem. Inf. Model. 56 (2016) 599-604.
[251] S. Zheng, Q. Tang, J. He, S. Du, S. Xu, C. Wang, Y. Xu, F. Lin, J. Chem. Inf. Model. 56 (2016) 811-818.
[252] P. Li, K.M. Merz, Chem. Rev. 117 (2017) 1564-1686.
[253] J. Contreras-García, E.R. Johnson, S. Keinan, R. Chaudret, J.-P. Piquemal, D.N. Beratan, W. Yang, J. Chem. Theory Comput. 7 (2011) 625-632.
[254] C. Harford, B. Sarkar, Acc. Chem. Res. 30 (1997) 123-130.
[255] S. Al-Harthi, J.I. Lachowicz, M.E. Nowakowski, M. Jaremko, Ł. Jaremko, J. Inorg. Biochem. 198 (2019) 110716.
[256] T. Kiss, T. Jakusch, J.C. Pessoa, I. Tomaz, Coord. Chem. Rev. 237 (2003) 123-133.

[257] D. Sanna, G. Micera, E. Garribba, Inorg. Chem. 49 (2010) 174-187.
[258] B.M. Hoffman, D. Lukoyanov, Z.Y. Yang, D.R. Dean, L.C. Seefeldt, Chem. Rev. 114 (2014) 4041-4062.
[259] Y. Hu, M.W. Ribbe, Annual Rev. Biochem. 85 (2016) 455-483.
[260] R.R. Eady, Vanadium Nitrogenases of Azotobacter, in: H. Sigel, Sigel, A. (Ed.) Metal Ions in Biological Systems, Vanadium and its role in Life, Maecel Dekker, Inc., New York, 1995, pp. 363-405.
[261] C. Rüttimann-Johnson, R. Chatterjee, V.K. Shah, P.W. Ludden, The Vanadium-Containing Nitrogenase System of Azotobacter vinelandii, in: A.S. Tracey, D.C. Crans (Eds.) Vanadium Compounds: Chemistry, Biochemistry, and Therapeutic Applications, ACS, Washington, 1998, pp. 228-240.
[262] D.F. Harris, D.A. Lukoyanov, H. Kallas, C. Trncik, Z.Y. Yang, P. Compton, N. Kelleher, O. Einsle, D.R. Dean, B.M. Hoffman, L.C. Seefeldt, Biochemistry 58 (2019) 3293-3301.
[263] D. Rehder, J. Inorg. Biochem. 80 (2000) 133–136.
[264] L.C. Seefeldt, B.M. Hoffman, D.R. Dean, Ann. Rev. Biochem. 78 (2009) 701–722.
[265] R.R. Eady, Coord. Chem. Rev. 237 (2003) 23–30.
[266] R.R. Eady, Chem. Rev. 96 (1996) 3013–3030.
[267] R. Darnajoux, N. Magain, M. Renaudin, F. Lutzoni, J.-P. Bellenger, X. Zhang, PNAS 116 (2019) 24682-24688.
[268] K.E. Luxem, A.M.L. Kraepiel, L. Zhang, J.R. Waldbauer, X. Zhang, Environ. Microbiol. 22 (2020) 1397-1408.
[269] D. Sippel, O. Einsle, Nature Chem. Biol. 13 (2017) 956-960.
[270] D. Sippel, M. Rohde, J. Netzer, C. Trncik, J. Gies, K. Grunau, I. Djurdjevic, L. Decamps, S.L.A. Andrade, O. Einsle, Science 359 (2018) 1484-1489.
[271] C.K. Rofer-DePoorter, Chem. Rev. 81 (1981) 447–474.
[272] C.C. Lee, Y. Hu, M.W. Ribbe, Angew. Chem. Int. Ed. Engl. 50 (2011) 5545–5547.
[273] R.N.F. Thorneley, D.J. Lowe, Biochem. J. 224 (1984) 887–894.
[274] Y. Hu, M.W. Ribbe, J. Biol. Inorg. Chem. 20 (2015) 435-445.
[275] Y. Hu, C.C. Lee, M.W. Ribbe, Science 333 (2011) 753-755.
[276] C.C. Lee, Y. Hu, M.W. Ribbe, Science 329 (2010) 642.
[277] M.J. Dilworth, R.R. Eady, Biochem. J. 277 (1991) 465–468.
[278] N.S. Sickerman, Y.L. Hu, M.W. Ribbe, Chem. Asian J. 12 (2017) 1985-1996.
[279] M. Rohde, K. Grunau, O. Einsle, Angew. Chem. Int. Ed. 59 (2020) 23626-23630.
[280] T. Spatzal, K.A. Perez, O. Einsle, J.B. Howard, D.C. Rees, Science 345 (2014) 1620-1623.

[281] B. Benediktsson, A.T. Thorhallsson, R. Bjornsson, Chem. Comm. 54 (2018) 7310-7313.
[282] J. Huang, A.D. MacKerell Jr, J. Comput. Chem. 34 (2013) 2135-2145.
[283] L. Cao, O. Caldararu, U. Ryde, J. Biol. Inorg. Chem. 25 (2020) 847-861.
[284] A.T. Brunger, P.D. Adams, G.M. Clore, W.L. DeLano, P. Gros, R.W. Grosse-Kunstleve, J.-S. Jiang, J. Kuszewski, M. Nilges, N.S. Pannu, R.J. Read, L.M. Rice, T. Simonson, G.L. Warren, Acta Cryst.Section D 54 (1998) 905-921.
[285] B. Benediktsson, R. Bjornsson, Inorg. Chem. 59 (2020) 11514-11527.
[286] C.C. Lee, A.W. Fay, T.C. Weng, C.M. Krest, B. Hedman, K.O. Hodgson, Y. Hu, M.W. Ribbe, Proc. Natl. Acad. Sci. USA 112 (2015) 13845–13849.
[287] H. Vilter, Phytochemistry 23 (1984) 1387-1390.
[288] T.L. Johnson, B. Brahamsha, B. Palenik, J. Muhle, Limnol. Oceanogr. 60 (2015) 1823-1835.
[289] R. Wever, P. Barnett, Chem. Asian J. 12 (2017) 1997-2007.
[290] A. Messerschmidt, Prade, L., Wever, R., Chloroperoxidase from Curvularia inaequalis: X-ray Structures of Native and Peroxide Form Reveal Vanadium Chemistry in Vanadium Haloperoxidases, in: A.S. Tracey, Crans, D.C. (Ed.) Vanadium Compounds. Chemistry, Biochemistry, and Therapeutic Applications, American Chemical Society, Washington, 1998 pp. 186-201.
[291] R. Wever, Krenn, B.E., Vanadium Haloperoxidases, in: N.D. Chasteen (Ed.) Vanadium in Biological Systems, Physiology and Biochemistry, Kluwer, Dordrecht, 1990, pp. 81-97.
[292] R. Wever, Hemrika, W., Vanadium in Enzymes, in: J.O. Nriagu (Ed.) Vanadium in the Environment, Jonh Wiley and Sons, New York, 1998, pp. 285-305.
[293] R. Wever, Structure and Function of Vanadium Haloperoxidases, in: H. Michibata (Ed.) Biochemical and Molecular Biological Approaches, Springer, Dordrecht, 2012, pp. 95-125.
[294] H. Vilter, Vanadium-Dependent Haloperoxidases, in: H. Sigel, Sigel, A. (Ed.) Vanadium and its Role in Life, Mardel Dekker, New York, 1995, pp. 325-362.
[295] C.C. McLauchlan, H.A. Murakami, C.A. Wallace, D.C. Crans, J. Inorg. Biochem. 186 (2018) 267-279.
[296] G. Licini, V. Conte, A. Coletti, M. Mba, C. Zonta, Coord. Chem. Rev. 255 (2011) 2345-2357.
[297] W. Plass, Coord. Chem. Rev. 255 (2011) 2378–2387.
[298] D. Wischang, O. Brucher, J. Hartung, Coord. Chem. Rev. 255 (2011) 2204-2217.
[299] A. Timmins, S.P. De Visser, in: Adv. Protein Chem. Struct. Biol., 2015, pp. 113-151.
[300] A. Timmins, S.P.d. Visser, Catalysts 8 (2018) 314.
[301] A. Messerschmidt, R. Wever, Proc. Natl. Acad. Sci. U. S. A. 93 (1996) 392-396.
[302] A. Messerschmidt, L. Prade, R. Wever, in: Biol. Chem., 1997, pp. 309.

[303] M.N. Isupov, A.R. Dalby, A.A. Brindley, Y. Izumi, T. Tanabe, G.N. Murshudov, J.A. Littlechild, J. Mol. Biol. 299 (2000) 1035-1049.
[304] J. Littlechild, E. Garcia-Rodriguez, A. Dalby, M. Isupov, J. Mol. Recognit. 15 (2002) 291-296.
[305] S. Macedo-Ribeiro, W. Hemrika, R. Renirie, R. Wever, A. Messerschmidt, J. Biol. Inorg. Chem. 4 (1999) 209-219.
[306] W. Hemrika, R. Renirie, S. Macedo-Ribeiro, A. Messerschmidt, R. Wever, J. Biol. Chem. 274 (1999) 23820–23827.
[307] T. Ohshiro, J. Littlechild, E. Garcia-Rodriguez, M.N. Isupov, Y. Iida, T. Kobayasi, Y. Yzumi, Protein Sci. 13 (2004) 1566-1571.
[308] A. Frank, C.J. Seel, M. Groll, T. Gulder, ChemBioChem 17 (2016) 2028-2032.
[309] R. Renirie, W. Hemrika, S.R. Piersma, R. Wever, Biochemistry 39 (2000) 1133-1141.
[310] C. Kimblin, X.H. Bu, A. Butler, Inorg. Chem. 41 (2002) 161-163.
[311] N. Tanaka, Z. Hasan, R. Wever, Inorg. Chim. Acta 356 (2003) 288-296.
[312] M. Bangesh, W. Plass, J. Mol. Struct. Theochem 725 (2005) 163-175.
[313] J.Y. Kravitz, V.L. Pecoraro, Pure Appl. Chem. 77 (2005) 1595-1605.
[314] G. Zampella, P. Fantucci, V.L. Pecoraro, L. De Gioia, J. Am. Chem. Soc. 127 (2005) 953–960.
[315] G. Zampella, P. Fantucci, V.L. Pecoraro, L. De Gioia, Inorg. Chem. 45 (2006) 7133-7143.
[316] S. Raugei, F.L. Gervasio, P. Carloni, Phys. Status Solidi B 243 (2006) 2500-2515.
[317] W. Plass, M. Bangesh, S. Nica, A. Buchholz, Vanadium: The Verastile Metal 974 (2007) 163-177.
[318] K.R. Geethalakshmi, M.P. Waller, W. Thiel, M. Bühl, J. Phys. Chem. B 113 (2009) 4456–4465.
[319] M.Q.E. Mubarak, E.F. Gérard, C.F. Blanford, S. Hay, S.P. De Visser, ACS Catal. 10 (2020) 14067-14079.
[320] C.J. Schneider, G. Zampella, L. DeGioa, V.L. Pecoraro, Understanding the Mechanism of Vanadium-Dependent Haloperoxidases and Related Biomimetic Catalysis, in: K. Kustin, J. Costa Pessoa, D.C. Crans (Eds.) Vanadium: The Verastile Metal, ACS, Washington, DC, 2007, pp. 148-162.
[321] L.F. Pacios, O. Gálvez, J. Chem. Theory Comput. 6 (2010) 1738–1752.
[322] A.N. Antipov, N.N. Lyalikova, N.P. L'vov, IUBMB Life 49 (2000) 137-141.
[323] A.N. Antipov, D.Y. Sorokin, N.P. L'Vov, J.G. Kuenen, Biochem. J. 369 (2003) 185-189.
[324] D. Rehder, Org. Biomol. Chem. 6 (2008) 957-964.

[325] N.A. Yukova, N.D. Saveljeva, N.N. Lyalikova, Mikrobiologiya 62 (1993) 597-603.
[326] J.T. Csotonyi, E. Stackebrandt, Y. Yorkov, Appl. Environ. Microbiol., 72, 4950-4956, Appl. Environ. Microbiol. 72 (2006) 4950-4956.
[327] J. Zhang, H. Dong, L. Zhao, R. McCarrick, A. Agrawal, Chem. Geol. 370 (2014) 29-39.
[328] W. Carpentier, L. De Smet, J. Van Beeumen, A. Brigé, J. Bacteriol. 187 (2005) 3293-3301.
[329] I. Ortiz-Bernad, R.T. Anderson, H.A. Vrionis, D.R. Loveley, Appl. Environ. Microbiol. 70 (2004) 3091-3095.
[330] J. van Marwijk, D.J. Opperman, L.A. Piater, E. van Heerden, Biotechnol. Lett. 31 (2009) 845-849.
[331] B. Zhang, Y. Li, Y. Fei, Y. Cheng, Environ. Sci. Technol. 55 (2021) 2121-2131.
[332] L. Chen, J.-R. Liu, J. Gao, W.-F. Hu, J.-Y. Yang, J. Hazard. Mater. 5 (2021) 124200.
[333] B. Zhang, Y. Jiang, K. Zuo, C. He, Y. Dai, Z.J. Ren, J. Hazard. Mater. 382 (2020) 121228.
[334] J. Zhai, M.H. Rahaman, X. Chen, H. Xiao, K. Liao, X. Li, C. Duan, B. Zhang, G. Tao, T. John, J. Vymazal, Ecol. Eng. 87 (2016) 434-443.
[335] J. Ma, H. Wu, Y. Wan, G. Qiu, B. Fu, C. Wu, C. Wei, Bioresour. Technol. 289 (2019) 121616.
[336] Z. Zhao, C. Sun, Y. Li, Q. Yu, Z. Jin, M. Wang, L. Liang, Y. Zhang, Chem. Eng. J. 393 (2020) 124801.
[337] C. He, B. Zhang, J. Lu, R. Qiu, Water Res. 189 (2021) 116664.
[338] D. Rehder, G. Santoni, G.M. Licini, C. Schulzke, B. Meier, Coord. Chem. Rev. 237 (2003) 53-63.
[339] F. van de Velde, I.W.C.E. Arends, R.A. Sheldon, J. Inorg. Biochem. 80 (2000) 81-89.
[340] F. van de Velde, I.W.C.E. Arends, R.A. Sheldon, Top. Catal. 13 (2000) 259.
[341] F. van de Velde, L. Könemann, F. van Rantwijk, R.A. Sheldon, Biotechnol. Bioeng. 67 (2000) 87-96.
[342] A. Pordea, M. Creus, J. Panek, C. Duboc, D. Mathis, M. Novic, T.R. Ward, J. Am. Chem. Soc. 130 (2008) 8085-8088.
[343] I. Correia, S. Aksu, P. Adão, J. Costa Pessoa, R.A. Sheldon, I.W.C.E. Arends, J. Inorg. Biochem. 102 (2008) 318-329.
[344] M.R. Maurya, Coord. Chem. Rev. 383 (2019) 43-81.
[345] A. Butler, M. Sandy, Nature 460 (2009) 848–854.
[346] E. de Boer, H. Plat, M.G. Tromp, R. Wever, M.C. Franssen, H.C. van der Plas, E.M. Meijer, H.E. Shoemaker, Biotechnol. Bioeng. 30 (1987) 607-610.

[347] E.E. Coupe, M.G. Smyth, A.P. Fosberry, R.M. Hall, J.A. Littlechild, Protein Expr. Purif. 52 (2007) 265–272.
[348] D. Wischang, J. Hartung, Tetrahedron 67 (2011) 4048-4054.
[349] D. Wischang, M. Radlow, H. Schulz, H. Vilter, L. Viehweger, M.O. Altmeyer, C. Kegler, J. Herrmann, R. Muller, F. Gaillard, L. Delage, C. Leblanc, J. Hartung, Bioinorg. Chem. 44 (2012) 25-34.
[350] P. Bernhardt, T. Okino, J.M. Winter, A. Miyanaga, B.S. Moore, J. Am. Chem. Soc. 133 (2011) 4268-4270.
[351] A. But, J. Le Notre, E.L. Scott, R. Wever, J.P.M. Sanders, ChemSusChem 5 (2012) 1199-1202.
[352] J.J. Dong, E. Fernández-Fueyo, J. Li, Z. Guo, R. Renerie, R. Wever, F. Hollmann, Chem. Commun. 53 (2017) 6207-6210.
[353] D. Wischang, J. Hartung, T. Hahn, R. Ulber, T. Stumpf, C. Fecher-Trost, Green Chem. 13 (2011) 102-108.
[354] E. Fernandez-Fueyo, M. van Wingerden, R. Renirie, R. Wever, Y. Ni, D. Holtmann, F. Hollmann, ChemCatChem 7 (2015) 4035-4038.
[355] M. Andersson, A. Willetts, S. Allenmark, J. Org. Chem. 62 (1997) 8455–8458.
[356] H.B. ten Brink, H.L. Dekker, H.E. Schoemaker, R. Wever, J. Inorg. Biochem. 80 (2000) 91–98.
[357] H.B. ten Brink, H.L. Holland, H.E. Schoemaker, H. Van Lingen, R. Wever, Tetrahedron: Asymmetry 10 (1999) 4563-4572.
[358] W. Hemrika, Renerie, R., Dekker, H., Wever, R., Vanadium Containing Haloperoxidases and Acid Phosphatases: the conserved active site, in: A.S. Tracey, Crans, D.C. (Ed.) Vanadium Compounds. Chemistry, Biochemistry and Therapeutic Applications, ACS, Washington, 1998, pp. 216-227.
[359] A.F. Neuwald, Protein Sci. 6 (1997) 1764-1767.
[360] R. Renirie, W. Hemrika, R. Wever, J. Biol. Chem. 275 (2000) 11650-11657.
[361] F. van de Velde, L. Könemann, Chem. Commun. (1998) 1891-1892.
[362] R.T. MacGillivray, E. Mendez, J.G. Shewale, S.K. Sinha, J. Lineback-Zins, K. Brew, J. Biol. Chem. 258 (1983) 3543-3553.
[363] J. Schaller, S. Gerber, U. Kämpfer, S. Lejon, C. Trachsel, Human Blood Plasma Proteins: Structure and Function, John Wiley & Sons Ltd., Chichester, 2008.
[364] J. Williams, K. Moreton, Biochem. J. 185 (1980) 483-488.

[365] R. Crichton, Iron Metabolism - From Molecular Mechanisms to Clinical Consequences, 3rd Edition, John Wiley & Sons, Ltd, Chichester, 2009.
[366] J.A. Benjamín-Rivera, A.E. Cardona-Rivera, Á.L. Vázquez-Maldonado, C.Y. Dones-Lassalle, H.L. Pabón-Colon, H.M. Rodríguez-Rivera, I. Rodríguez, J.C. González-Espiet, J. Pazol, J.D. Pérez-Ríos, J.F. Catala-Torres, M. Carrasquillo Rivera, M.G. De Jesus-Soto, N.A. Cordero-Virella, P.M. Cruz-Maldonado, P. González-Pagan, R. Hernández-Ríos, K. Gaur, S.A. Loza-Rosas, A.D. Tinoco, Inorganics 8 (2020) 48.
[367] G.C. Justino, E. Garribba, J. Costa Pessoa, J. Biol. Inorg. Chem. 18 (2013) 803-813.
[368] H. Sun, M. Cox, H. Li, P. Sadler, Struct. Bonding (Berlin) 88 (1997) 71-102.
[369] D.N. Chasteen, Coord. Chem. Rev. 22 (1977) 1-36.
[370] J. Costa Pessoa, I. Tomaz, Curr. Med. Chem. 17 (2010) 3701-3738.
[371] T. Jakusch, J. Costa Pessoa, T. Kiss, Coord. Chem. Rev. 255 (2011) 2218-2226.
[372] D. Sanna, P. Buglyo, G. Micera, E. Garribba, J. Biol. Inorg. Chem. 15 (2010) 825-839.
[373] D.C. Harris, Biochemistry 16 (1977) 560-564.
[374] D. Rehder, Future Med. Chem. 4 (2012) 1823-1837.
[375] D. Sanna, G. Micera, E. Garribba, Inorg. Chem. 52 (2013) 11975-11985.
[376] R.J. DeKoch, D.J. West, J.C. Cannon, N.D. Chasteen, Biochemistry 13 (1974) 4347-4354.
[377] G. Gonçalves, I. Tomaz, I. Correia, L.F. Veiros, M.M.C.A. Castro, F. Avecilla, L. Palacio, M. Maestro, T. Kiss, T. Jakusch, M.H.V. Garcia, J. Costa Pessoa, Dalton Trans. 42 (2013) 11841-11861.
[378] D. Sanna, L. Bíró, P. Buglyó, G. Micera, E. Garribba, Metallomics 4 (2012) 33-36.
[379] D. Sanna, V. Ugone, G. Sciortino, P. Buglyo, Z. Bihari, P.L. Parajdi-Losonczi, E. Garribba, Dalton Trans. 47 (2018) 2164-2182.
[380] W. Bal, M. Sokołowska, E. Kurowska, P. Faller, Biochim. Biophys. Acta, Gen. Subj. 1830 (2013) 5444-5455.
[381] M. Fasano, S. Curry, E. Terreno, M. Galliano, G. Fanali, P. Narciso, S. Notari, P. Ascenzi, IUBMB Life 57 (2005) 787-796.
[382] B.P. Espósito, R. Najjar, Coord. Chem. Rev. 232 (2002) 137-149.
[383] J. Christodoulou, P.J. Sadler, A. Tucker, Eur. J. Biochem. 225 (1994) 363-368.
[384] N.D. Chasteen, J. Francavilla, J. Phys. Chem. 80 (1976) 867-871.
[385] K. Fukui, H. Ohya-Nishiguchi, M. Nakai, H. Sakurai, H. Kamada, FEBS Lett. 368 (1995) 31-35.
[386] M. Purcell, J.F. Neault, H. Malonga, H. Arakawa, H.A. Tajmir-Riahi, Can. J. Chem. 79 (2001) 1415-1421.

[387] B.D. Liboiron, K.H. Thompson, G.R. Hanson, E. Lam, N. Aebischer, C. Orvig, J. Am. Chem. Soc. 127 (2005) 5104-5115.
[388] D. Sanna, E. Garribba, G. Micera, J. Inorg. Biochem. 103 (2009) 648-655.
[389] D. Sanna, G. Micera, E. Garribba, Inorg. Chem. 48 (2009) 5747-5757.
[390] E. Cobbina, S. Mehtab, I. Correia, G. Gonçalves, I. Tomaz, I. Cavaco, T. Jakusch, E. Enyedi, T. Kiss, J. Costa Pessoa, J. Mex. Chem. Soc. 57 (2013) 180-191.
[391] I. Correia, T. Jakusch, E. Cobbinna, S. Mehtab, I. Tomaz, N.V. Nagy, A. Rockenbauer, J. Costa Pessoa, T. Kiss, Dalton Trans. 41 (2012) 6477-6487.
[392] P. Eastman, J. Swails, J.D. Chodera, R.T. McGibbon, Y. Zhao, K.A. Beauchamp, L.-P. Wang, A.C. Simmonett, M.P. Harrigan, C.D. Stern, R.P. Wiewiora, B.R. Brooks, V.S. Pande, PLoS Comput. Biol. 13 (2017) e1005659.
[393] V. Hornak, R. Abel, A. Okur, B. Strockbine, A. Roitberg, C. Simmerling, Proteins: Struct., Funct., Bioinf. 65 (2006) 712-725.
[394] A.J. Stewart, C.A. Blindauer, S. Berezenko, D. Sleep, P.J. Sadler, Proc. Natl. Acad. Sci. U. S. A. 100 (2003) 3701-3706.
[395] E. Mothes, P. Faller, Biochemistry 46 (2007) 2267-2274.
[396] M. Sokołowska, M. Wszelaka-Rylik, J. Poznański, W. Bal, J. Inorg. Biochem. 103 (2009) 1005-1013.
[397] K.B. Handing, I.G. Shabalin, O. Kassaar, S. Khazaipoul, C.A. Blindauer, A.J. Stewart, M. Chruszcz, W. Minor, Chem. Sci. 7 (2016) 6635-6648.
[398] H. Yasui, Y. Kunori, H. Sakurai, Chem. Lett. 32 (2003) 1032-1033.
[399] G. Heinemann, B. Fichtl, M. Mentler, W. Vogt, J. Inorg. Biochem. 90 (2002) 38-42.
[400] A. Banerjee, M. Mohanty, S. Lima, R. Samanta, E. Garribba, T. Sasamori, R. Dinda, New J. Chem. 44 (2020) 10946-10963.
[401] P. Nunes, I. Correia, F. Marques, A.P. Matos, M.M.C. dos Santos, C.G. Azevedo, J.-L. Capelo, H.M. Santos, S. Gama, T. Pinheiro, I. Cavaco, J. Costa Pessoa, Inorg. Chem. 59 (2020) 9116-9134.
[402] D. Sanna, G. Micera, E. Garribba, Inorg. Chem. 50 (2011) 3717-3728.
[403] S. Nishihara, A. Shimizu, Y. Arata, Mol. Immunol. 23 (1986) 285-290.
[404] D. Sanna, L. Bíró, P. Buglyó, G. Micera, E. Garribba, J. Inorg. Biochem. 115 (2012) 87-99.
[405] M. Bruech, M.E. Quintanilla, W. Legrum, J. Koch, K.J. Netter, G.F. Fuhrmann, Toxicology 31 (1984) 283-295.
[406] T.C. Delgado, A.I. Tomaz, I. Correia, J. Costa Pessoa, J.G. Jones, C.F.G.C. Geraldes, M.M.C.A. Castro, J. Inorg. Biochem. 99 (2005) 2328-2339.

[407] M. Garner, J. Reglinski, W.E. Smith, J. McMurray, I. Abdullah, R. Wilson, J. Biol. Inorg. Chem. 2 (1997) 235-241.
[408] T.V. Hansen, J. Aaseth, J. Alexander, Arch. Toxicol. 50 (1982) 195-202.
[409] A. Heinz, K.A. Rubinson, J.J. Grantham, J. Lab. Clin. Med. 100 (1982) 593-612.
[410] X. Yang, K. Wang, J. Lu, D.C. Crans, Coord. Chem. Rev. 237 (2003) 103-111.
[411] B. Zhang, L. Ruan, B. Chen, J. Lu, K. Wang, BioMetals 10 (1997) 291-298.
[412] D. Sanna, M. Serra, G. Micera, E. Garribba, Inorg. Chem. 53 (2014) 1449-1464.
[413] K. De Cremer, M. Van Hulle, C. Chéry, R. Cornelis, K. Strijckmans, R. Dams, N. Lameire, R. Vanholder, J. Biol. Inorg. Chem. 7 (2002) 884-890.
[414] I.G. Macara, K. Kustin, L.C. Cantley Jr, Biochim. Biophys. Acta, Gen. Subj. 629 (1980) 95-106.
[415] A. Levina, A.I. McLeod, S.J. Gasparini, A. Nguyen, W.G.M. De Silva, J.B. Aitken, H.H. Harris, C. Glover, B. Johannessen, P.A. Lay, Inorg. Chem. 54 (2015) 7753-7766.
[416] V. Simplaceanu, J.A. Lukin, T.-Y. Fang, M. Zou, N.T. Ho, C. Ho, Biophys. J. 79 (2000) 1146-1154.
[417] D. Sanna, J. Palomba, G. Lubinu, P. Buglyó, S. Nagy, F. Perdih, E. Garribba, J. Med. Chem. 62 (2019) 654-664.
[418] T. Jakusch, É.A. Enyedy, K. Kozma, Z. Paár, A. Bényei, T. Kiss, Inorg. Chim. Acta 420 (2014) 92-102.
[419] H.A. McKenzie, F.H. White, Lysozyme and α-Lactalbumin: Structure, Function, and Interrelationships, in: C.B. Anfinsen, F.M. Richards, J.T. Edsall, D.S. Eisenberg (Eds.) Adv. Protein Chem., Academic Press, 1991, pp. 173-315.
[420] S.A. Ragland, A.K. Criss, PLoS Pathog. 13 (2017) e1006512.
[421] Lysozymes: model enzymes in biochemistry and biology, Jollès, P., Ed.; Birkhaüser Verlag, Basel, 1996.
[422] M. Dumoulin, R.J.K. Johnson, V. Bellotti, C.M. Dobson, Human lysozyme, in: V.N. Uversky, A.L. Fink (Eds.) Protein misfolding, aggregation, and conformational diseases: Part B: molecular mechanisms of conformational diseases, Springer US, Boston, MA, 2007, pp. 285-308.
[423] G.A. Ordway, D.J. Garry, J. Exp. Biol. 207 (2004) 3441-3446.
[424] S.V. Evans, G.D. Brayer, J. Mol. Biol. 213 (1990) 885-897.
[425] D. Sanna, M. Serra, G. Micera, E. Garribba, Inorg. Chim. Acta 420 (2014) 75-84.
[426] T. Zhao, F.L. King, J. Inorg. Biochem. 104 (2010) 186-192.
[427] E. Moreno-Gordaliza, B. Cañas, M.A. Palacios, M.M. Gómez-Gómez, Talanta 88 (2012) 599-608.

[428] C.M. Pickart, M.J. Eddins, Biochim. Biophys. Acta Mol. Cell Res. 1695 (2004) 55-72.
[429] X. Jiang, X. Wang, Annu. Rev. Biochem. 73 (2004) 87-106.
[430] M. Aureliano, C.A. Ohlin, J. Inorg. Biochem. 137 (2014) 123-130.
[431] M. Aureliano, D.C. Crans, J. Inorg. Biochem. 103 (2009) 536-546.
[432] M. Aureliano, Oxid Med Cell Longev 2016 (2016) 6103457.
[433] A. Bijelic, M. Aureliano, A. Rompel, Chem. Commun. 54 (2018) 1153-1169.
[434] A. Bijelic, M. Aureliano, A. Rompel, Angew. Chem. Int. Ed. 58 (2019) 2980-2999.
[435] M. Zhao, X. Chen, G. Chi, D. Shuai, L. Wang, B. Chen, J. Li, Inorg. Chem. Front. 7 (2020) 4320-4332.
[436] D. Marques-da-Silva, G. Fraqueza, R. Lagoa, A.A. Vannathan, S.S. Mal, M. Aureliano, New J. Chem. 43 (2019) 17577-17587.
[437] T. Douglas, M. Young, Nature 393 (1998) 152-155.
[438] S. Shigeta, S. Mori, E. Kodama, J. Kodama, K. Takahashi, T. Yamase, Antiviral Res. 58 (2003) 265-271.
[439] N. Yamamoto, D. Schols, E. De Clercq, Z. Debyser, R. Pauwels, J. Balzarini, H. Nakashima, M. Baba, M. Hosoya, R. Snoeck, Mol. Pharmacol. 42 (1992) 1109-1117.
[440] G.A. Donzella, D. Schols, S.W. Lin, J.A. Esté, K.A. Nagashima, P.J. Maddon, G.P. Allaway, T.P. Sakmar, G. Henson, E. DeClercq, J.P. Moore, Nat. Med. 4 (1998) 72-77.
[441] T. Yamase, J. Mater. Chem. 15 (2005) 4773-4782.
[442] R.L. Felts, T.J. Reilly, J.J. Tanner, J. Biol. Chem. 281 (2006) 30289-30298.
[443] M. Zebisch, M. Krauss, P. Schäfer, N. Sträter, J. Mol. Biol. 415 (2012) 288-306.
[444] M. Zebisch, M. Krauss, P. Schäfer, P. Lauble, N. Sträter, Structure 21 (2013) 1460-1475.
[445] J.H. Bae, E.D. Lew, S. Yuzawa, F. Tomé, I. Lax, J. Schlessinger, Cell 138 (2009) 514-524.
[446] M. Arefian, M. Mirzaei, H. Eshtiagh-Hosseini, A. Frontera, Dalton Trans. 46 (2017) 6812-6829.
[447] M. Aureliano, G. Fraqueza, C.A. Ohlin, Dalton Trans. 42 (2013) 11770-11777.
[448] G. Fraqueza, C.A. Ohlin, W.H. Casey, M. Aureliano, J. Inorg. Biochem. 107 (2012) 82-89.
[449] S. Ramos, J.J.G. Moura, M. Aureliano, J. Inorg. Biochem. 104 (2010) 1234-1239.
[450] S. Ramos, J.J.G. Moura, M. Aureliano, Metallomics 4 (2012) 16-22.
[451] T. Tiago, M. Aureliano, C. Gutiérrez-Merino, Biochemistry 43 (2004) 5551-5561.
[452] T. Tiago, P. Martel, C. Gutiérrez-Merino, M. Aureliano, Biochim. Biophys. Acta, Proteins Proteom. 1774 (2007) 474-480.
[453] S. Ramos, M. Manuel, T. Tiago, R. Duarte, J. Martins, C. Gutiérrez-Merino, J.J.G. Moura, M. Aureliano, J. Inorg. Biochem. 100 (2006) 1734-1743.

[454] U. Pick, J. Biol. Chem. 257 (1982) 6111-6119.
[455] P. Csermely, A. Martonosi, G.C. Levy, A.J. Ejchart, Biochem. J. 230 (1985) 807-815.
[456] T. Tiago, M. Aureliano, J.J.G. Moura, J. Inorg. Biochem. 98 (2004) 1902-1910.
[457] G. Sciortino, M. Aureliano, E. Garribba, Inorg. Chem. 60 (2021) 334-344.
[458] S. Genheden, U. Ryde, Expert Opinion on Drug Discovery 10 (2015) 449-461.
[459] I. Andersson, A. Gorzsás, C. Kerezsi, I. Tóth, L. Pettersson, Dalton Trans. (2005) 3658-3666.
[460] G. Fraqueza, J. Fuentes, L. Krivosudský, S. Dutta, S.S. Mal, A. Roller, G. Giester, A. Rompel, M. Aureliano, J. Inorg. Biochem. 197 (2019) 110700.
[461] D. Althumairy, H.A. Murakami, D. Zhang, B.G. Barisas, D.A. Roess, D.C. Crans, J. Inorg. Biochem. 203 (2020) 110873.
[462] N. Samart, D. Althumairy, D. Zhang, D.A. Roess, D.C. Crans, Coord. Chem. Rev. 416 (2020) 213286.
[463] D. Althumairy, K. Postal, B.G. Barisas, G.G. Nunes, D.A. Roess, D.C. Crans, Metallomics 12 (2020) 1044-1061.
[464] B.M. Dorsey, C.C. McLauchlan, M.A. Jones, Front. Chem. 6 (2018).
[465] A. Levina, A.I. McLeod, L.E. Kremer, J.B. Aitken, C.J. Glover, B. Johannessen, P.A. Lay, Metallomics 6 (2014) 1880-1888.
[466] H. Sakurai, J. Fugono, H. Yasui, Mini-Rev. Med. Chem. 4 (2004) 41-48.
[467] D. Sanna, M. Serra, V. Ugone, L. Manca, M. Pirastru, P. Buglyo, L. Biro, G. Micera, E. Garribba, Metallomics 8 (2016) 532-541.
[468] D. Rehder, Dalton Trans. 42 (2013) 11749–11761.
[469] S. Treviño, A. Diaz, J. Inorg. Biochem. 208 (2020) 111094.
[470] Y. Yoshikawa, H. Sakurai, D.C. Crans, G. Micera, E. Garribba, Dalton Trans. 43 (2014) 6965-6972.
[471] D.C. Crans, L. Yang, A. Haase, X. Yang, Health Benefits of Vanadium and Its Potential as an Anticancer Agent, Met. Ions Life Sci., in: H.S. A. Sigel, E. Freisinger, R.K.O. Sigel (Ed.) Metallo-Drugs Development & Action of Anticancer Agents, Walter de Gruyter GmbH, Berlin, 2018, pp. 251–279.
[472] D. Gambino, Coord. Chem. Rev. 255 (2011) 2193– 2203.
[473] Y.C. Wong, S. Kim, W. Peng, D. Krainc, Trends Cell Biol. 29 (2019) 500-513.
[474] T.T. Liu, Y.J. Liu, Q. Wang, X.G. Yang, K. Wang, J. Biol. Inorg. Chem. 17 (2012) 311-320.
[475] S. Kowalski, S. Hać, D. Wyrzykowski, A. Zauszkiewicz-Pawlak, I. Inkielewicz-Stępniak, Oncotarget 8 (2017) 60324-60341.
[476] J.X. Wu, Y.H. Hong, X.G. Yang, J. Biol. Inorg. Chem. 21 (2016) 919-929.

[477] A. Papaioannou, M. Manos, S. Karkabounas, R. Liasko, A.M. Evangelou, I. Correia, V. Kalfakakou, J. Costa Pessoa, T. Kabanos, J. Inorg. Biochem. 98 (2004) 959-968.
[478] R. Parrondo, A. de las Pozas, T. Reiner, P. Rai, C. Perez-Stable, Mol. Cancer 9 (2010) 182-195.
[479] M. A., S. Yamamoto, B. Wang, K. Tanaka, N. Suzuki, S. Aoki, A. Ito, T. Nanao, S. Ohya, M. Yoshino, J. Zhu, A. Enomoto, Y. Matsumoto, O. Funatsu, Y. Hosoi, M. Ikekita, Cancer Res. 70 (2010) 257-265.
[480] M. Pisano, C. Arru, M. Serra, G. Galleri, D. Sanna, E. Garribba, G. Palmieri, C. Rozzo, Metallomics 11 (2019) 1687-1699.
[481] T.L. Turner, V.H. Nguyen, C.C. McLauchlan, Z. Dymon, B.M. Dorsey, J.D. Hooker, M.A. Jones, J. Inorg. Biochem. 108 (2012) 96-104.
[482] R.S. Mendez, B.M. Dorsey, C.C. McLauchlan, M. Beio, T.L. Turner, V.H. Nguyen, A. Su, W. Beynon, J.A. Friesen, M.A. Jones, Int. J. Chem. 6 (2014) 35-49.
[483] R. Wever, Application of peroxidases, in: H.B. Dunford (Ed.) Peroxidases and catalases: Biochemistry, biophysics, biotechnology and physiology, John Wiley & Sons, Inc., New Jersey, 2010, pp. 403-423.
[484] A. Levina, A. Pires Vieira, A. Wijetunga, R. Kaur, J.T. Koehn, D.C. Crans, P.A. Lay, Angew. Chem. Int. Ed. 59 (2020) 15834–15838.
[485] V.P. Torchilin, AAPS J. 9 (2007) E128–E147.
[486] M. Selman, C. Rousso, A. Bergeron, H.H. Son, R. Krishnan, N.A. El-Sayes, O. Varette, A. Chen, F. Le Boeuf, F. Tzelepis, J.C. Bell, D.C. Crans, J.-S. Diallo, Mol. Ther. 26 (2018) 56-69.

Graphical Abstract

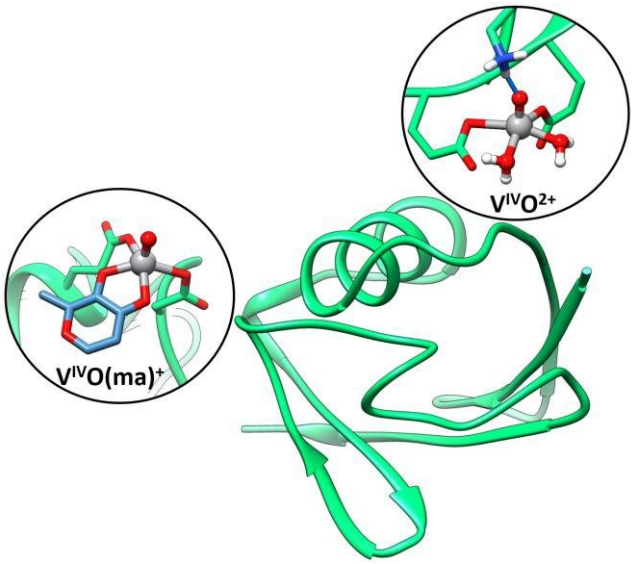

Synopsis

Recent developments on the understanding of binding of vanadium species with proteins and enzymes and on the experimental and computational methods to study these systems are reviewed. The biological and therapeutic implications of such interactions, challenges and future directions on applications of vanadium compounds are presented.